The westward displacement along this thrust fault is indicated in section by an offset (known from drill-hole data) of parts of the porphyry mass existing east of the pit. The amount of displacement might amount to a few hundred feet.

3. Mineralization.

The three formations seen in the pit are the diabase, a dark-gray color, the schist ranging from a light pink to a reddish brown and the porphyry often lighter in color.

Hypogene mineralization occurs more conspicuously in the diabase under the form of chalcopyrite and pyrite. The rock is fractured and broken, although fine-grained and dense. It is hard to break, hard to drill and hard to crush; however it crumbles easily by disintegration after a few months of exposure in the air. A hammer blow breaks it along pre-existing fractures and each new blow breaks it along more tiny fractures all of which are mineralized. This mineralization does not extend far away from the fracture, perhaps a tenth or 2 tenths of an inch. It is not truly disseminated therefore, and it could better be called reticulated for example, as E. N. Pennebaker labeled it (verbal communication).

It is difficult to distinguish chalcocite in this dark rock and the amount of supergene enrichment is ~~now~~ not well known.

The schist in the pit usually shows chalcocite as copper mineral either as tiny specks or as veinlets. This is understand-

ably secondary because we are still in the supergene zone.

In the schist also, we can detect the same "reticulation" in mineralization as noticed in the diabase.

The porphyry in the pit shows chalcopyrite, pyrite and secondary chalcocite; much of the chalcopyrite and the pyrite have indeed been already replaced.

Gold and silver in minute quantity accompany the copper minerals with some molybdenum.

Native copper has been one of the copper minerals frequently found in the Ray ore zones. Cuprite sometimes under the form of chalcotrichite with its delicate hairlike crystals, is also abundant in places.

4. Alteration.

Little hydrothermal alteration as such seems to have affected the diabase. The schist, on the other hand, exhibits much more alteration although less than at other mines, such as Chino, etc. Sericitization is the main phenomenon and it occurs generally along with mineralization; it is well displayed in the whole western portion of the Pearl Handle Pit. Some silicification mainly along faults also shows at places. It has been repeatedly observed in field specimens from the pit and outside, that a small bleached zone of sericitization occurs on either side of pyrite veins but the phenomenon does not occur along quartz veins.

Another type of alteration connected with thermal metamorphism is seen in the pit west of the diabase: this is the occurrence of larger masses of a siliceous rock quite sericitic, grayish and fine-grained, occasionally still showing remnants of schistosity. It breaks, however, like diabase with a similar occurrence of mineralization, often then having a darker grayish color.

Two such occurrences have been found. One shows in the diabase, near its underface, north of the pit, where it looks more like a stoped mass of schist in the diabase. The other, quite extensive, shows on the west side of the pit below but adjacent to the diabase. The occurrence seems in this case to be more of a transitional type. The color is generally light gray, sometimes whitish gray showing a marked contrast with the dark diabase to the east and the brown reddish schist further west. Thin sections made from this rock showed it to be a sericitized quartzite.

The porphyry, mainly found east of the pit, displays some alteration mainly in the plagioclase felspars. It has a pinkish appearance and shows well-formed biotite books, shiny and well crystallized. Here too, we see that along pyrite veinlets there is a bleached sericitized band on either side. These bands are wider here than in the schist, often 1 or 2 inches wide in total. The color becomes creamy-tan.

To the south of the pit we also find a transitional zone between schist and porphyry this time where the two rock characteristics have been blended together.

---

5. Origin of the Ore.

There is much speculation about this question. It appears, however, that one of the small stocks of Granite Mountain porphyry is much more broken and shattered than others; it is located east of the present pit and on the Ray fault within the ore body.

A well shattered porphyry stock in the middle of a heavy fault zone, accompanied by a general rustiness of the rocks in the area, seems a valid criteria for good porphyry copper. The presence of diabase, as is seen in other mines of the vicinity, is an additional favorable factor influencing the orebody.

J. Wertz

(Paper presented at the Spring Meeting AIME, Geology Division, Ray, Arizona on April 12, 1958).

Ray

compiled by L. Worly
1958

A BRIEF HISTORY OF THE RAY DISTRICT

The Mineral Creek Mining District, which includes the Ray area, was organized by silver prospectors in 1873. In 1880 the Mineral Creek Mining Co. built a five-stamp mill, then in 1883 the Ray Copper Co. took over and built a 30-ton copper furnace. The ore of the area was described as principally native copper. There was little activity until 1898 when the claims were purchased by the Globe Mines Exploration Company, (Ltd.), of London. The following year the ground was acquired by the Ray Copper Mines, (Ltd.), another British Company.

During the first year of its existence the new company founded the town of Kelvin and erected a 250-ton mill there. Ray and Kelvin were connected by a 7 mile narrow gauge railroad, various shops and offices were erected, and a 344 ft. shaft was sunk at Ray. Supplies were transported by steam traction engine 43 miles from Red Rock, the nearest shipping point on the railroad. There was no mining activity between 1901 and 1905.

D. C. Jackling was attracted to the district in 1906. The Ray Copper Co. and Gila Copper Co. were organized to acquire the English Company's holdings; they were merged as the Ray Consolidated Copper Co. in 1910. Other companies to become active in the district in 1906 and 1907 were the Arizona Hercules Copper Mining Co., Kelvin Calumet Mining Co. and Ray Central Mining Co.

The properties of all these Companies were acquired by the Ray Consolidated Copper Co. through the years. A mill was placed in operation at Hayden during 1911 and production started from the mines at Ray. In 1912 a smelter was built by A.S.& R. at Hayden. In 1924 Ray Consolidated Copper acquired the Chino Copper Co. in New Mexico. In 1926 the Nevada Consolidated Copper Co. absorbed the Ray Consolidated holdings and these holdings were later absorbed by Kennecott Copper Corp.

Mining methods underground and metallurgical processes at the mill underwent a slow but constant improvement. The Ray Mines were the first underground operation to produce 8000 tons of ore per day by the block caving method.

There was a brief shut-down of mining operations in 1921. Operations were again shut down during the depression between 1933 and 1937.

In 1938 the first unit of a modern precipitating plant was placed in operation. The plant has now expanded to six units which handle 2000 gallons of solution per minute, from underground workings and waste dumps.

During 1948 it was decided to mine the remaining ore by open pit methods. The Isbell Construction Company stripped waste from the Pearl Handle Pit under contract from 1948 to 1952. First ore was mined by open pit methods in 1950. The capacity of the Mill at Hayden was increased to 15,000 tons a day. A new Crushing Plant was built at Ray to handle the pit ore. Ore from the pit was gradually increased and from the underground mine decreased, until February 1, 1955, when underground mining was discontinued.

To increase recovery of non-sulphide copper in the ore, a Leach-Precipitation-Flotation Plant (L-P-F Plant) has been built at Hayden at a cost of over $5,000.000. This involves a special flotation section for recovery of previously rejected pyrite. This is roasted to produce sponge iron and sulphuric acid. The acid is used to leach the ore in the Mill feed and remove the soluble copper which is then precipitated on the sponge iron and recovered by flotation.

During 1956, work was started on an expansion program to increase production capacity to 22,500 tons of ore a day. A new Smelter is being constructed at Hayden to treat the concentrates which have previously been treated by the American Smelting and Refining Company.

Reference: Ransome - U.S.G.S. Professional Paper #115
1919, 1923
Notes from Mr. Leroy Hoyt

Ray

WELCOME

TO

KENNECOTT COPPER CORPORATION

RAY MINES DIVISION,
RAY, ARIZONA.

A. P. MORRIS
General Manager

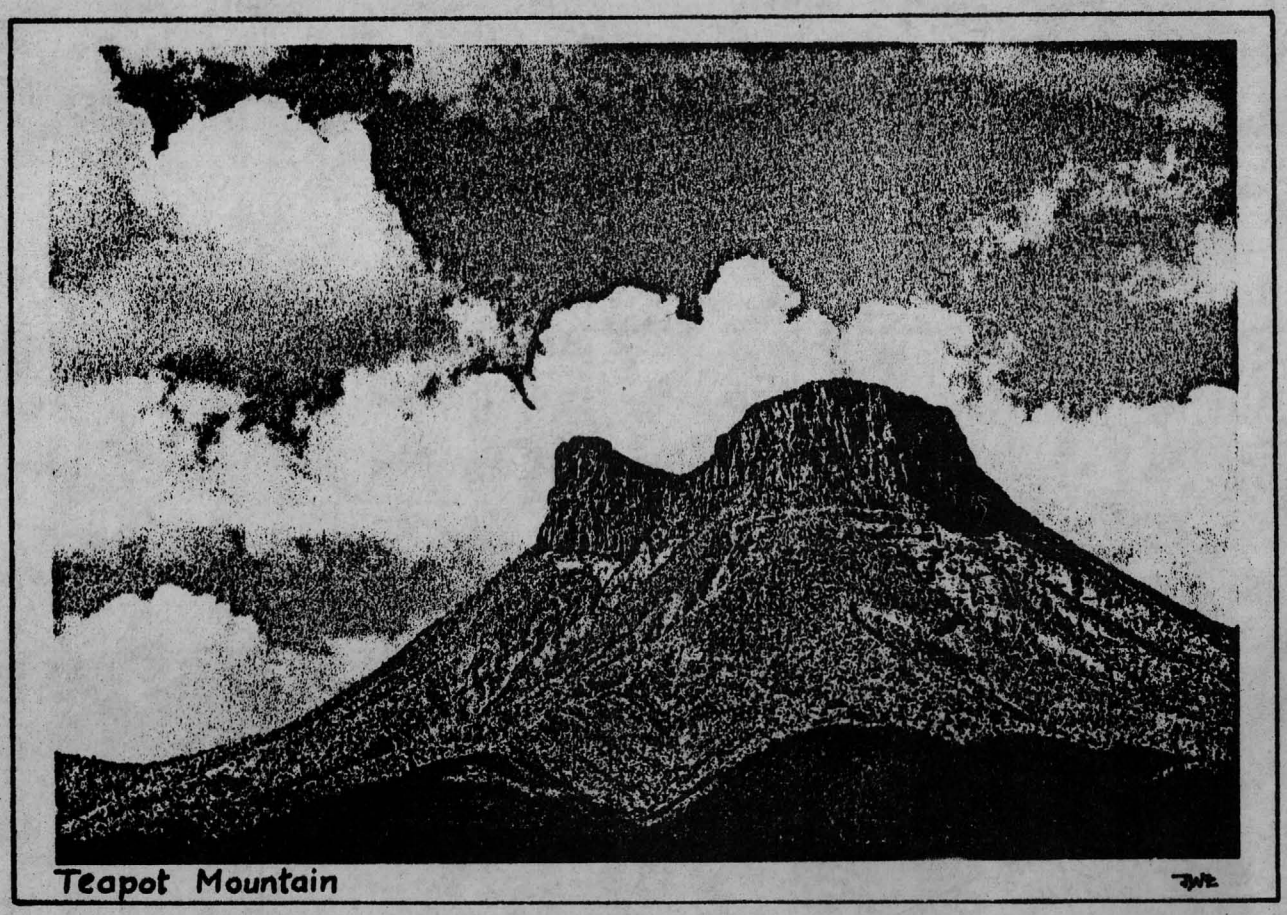

Teapot Mountain

SPRING MEETING

A.I.M.E. — GEOLOGY Division

APRIL 12, 1958

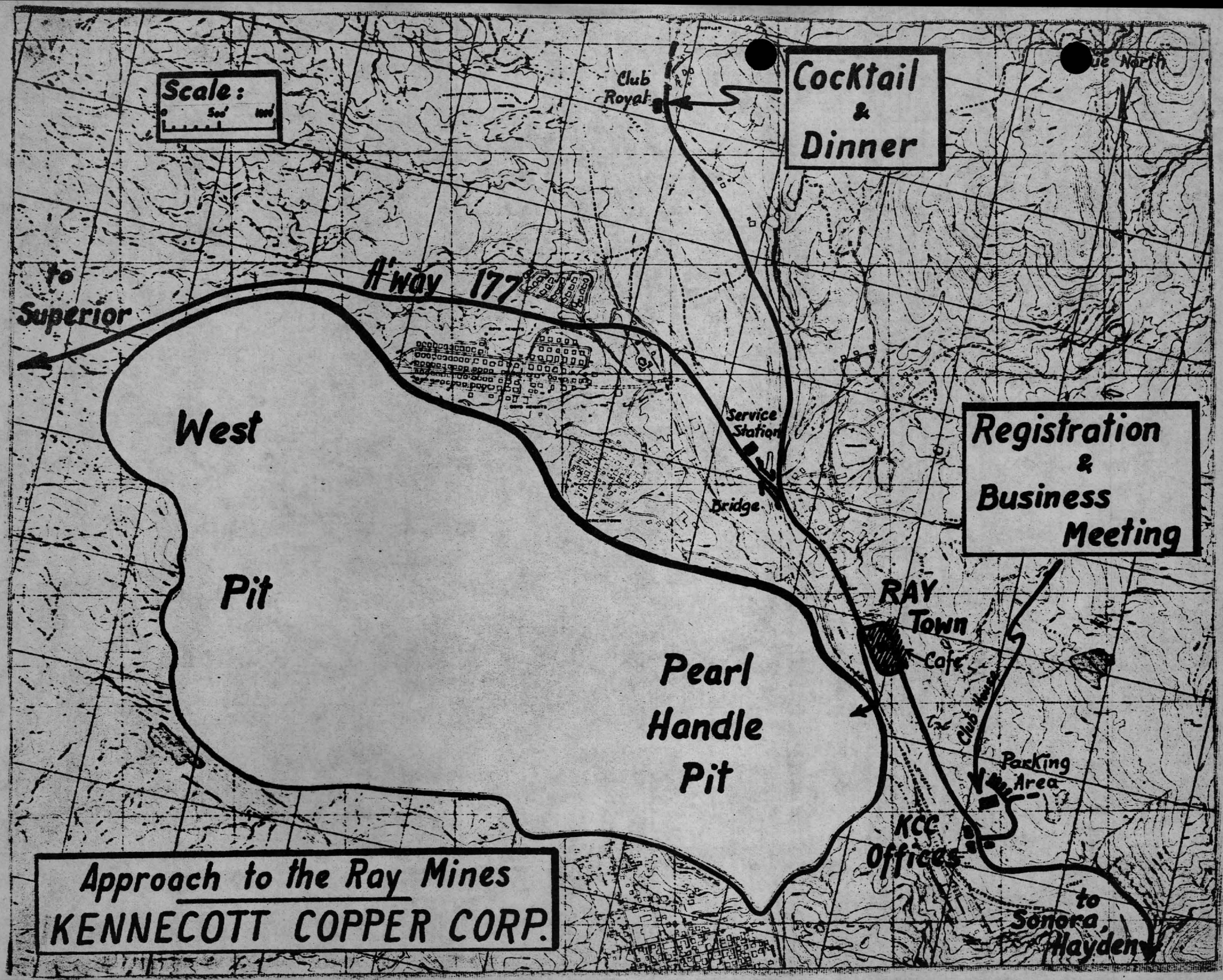
Scale:
0 500' 1000'
Club Royal
Cocktail & Dinner
to Superior
H'way 177
West Pit
Service Station
Bridge
Registration & Business Meeting
RAY Town
Cafe
Pearl Handle Pit
Club House
Parking Area
KCC Offices
to Sonora, Hayden
Approach to the Ray Mines
KENNECOTT COPPER CORP.

Schedule of the Day.

9:00 - 10:00 AM Registration

10:00 - 12:00 AM Business Meeting

1. Welcome Address by Mr. A.P. Morris, General Manager, and Chairman of the Arizona Section A.I.M.E.

2. New Developments on the Geology of the Ray Deposit by Mr. Jacques B. Wertz, Chairman Geology Division.

3. A discussion on adjacent districts will be held next.

12:15 - 1:30 PM Lunch period (at or around the Club House)

It is advised to bring lunches, cokes and coffee being available at the Canteen. (The company will not intervene in the cost of this meal.)

1:30 - 2:00 PM Film (17 min.) at Club House:

"Four-Day Cycle from Ore to Copper"

Club House

2:00 - 3:30 PM Visit of the pit, by van.

(the cars are left parked near the Club House)

3:30 - 4:15 PM Final stop at the bottom of the pit; collecting of samples.

(The vans have left but will be back by 4:15 PM)

4:30 - 4:45 PM Back to the Club House by vans.

Drive to Club Royal by private cars.
(Wash-up period either at Club House or Club Royal)

Pit Tour

5:15 - 6:15 PM Cocktails.

6:15 - on Mexican dinner.

(Choice Mexican dinner or steak)
Dinner and cocktails on the Company.

Club Royal

JDC
RAY

GEOLOGY AND MINERALIZATION OF THE RAY SILICATE OREBODY

by

Neil A. Gambell

Division Geologist

Ray Mines Division

Kennecott Copper Corporation

Presented at the

Arizona Geological Society and the University of Arizona

Porphyry Copper Symposium

Tucson, Arizona

March 18, 1976

and after revision at the

Arizona Conference - AIME

Mining Geology Division Meeting

Ray Mine, Arizona

April 16, 1977

Geology and Mineralization of the Ray Silicate Orebody

Associated with the sulfide deposit is a complex body of silicate copper mineralization. The use of the term silicate, when referring to the orebody, is due to the abundance of chrysocolla; however, the deposit also contains major quantities of copper bearing manganese wad, copper montmorillonite and halloysite, copper-iron oxide complexes, cuprite, malachite, native copper, with lesser amounts of cupriferous allophane, dioptase, azurite, libethenite, torbernite, and chalcocite.

By the early 1960's, drilling had delineated some 93 million tons of potential ore and a program of research and pilot plant studies was initiated with the objective of developing a viable extraction process. Success was realized in 1969 when a vat leaching system, utilizing sulfuric acid from the smelter acid plant, went into production. The most recent estimate of the silicate ore reserve is 156 million tons which averages 0.9 percent copper (total). The portion of this that is readily soluble is not known with certainty but a reasonable estimate would be 55 percent (.50 percent copper). The uncertainty arises from what technique is used to determine readily soluble copper. Ray Mines Division defines readily soluble copper as that portion of the total copper that is dissolved from a minus 100 mesh sample by boiling the sample for one minute in a 10 percent by weight sulfuric acid solution.

Currently we subdivide our mineralization into seven categories. These are primary sulfide, secondary sulfide, native, silicate, mixed native-sulfide, mixed native-silicate and oxide.

Slide 1 - Ore Type Distribution

The slide you see shows, in plan view, the distribution of the primary sulfide ore zone in the diabase, the secondary sulfide ore zone and the silicate ore zone.

The primary ore zone in the diabase is horseshoe shaped. The open end of the horseshoe results from a combination of the following: orebody uplift and tilting 15 to 20° to the southeast, the elimination of the diabase by deep pre-Whitetail (Oligocene) erosion, and the intrusion of a postmineral Teapot Mountain Porphyry stock.

The secondary ore zone (chalcocite) occurs largely in the Pinal Schist. The zone is extended to the west along the Last Turn shear zone. For the most part, it occupies the West Pit, Emperor Hill, and Pearl Handle Pit areas. In the later case, it is largely restricted to the area west of the Diabase Fault which bisects and down-drops the orebody. An interesting thing to note is that approximately half of the chalcocite blanket is located in the pyrite halo west of the underlying primary sulfide orebody. The enrichment blanket here represents at least a ten-fold increase in the hypogene copper grade.

The silicate orebody is subdivided into that which occurs in premineral rocks (horizontal pattern) and that which occurs in postmineral rocks (square pattern). Note that the bulk of the silicate orebody is located in the low-sulfide core area of the system. The Diabase Fault approximates the western boundary of the orebody. With illustration in hand, one can immediately recognize some potention metallurgical nightmares. Specifically, we can see areas where we could penetrate silicate ore, secondary sulfide ore, and primary sulfide ore, encountering several

transition zones characterized by complex mineral assemblages. This picture would be considerably complicated and undoubtedly impossible to illustrate if the oxide, native, mixed native-silicate, and mixed native-sulfide types were included.

Slide 2 - Aerial Oblique (Looking Southeast) of Silicate Orebody

Silicate copper mineralization is found in the Precambrian Pinal Schist, Pioneer Formation, Dripping Spring Quartzite, diabase and to a lesser extent, in the Granite Mountain Porphyry. In postmineral rocks, significant amounts of silicate copper is present in the Whitetail Conglomerate and the Apache Leap Tuff. This slide was taken from above Emperor Hill (foreground) and is directed toward the southeast.

Pronounced silicate ore in the diabase is represented by the blue area (top center) of the pit wall. The light colored areas are lenses of Apache Group quartzite and siltstones. The red area above the diabase is a channel fill deposit of Whitetail Conglomerate. The onlap of the younger Tertiary rocks is illustrated by the white zone which is the basal ash unit of the Apache Leap Tuff. Moving back down below the diabase, the red zone is the trace of the Diabase Fault. The pink zone on the adjacent bench is leached Pinal Schist and the white zone below is the Emperor Fault, which separates the schist from the Apache Group and diabase in the bottom of the Pearl Handle Pit. The offset on the Diabase Fault here is 1600 feet, west side down.

Slide 3 - Aerial Oblique (Looking East) of Silicate Orebody

This slide was taken from above the old town of Sonora (foreground) and shows a closer view of the features discussed in the last slide. Note how the diabase fault essentially terminates the silicate copper mineralization.

Slide 4 - Thickness of Silicate Ore - Premineral Rocks

The contour maps that are presented in the following slides were generated by manipulating the assay data from 137 diamond drill holes. I feel these types of illustrations are basic to understanding where the ore is, why it is there and where some problem areas may be located from a metallurgical standpoint.

This slide shows the thickness of silicate ore in all premineral rocks. The contour interval is 100 feet. A feature that really stands out is the linear zone where the silicate ore is plus 300 feet thick. The protrusion of thin ore corresponds exactly with a Granite Mountain Porphyry intrusive.

Slide 5 - Feet Percent Copper in Premineral Rocks

Here we have a feet percent copper map for premineral rocks. The linear zone observed in the previous slide is enhanced, and we can see that not only is the silicate orebody thick here, but it also contains a lot of copper.

Slide 6 - Feet Percent Copper in Diabase

This feet percent copper map shows the effect of isolating the diabase from the other premineral rocks. Again we see the linear feature observed previously and we now know the orebody is thick in this area, it contains large amounts of copper and a lot of the copper is in the diabase. The dead area between the two high zones is due to intense leaching of the diabase on a pre-Whitetail erosion surface, leaving hematite and minor native copper mineralization.

Slide 7 - Percent RSCu of TCu in Premineral Rocks

This is a plot of percentage of readily soluble copper of the total copper in premineral rocks. The contour interval is 10 percent. This map is the most important

from an operation standpoint because it identifies the potential areas of good and bad recoveries. If we use the 60 percent contour as the minimum for good recovery ore, we see that most of the thick zone of high copper content is included, but we also see some good recovery zones where the orebody is thin and low grade. The embayment of less than 40 percent readily soluble copper are partly due to the location of two Granite Mountain Porphyry masses and the influence of old drilling data. In the year since this paper was originally presented, we have generated a formula which allows upgrading of the old assay data resulting in the expansion of the 60 percent contour.

Slide 8 - Percent RSCu of TCu in Diabase

Again, isolating the diabase, this time relative to the readily soluble copper we see that most of the linear feature is enclosed by the 60 percent contour. Outlining the extent of mineralized diabase, a lot of it can be predicted to yield recovery problems.

Slide 9 - Feet Percent Copper in the Apache Leap Tuff

Moving on to silicate copper in postmineral rocks, this slide illustrates the feet percent copper in the 20 m.y. old Apache Leap Tuff. In the middle portion, we see a sizable zone of the equivalent of a 110 feet of one percent copper. The bow shape is important to note because the axis of a synclinal fold passes through this area (point out). Perhaps this structure played a role in localizing copper concentrations.

Slide 10 - Percent RSCu of TCu in the Apache Leap Tuff

Once again, using 60 percent as the cutoff for acceptable copper recovery in the leaching process, we can recognize a fair sized area of potential. An additional point about this map is that it is the best one to suggest that oxide copper deposits are

zoned because we have precluded the possibility of residual sulfide interference producing the difference between the readily soluble and total copper assays. Not only are they zoned horizontally, as the map shows, they are also zoned vertically.

Slide 11 - Feet Percent Copper in the Whitetail Conglomerate

The final contour map shows the feet percent copper in the 32 m.y. old Whitetail Conglomerate. The slide shows the scattered nature of the mineralization with the smaller areas being isolated to the contact zones with the underlying premineral rocks. The largest area of copper is associated with a paleochannel cut into the basement schist.

The Ray silicate orebody was developed largely in association with a major zone of normal faulting. The Diabase Fault forms the western boundary of the zone. East of the Diabase Fault, there are numerous small, parallel and sympathetic faults. The total displacement across the entire zone is on the order of 1500 to 2000 feet. The northwest trending linear characterized by a great thickness of ore and large amounts of copper in premineral rocks correlates well with this fault system.

The formation of the silicate orebody was an enrichment process. From what we can infer from the hypogene sulfide zoning pattern, it is probable that if the silicate orebody had not formed, we would be looking at 0.2 percent hypogene copper grades or less; therefore, the average grade of the silicate orebody (0.9 percent copper) represents an enrichment factor of at least 4.5.

Copper silicate mineralization formed as replacements of the original sulfide veins, as replacement (or copper soaking) of the wall rock clays, as (in the case of the Whitetail Conglomerate) replacement of reactive rock fragments and matrix, and most importantly as a filling in open fractures and joints.

Slide 12 - Southwest-Northeast Cross Section (Looking Northwest Through the Silicate Orebody

This geologic section, which looks to the northwest, is fairly typical of the silicate orebody and illustrates most of the features I have discussed. All the major pre- and postmineral rocks are represented (explain rock type symbols). The Diabase Fault is located just off the left side of the illustration. The fault shown is seen to be pre-Whitetail in age. The solid black lines on the drill holes represent intercepts of silicate ore. The sawtooth pattern is primary sulfide ore and the open blocks are secondary sulfide ore. Note the thickness of silicate ore in the schist below the pre-Whitetail channel and in the footwall of the fault. On the other sections, the bulk of the ore is in the hanging wall of the fault. The schist is the oldest rock in the area and hence it has been subjected to every ground preparation event since the Precambrian.

Slide 13 - Ore Type Overlay of Geologic Cross Section

This slide is intended to be an overlay to the last slide. It shows just the ore zones and their relationships. In this case, the solid black area is primary sulfide ore with the sulfide content of the rock increasing both to the left and right sides of the illustration. The vertical bar pattern shows the extent of secondary sulfide ore and the unshaded areas are silicate ore. The bulk of the silicate ore located below the channel was formed in a low total sulfide environment by the direct conversion of chalcopyrite to pitch limonite, the conversion of weak chalcocite mineralization to malachite and chrysocolla, and the introduction of copper bearing solutions along zones of high permeability.

At Ray, we have initiated a detailed investigation of the silicate orebody which will probably take years to complete. The goals of the project are: 1) to document the mineralization as it is mined, and 2) to assist in the efficient mining and benefaction of the ore by recognition and characterization of both distinct mineral zones and transition mineral zones.

Drill core observations are being supplemented by detailed pit mapping at a scale of 1" = 200', with representative samples being taken at least every 50 feet or less if a change in lithology occurs.

Some preliminary observations on supergene mineral zoning and paragenesis are as follows:

1. In the area west of the Diabase Fault, formerly characterized by a moderate to high, probably slightly pyritic, sulfide content, the following zones occur: a) hematitic leached capping, b) cuprite, c) chalcotrichite-native copper, d) native copper, e) native copper—chalcocite, f) chalcocite, and g) hypogene pyrite-chalcopyrite.

2. On the fringe of the silicate orebody, formerly moderate to low sulfide content in diabase adjacent to hypogene sulfides, there is extensive development of cupriferous wad on fractures with copper bearing clays in the rock matrix. Quartzitic rocks in this zone show strong iron oxide mineralization on fractures, some of which is copper bearing.

3. Below this zone, chrysocolla and some malachite begins to appear with the cupriferous wad and copper clays.

4. Adjacent to this zone, chrysocolla becomes more abundant, with cupriferous wad and copper bearing clays still present.

5. In diabase, the above zone begins to pick up cuprite with depth and finally cuprite and native copper prevail. In the siliceous rocks, the chrysocolla zone yields to a malachite-chalcocite zone.

6. In the larger vein structures, the following assemblages can be seen from the inside out: chacocite, cuprite, malachite, black and blue chrysocolla. If the vein was largely chalcopyrite, you see pitch linonite which is being replaced by chrysocolla.

7. In some cases, malachite and azurite seem to be the direct result of sulfide destruction and the common occurrence of malachite being replaced by chrysocolla in some of the larger veins suggests that the bulk of our copper silicate orebody may have once been a copper carbonate orebody.

Slide 14 - Pit Wall in Silicate Orebody (Looking East)

The following slide series will illustrate some of the above points.

This is a view of the silicate orebody as it is currently exposed in the pit wall. Immediately below the natural topography at the top, we can see three or four dark gray bench faces. This area represents the upper and outer zone of cupriferous wad and copper clay mineralization in the diabase. The blue-gray zone below is the strong chrysocolla zone.

Slide 15 - Clope-Up of Cupriferous Wad Zone

This is a close-up of the cupriferous wad-copper clay zone. The upper benches are recent gravelly deposits with a manganese rich layer at the bedrock contact.

Slide 16 - 2460 Level Close-Up

Going deeper or inward, we can see chrysocolla and malachite beginning to show up.

Slide 17 - Chrysocolla Zone in Diabase

Here we see a contact between a diabase sill and the Pioneer Formation. Strong chrysocolla has been developed in the diabase. The reasons for this are the fact that the hypogene copper mineralization preferred the mafic diabase, the reactive nature of the rock undoubtedly affected the pH of the supergene copper solutions, and the diabase contains abundant clay which soaked up the copper. Lastly, note the closely spaced sheeting at the top of the diabase. Many of these low angle fractures show evidence of movement. In any period of post diabase structural readjustment, movement occurred in the weaker diabase which is conducive to the all important ground preparation phenomena.

Slide 18 - Close-Up of Diabase Silicate Ore

This close-up illustrates the nature of the good chrysocolla zone in the diabase. Note the abundant veins and fractures. A close-up of the adjacent gray wall rock areas would show copper soaked clays after the feldspars.

Slide 19 - 1980 Bench

This view of the pit wall shows the influence of the diabase on the mineralization. In this particular area, we see a reddish tint along the top of the sill below the strong chrysocolla at the contact. The red color is the result of cuprite, chalcotrichite, and native copper. I will use the bench face in front of the haulage truck to illustrate the complex mineralization that can be encountered during mining operations.. Although the contacts aren't clearly visible in the slide, the following rock types are present from right to left; Dripping Springs Quartzite with its basal Barnes Conglomerate member,

the Pioneer Formation and the diabase. The Dripping Springs contains disseminated chalcocite with malachite, minor cupriferous wad, and chrysocolla on the fractures. The sulfide gradually disappears, resulting in a dioptase, chrysocolla, malachite assemblage just above the Barnes. The Barnes contains malachite with some cupriferous wad and chrysocolla. The upper Pioneer contains malachite and cupriferous wad which yields to a cuprite, chrysocolla, malachite, and native copper zone near the diabase contact. The diabase contains cuprite, copper clay, native copper, and chrysocolla. This boils down to a sulfide-silicate zone, a silicate zone, and a native-silicate zone occurring along this 1000 feet of bench face.

Slide 20 - Close-Up of Cuprite Zone

This slide is a close-up of the cuprite-native copper zone along the upper portion of the diabase sill.

Slide 21 - Whitetail Conglomerate - Granite Mountain Porphyry Contact

The next series of slides will show the nature of copper silicate mineralization in the postmineral rocks. The first slide shows the spotty nature of some of the ore along the contact zone. Here, the Whitetail Conglomerate onlaps the Granite Mountain Porphyry.

Slide 22 - Silicate Copper Mineralization in the Whitetail Conglomerate

Here we see more extensive silicate copper mineralization along selected beds near the base of the Whitetail Conglomerate.

Slide 23 - Close-Up of Silicate Ore in the Whitetail Conglomerate

This close-up view of a boulder of Whitetail ore shows the preferential replacement of limestone cobbles.

Slide 24 - Apache Leap Tuff with Copper Silicate Copper Mineralization

This slide shows the contact between the diabase and the Apache Leap Tuff on the 2020 level. The dark zone in the tuff above the basal ash unit is the result of cupriferous wad with some chrysocolla coating the fracture surfaces. The clay minerals in the tuff matrix also contain copper. The intense fracturing in the tuff here is the result of its proximity to a postmineral reverse fault which produced the syn linal fold noted earlier. Minor amounts of silicate copper mineralization also occur in the 17 million year old Big Dome Formation and as noted by Phillips, Cornwall, and Rubin (1971); a small deposit of exotic copper mineralization was found in recent stream gravels which contained a fossil log dated at 7.35 thousand years.

The non-copper bearing minerals in the deposit that may give some clues to its origin are: 1) calcite in the Whitetail Conglomerate, especially near its base and in the diabase where it is apparently of hypogene origin and was stable during the development surrounding and intergrowing cuprite and native copper mineralization, and 2) minor megascopic opal with chrysocolla in the Whitetail Conglomerate. On the microscopic level, opal may be abundant in the orebody. 3) Both early and late occurrences of selenite. Some specimens of malachite appear to be pseudomorphs after selenite as do some specimens of chrysocolla. 4) Extensive development of clinoptilolite and huelandite mineralization, most of which postdates the formation of chrysocolla but predates most, if not all, libethenite. 5) Small rosettes of barite have been found growing on some native copper and malachite specimens.

Metz and Rose, 1964, suggest that hot springs activity may have aided in the formation of the silicate orebody.

In the Inspiration Mine area, Throop and Buseck, 1971, suggest that silica may have been released during the alteration of the volcanic glass to heulandite. At Ray, zeolites coat fractures and much of the chrysocolla in all the rock types.

At this state of the research, I offer no speculations on the silica source. However, I will re-emphasize a point made earlier - I feel that in its initial stages, the Ray silicate deposit was characterized by strong copper carbonate mineralization.

Slide 25 - View (Looking East) of the Silicate Ore Leaching Plant

Some vital statistics on the silicate ore processing plant you see here are as follows:

1. 10,000 tons of $-\frac{1}{2}$ inch ore per day to leach vats.

2. Sulfuric acid concentration in vats is maintained at 35 grams per liter.

3. Plant life acid consumption has averaged 100 pounds per ton of ore.

4. Currently, plant recoveries are 60 to 65 percent of the total copper. Plant recoveries have varied from 45 to 75 percent of the total copper.

5. The solution to electrowinning contains 20 to 35 grams per liter copper.

6. 4,000 tons of -10 mesh silicate ore per day to new agitation leaching plant with production being achieved by the precipitation method.

7. At current operating rates, the combined output of both sections will be 28,000 tons of copper per year.

Rock related factors that affect copper recovery in the leaching process are: 1) the mineralogy of the ore minerals. Malachite, chrysocolla, cuprite, azurite, cupriferous wad and copper bearing halloysite leach well. Copper bearing montmorillonite,

as noted by Metz and Stephens, 1967, and some copper iron-oxide complexes leach poorly. The copper bearing phosphates, libethenite, and torbernite don't leach at all. 2) The mineralogy of the gangue minerals. Calcite and biotite are two abundant types that can consume or neutralize sulfuric acid. 3) Rock type. The Apache Leap Tuff slimes rapidly in the acid environment as does the diabase only to a lesser extent. The siliceous rocks retain their competency, allowing better solution circulation and access. 4) How the mineralization occurs in the rock. In the quartzites, most of the mineralization occurs on fractures and in veins which become well exposed in the crushing process. In the diabase and the Apache Leap Tuff, a lot of the copper is disseminated throughout the rock in the clay sites requiring diffusion of the leach solution.

REFERENCES

1. Metz, R. A., and Rose, A. W., 1966. Geology of the Ray copper deposit, Ray, Arizona, in Titley, S. R., and Hicks, C. L., eds., Geology of the porphyry copper deposits, southwestern North America: Tucson, University of Arizona Press, p. 177-188.

2. Phillips, C. H., Cornwall, H. R., and Rubin Meyer, 1971, A Holocene ore body of copper oxides and carbonates at Ray, Arizona: Econ. Geology, v. 66, p. 495-498.

3. Stephens, J. D., and Metz., R. A., 1967, The occurrence of copper-bearing clay minerals in oxidized portions of the disseminated copper deposit at Ray, Arizona: oral presentation at the 1967 meeting of the Geological Society of America.

4. Throop, A. H., and Buseck, P. R., 1971, Nature and origin of black chrysocolla at the Inspiration Mine, Arizona: Econ. Geology, v. 66, p. 1166-1175.

Page 4 of original

missing.

+DL
JEK

A REVIEW OF THE RAY OREBODY

by

Neil A. Gambell

Division Geologist

Ray Mines Division

Kennecott Copper Corporation

Presented at the

Arizona Conference - AIME

Mining Geology Division Meeting

Ray Mine, Arizona

April 16, 1977

A REVIEW OF THE RAY OREBODY

INTRODUCTION

The Ray Mine is owned and operated by Kennecott Copper Corporation and is located in eastern Pinal County, Arizona, seventy miles southeast of Phoenix. The deposit has been a major copper source since 1911, producing an estimated 2.7 million tons of copper. The bulk of the production has been derived from sulfide ores. Mining was accomplished by underground techniques until 1955 when full conversion to open pit methods was achieved.

Currently we are mining 30,000 tons of sulfide ore and 14,000 tons of silicate ore on a five-day per week basis. The sulfide ore is crushed to minus 10 inches at the mine and shipped by rail some 18 miles to the concentrator and smelter works at Hayden. The silicate ore is processed entirely at the mine via a percolation/agitation leaching system with the final product being electrowon cathode copper.

LITHOLOGIES

The first slide shows the lithologic units which are important in the Ray deposit. The oldest rock is the Pinal Schist which is composed of quartz-sericite and quartz-chlorite-epidote metasediments, as well as some metavolcanic units. A metarhyolite unit in the schist has been dated at 1660 m.y. (Livingston and Damon, 1968). The Ruin or Oracle Granite, which is compositionally a quartz monzonite, intrudes the schist and has been dated in the Winkelman area at 1420 m.y. (Livingston and Damon, 1968). Following a long period of erosion, the younger Precambrian

quartzose sediments of the Apache Group were deposited.

The Pioneer Formation is approximately 230 feet thick and consists of interbedded arkose and tuffaceous siltstones with a basal conglomerate (Scanlan Conglomerate member). Above the Pioneer Formation, there is typically 40 feet of basal Dripping Spring (Barnes Conglomerate). Above this we have approximately 250 feet of the lower arkose-quartzite member of the Dripping Spring. Although the upper Dripping Spring, the Mescal Limestone and the Troy Quartzite are present east of the mine, they are not important from the standpoint of copper mineralization.

Extensive diabase intrusions, mostly as sills, occurred 1150 m.y. ago (Livingstone and Damon, 1968). The preore mineralogy of the diabase is variable; however, the bulk of it appears to have been a hornblende-pyroxene labradorite diabase with minor quartz, biotite orthoclase, magnetite, and apatite. At Ray, this diabase is an important host rock. In the mine area there are two sills which average about 500 feet in thickness. The sills prefer certain stratigraphic horizons which are: (1) the Pinal Schist-Ruin Granite about 300 feet below the Apache Group, (2) the middle of the Pioneer Formation, and (3) between the lower arkose and upper siltstone members of the Dripping Spring Quartzite. Going north through the mine, the sill in the Pioneer migrates downward into the schist and granite. Likewise, the upper sill in the Dripping Spring Quartzite migrates downward into the Pioneer Formation. Economic hypogene copper mineralization is not found in Precambrian rocks above the upper diabase sill in the Dripping Spring Quartzite.

Referring to the left side of the first slide, we have four Laramide intrusives which warrant description. The Tortilla Quartz Diorite (Sonora Diorite) dated at approximately 70 m.y. (Banks and others, 1973) is largely restricted to the south and

and west sides of the deposit, while the main mass of diorite porphyry is found on the east side of the deposit. Depending upon their location within the sulfide system, both of the rocks can contain significant amounts of ore grade (at least 0.40% copper) hypogene copper mineralization. Within the Ray deposit, neither the Tortilla Quartz Diorite nor the diorite porphyry has been found intruding any lithologies above the diabase sill in the Pioneer Formation.

The Granite Mountain Porphyry has been dated at 60 m.y. (see Banks and others, 1972-1973, Livingston and others, 1968, and McDowell, 1971) and has been long thought to be the causative intrusive at Ray. The rock is in reality a porphyritic granodiorite composed of oligoclase, quartz, biotite-magnetite, and orthoclase phenocrysts with an orthoclase matrix (Cornwall and others, 1971). At the present surface, the main mass of Granite Mountain Porphyry is west of Ray in the Granite Mountain area where it is at least two miles in diameter and appears to have intruded near a northeast trending Pinal Schist/Ruin Granite contact. In the mine, there are several small masses of Granite Mountain Porphyry which are aligned in a N70^{o}E direction along a zone of weakness referred to as the "porphyry break" (Metz and Rose, 1966). Diamond drilling indicates that some of these masses may coalesce at depth to form a stock central to the hypogene ore mineralization.

The Teapot Mountain Porphyry is slightly younger than the Granite Mountain Porphyry and intrudes as stocks and dikes along a northeast trend north of Ray. The Teapot is characterized by large euhedral orthoclase and quartz phenocrysts. The Calumet Breccia Pipe may be associated with one of the Teapot

The Big Dome Formation was named for exposures south of the mine (Krieger and others, 1974). A biotite tuff within the Big Dome has been dated discordantly at 14 and 17 m.y. (Cornwall and others, 1971). In the deposit area, the Big Dome can be subdivided into a schist-porphyry facies and a coarser grained, gray mixed limestone-Apache Group facies.

The youngest rock unit at Ray is a water lain rhyolite tuff. This light pink to brown tuff appears to interfinger with the Big Dome in places and may closely resemble it in age.

Secondary copper mineralization can be found in any of the lithologies shown on the first figure with the exception of the Ruin Granite.

The second slide gives a general feeling for the distribution of the major rock units. The western part of the figure is predominately Pinal Schist, while the eastern portion is mixed diabase and undifferentiated Apache Group. Note the masses of Granite Mountain Porphyry and the onlap of the postmineral volcanics and sediments.

Hypogene Sulfide Zoning

The next slide illustrates the hypogene sulfide zoning. A high sulfide-low copper pyrite halo surrounds an ore zone of moderate sulfides with approximately equal amounts of pyrite and chalcopyrite. Inside the ore zone, there is a low sulfide-high chalcopyrite zone. The pyrite halo is elongate in an east-west direction and measures approximately 14,000 by 10,000 feet. The hypogene ore shell trends northwest and is about 6,000 feet wide and 8,000 feet long. Chalcopyrite is the dominant copper mineral.

Ore Type Distribution and Reserves

The fourth slide shows the distribution of the various ore types at Ray. Of interest is the location of the secondary chalcocite zone to the west of and above the western branch of the hypogene ore zone. Most of the chalcocite occurs in the Pinal Schist which, if you recall the second slide, is the dominant rock type in this area. The location of the chalcocite orebody if affected by structure. The hypogene orebody is horseshoe shaped with the open end being the result of the combined effects of postmineral faulting, intrusion, and erosion. The diabase fault bisects the hypogene ore zone.

The silicate/oxide orebody was developed in the low total sulfide-high chalcopyrite core zone.

The total reserve of all ore types is greater than 650-million tons, with an average grade of about 0.80 percent copper.

Hypogene Mineralization and Alteration

To discuss the hypogene alteration and copper-molybdenum distribution, it is convenient to divide the lithologies into quartzose Precambrian rocks/Granite Mountain Porphyry and diabase. Because of today's time constraints, I will give only the highlight features of the first group.

This slide shows a detailed copper distribution map for the quartzose Precambrian rocks. Only small areas of plus 0.4 percent copper are present with the best one being located on the east side and associated with Pinal Schist/Ruin Granite contact which may have acted as a barrier to the mineralizing solutions (Metz and Rose, 1966). Similarly, there is little ore grade copper mineralization in the Granite Mountain Porphyry. Unfortunately, molybdenite favors these rocks.

In the siliceous Precambrian rocks and the porphyry, the hypogene alteration pattern from the inside out is biotite-K-feldspar, quartz-sericite, and epidote-chlorite.

The remainder of this talk will be devoted to the most important host rock, the diabase (Metz and others, 1968, Metz and Rose, 1966, Phillips and others, 1974).

Looking at the hypogene copper distribution in the diabase, we note large areas of plus 0.4% copper as well as five distinct areas of plus 0.8% copper. Comparing this figure with the previous slide demonstrates the affinity of copper for the diabase. Approximately 85 percent of the Ray ore reserve is in the diabase.

In the next two slides we will look at the copper distribution in diamond drill holes along a-a' and b-b'. The diabase in this area intrudes the Pinal Schist and splits into two branches on the west side of the section. Along section a-a', the higher copper grade follows the top of the sill and plunges abruptly between holes 4 and 5. Note the lower copper grades in the schist. Along b-b', the zone of maximum copper concentration migrates uniformily down the sill from hole 8 through holes 9 and 10. The presence of the reactive diabase sill tends to broaden and flatten the top of the ore shell.

Using the six drill holes along section a-a', we can look at the variation in four significant parameters across the ore zone. The first graph is a plot of the percent copper encountered in the diabase in each drill hole (dotted line). You will recall that in holes 1 and 2 there is a small lens of schist in the diabase. The solid lines "a" and "b" represent the copper grades of the upper and lower sections of diabase while the "c" line shows the copper grade of the schist. Note the total copper

in the schist is lower than that in the diabase.

The second graph shows how the sulfide content varies. Here again the slashed line is the average for the diabase. Points "a" and "b" represent the upper and lower diabase sections respectively and "c" represents the schist lens and the average of the two diabases. Unfortunately, hole 2 is an old hole and samples couldn't be located for analysis, hence the question mark. Observe (1) the sulfide content of the schist and diabase are the same, and (2) the appearance of the high sulfide (7 wt. percent) pyrite zone in holes 5 and 6.

The third graph demonstrates the change in the chalcopyrite/pyrite ratio across section a-a'. Points "a" and "b" are the diabase and point "c" is the schist. From the previous slide, we know that hole one is close to the low sulfide core zone, yet this slide shows the schist lens to be pyritic, illustrating once again the affinity of the diabase for copper. The pyrite halo is also illustrated by the chalcopyrite content of holes 5 and 6.

The final graph shows the magnetite distribution in the drill holes. Points "a" and "b" are diabase and "c" is schist. The general shape of the graphs is similar to the copper distribution graph. The most magnetite is accompanied by the best copper mineralization.

Biotite is one of the most common alteration products in the diabase. It occurs as a fine-grained mesh in vein envelopes and as thin rims surrounding disseminated magnetite and sulfide grains in the wall rock. Biotite envelopes are easily distinguished from the less altered wall rock. The width of the vein envelopes is directly related to the size and frequency of occurrence of the quartz-sulfide veins.

In a well-mineralized area with strong stockwork veining, the wall rock may be totally altered for tens of feet. Coarse-grained (2.5 mm) secondary biotite is encountered in some quartz-sulfide veins and is most common in the low sulfide-high chalcopyrite core of the deposit.

Two distinct color varieties of secondary biotite are present - brown and olive-green. A small number of observations have shown that the olive-green variety becomes more abundant outward from the high copper zone. The difference in color may be due to variation of the titanium content of the biotite.

Within the vein envelopes, most of the secondary biotite is an alteration product of pyroxene and hornblende. The biotitization in vein envelopes is accompanied by alteration of the plagioclase to an orange-brown clay. Secondary biotite may be present along the twin planes in the plagioclase.

Secondary biotite in vein envelopes has a widespread lateral distribution in the lower diabase sill. It is present in the low sulfide-high chalcopyrite core outward through the high copper zone, where strong biotite alteration correlates with high copper values.

Secondary magnetite is found in the wall rock and vein envelopes as disseminated anhedral blebs and subhedral, needle-like crystals. Both forms commonly are enclosed by an inner envelope of sphene and an outer envelope of biotite or chlorite. Secondary magnetite also occurs in veins with quartz and sulfides. Chalcopyrite and pyrite veins appear to cut most magnetite veins.

Secondary sphene and rutile are present in the altered diabase, and they exhibit a zonal relationship with rutile closer to the veins than sphene. Light gray to white sphene envelops some anhedral magnetite grains in the wall rock. In most

cases the sphene is itself enveloped in secondary biotite or chlorite and may show some alteration to calcite. Bright orange, crystalline aggregates of alteration rutile are usually restricted to the vein envelopes associated with strong biotite alteration.

Both early and late barren quartz veins are present in the diabase. Mineralized quartz veins are abundant in the low sulfide-high chalcopyrite core outward through the high copper zone. In the pyrite halo, vein quartz decreases markedly. Fine anhedral quartz is present in many vein envelopes with biotite and clay.

The chief alteration product of the plogioclase in the diabase is a light orange-brown clay mineral. This alteration is most intense in vein envelopes and accompanies strong biotite alteration of the mafic minerals.

Secondary K-feldspar is a rare alteration product in the Ray diabase. Also, hypogene sericite in the diabase is not abundant. In the high sulfide-high pyrite zone, sericite and clay minerals are present as partial replacements of plagioclase in the vein envelopes. Late stage sphalerite-galena veins frequently have sericitic envelopes. Where these veins cut earlier quartz-sulfide veins with biotite envelopes, the biotite is altered to sericite.

Like biotite, chlorite may envelop disseminated sulfide and magnetite grains in the wall rock. Primary hornblende is partially to completely altered to chlorite-biotite. Chlorite in vein envelopes seems to be related to the introduction of late calcite in the vein. Such veins frequently exhibit an inner chlorite and an outer

biotite envelope. The frequency of chlorite occurrence in the diabase increases outward from the center of the sulfide system.

Though occasional epidote occurs in quartz-sulfide veins throughout the high copper zone, epidote is most abundant in the pyrite halo where it occurs in pyrite veins and more extensively in the vein envelope as an alteration product of plagioclase. Epidote rimming and veining a clay product in a plagioclase site suggests that the epidote is a late alteration.

Milky-white calcite occurs near the center of veins as a filling with microveinlets cutting the sulfide grains. In some cases calcite floods the vein envelopes and replaces earlier formed clay minerals. Although it appears to be largely a late mineral, calcite is most abundant in veins in the high copper zone and shows a tendency to decrease, both inward and outward, from this zone. Calcite crystallization or deposition may have been favorably influenced by the calcic nature of the plagioclase (labradorite) in the unaltered diabase.

Coarsely crystalline, light purple anyhydrite is present as a major constituent of some quartz-sulfide veins. The abundance of anhydrite increases with depth, and, for some unknown reason, the greatest concentration of purple anhydrite occurs in the high copper zone on the southwestern side of the orebody west of the Diabase Fault.

Minor quantities of orange to white crystalline chabazite occur in some quartz-sulfide veins in the ore zone and outward through the pyrite halo. Chabazite appears to be a late vein filling.

Much of the pyroxene in the diabase shows partial to complete alteration to fine-grained amphibole. The author believes that at least part of the uralitization in the diabase is the result of hydrothermal alteration. This is compatible with the tendency to form hydrous silicate alteration products, and petrographic studies indicate decreasing uralitization and increasing pyroxene with increasing distance outward from the orebody.

SUMMARY

The Ray orebody was developed in older and younger Precambrian rocks. Stratigraphically, the highest unit of the Apache Group affected by the hypogene ore solutions appears to be the arkose member of the Dripping Spring Quartzite. The deposit is thought to be genetically related to the 60 to 61 million year old Granite Mountain Porphyry. Secondary copper mineralization is found in the Precambrian rocks (excluding the Ruin Granite), the Laramide intrusives, and the Tertiary conglomerate and volcanic units.

Supergene chalcocite mineralization formed above and lateral to the hypogene copper orebody, largely in the pyrite halo. The bulk of the silicate/oxide orebody formed in a low total sulfide-high chalcopyrite environment.

The deposit exhibits a typical hypogene sulfide zoning pattern with an outer high sulfide-low copper pyrite halo, an ore zone of moderate sulfide content characterized by approximately equal amounts of chalcopyrite and pyrite, and an inner low sulfide-high copper zone which is chalcopyritic in the diabase and, in places, pyritic in the quartzose rocks.

The bulk of the ore grade (at least 0.40% copper) mineralization occurs in the semi-reactive, mafic, Precambrian diabase host rock. Molybdenite mineralization favored the quartzose lithologies.

In the siliceous Precambrian rocks and the Granite Mountain Porphyry, the hypogene alteration zones from the inside out are (1) biotote-K-feldspar, (2) quartz-sericite, and (3) epidote-clorite.

In the diabase, biotite-clay alternation predominates in both the core and ore zones. Chlorite and epidote increase outward into the pyrite halo. There is no extensive development of hypogene sericite or K-feldspar in the diabase.

In all rock types, the frequency of quartz veins decreases outward from the center of the deposit.

REFERENCES

1. Banks, N. G., Cornwall, H. R., Silberman, M. L., Creasey, S. C., and Marvin, R. F., 1972, Chronology of intrusion and ore deposition at Ray, Arizona -- Part I, K-Ar ages: Econ. Geology, v. 67, p. 864-878.

2. Banks, N. G., and Stuckless, J. S., 1973, Chronology of intrusion and ore deposition at Ray, Arizona -- Part II, Fission-track ages: Econ. Geology, v. 68, p. 657-664.

3. Cornwall, H. R., Banks, N. G., and Phillips, C. H., 1971, Geologic map of the Sonora quadrangle Pinal and Gila counties, Arizona: U. S. Geol. Survey Quad Map GQ-1021.

4. Creasey, S. C., and Kistler, R. W., 1962, Age of some copper-bearing porphyries and other igneous rocks in southeastern Arizona, in Geol. Sur. Research 1962: U. S. Geol. Survey Prof. Paper 450-D, p. D1-D5.

5. Krieger, M. H., Cornwall, H. R., and Bank, N. G., 1974, Big Dome Formation and revised Tertiary stratigraphy in the Ray-San Manuel area, Arizona, in U. S. Geol. Survey Bulletin 1394-A, Changes in stratigraphic nomenclature by the U. S. Geological Survey, 1972 by Cohee, G. V., and Wright, W. B., p. A54-A62.

6. Livingston, D. E., and Damon, P. E., 1968, The ages of stratified Precambrian rock sequences in central Arizona and northern Sonora: Canadian Journal of Earth Sciences, Vol. 5., p. 763-772.

7. Livingston, D. E., Mauger, R. L., and Damon, P. E., 1968, Geochronology of the emplacement, enrichment, and preservation of Arizona porphyry copper deposits: Econ. Geology, v. 63, p. 30-36.

8. McDowell, F. W., 1971, K-Ar ages of igneous rocks from the western United States: Isochron/West, No. 2, p. 1-17.

9. Metz, R. A., and Rose, A. W., 1966. Geology of the Ray copper deposit Ray, Arizona, in Titley, S. R., and Hicks, C. L., eds., Geology of the porphyry copper deposits, southwestern North America: Tucson, University of Arizona Press, p. 177-188.

10. Phillips, C. H., Gambell, N. A., and Fountain, D. S., 1974, Hydrothermal alteration, mineralization, and zoning in the Ray Deposit: Econ. Geology, v. 69, p. 1237-1250.

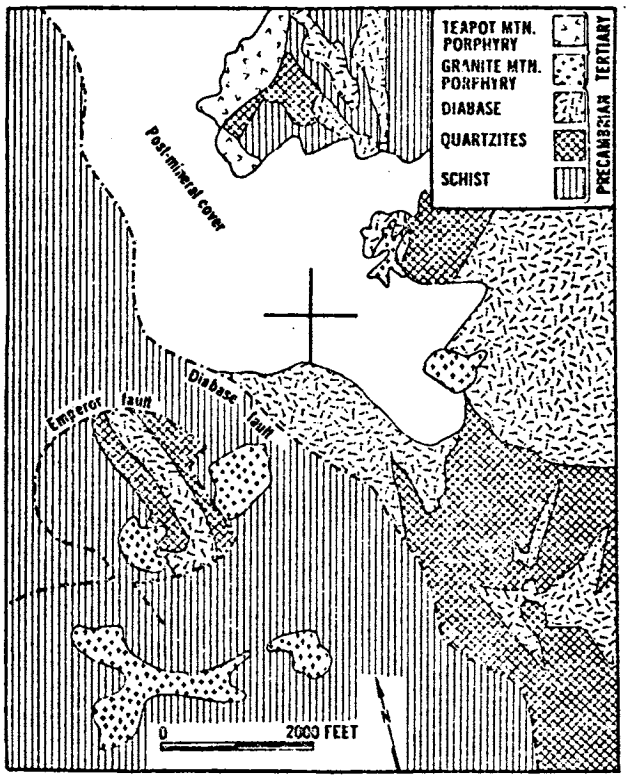

FIG. 2. Generalized geologic map of the Ray copper deposit. The cross on the figure is a reference point enabling the reader to correlate Figures 2, 3, 4, and 6A.

Slide 2

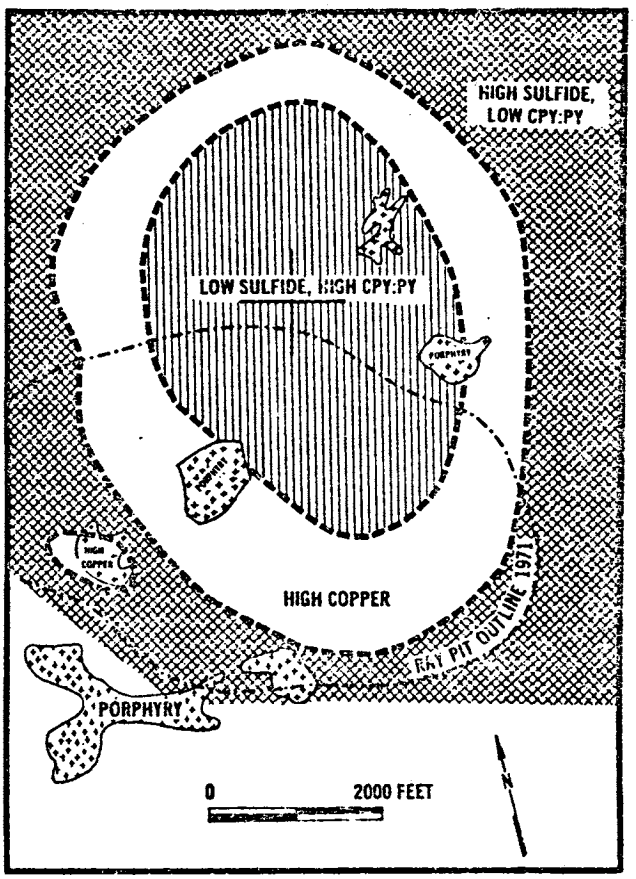

FIG. 3. Generalized zoning of hypogene sulfides in the Ray deposit. The porphyry shown is the Granite Mountain Porphyry.

Slide 3

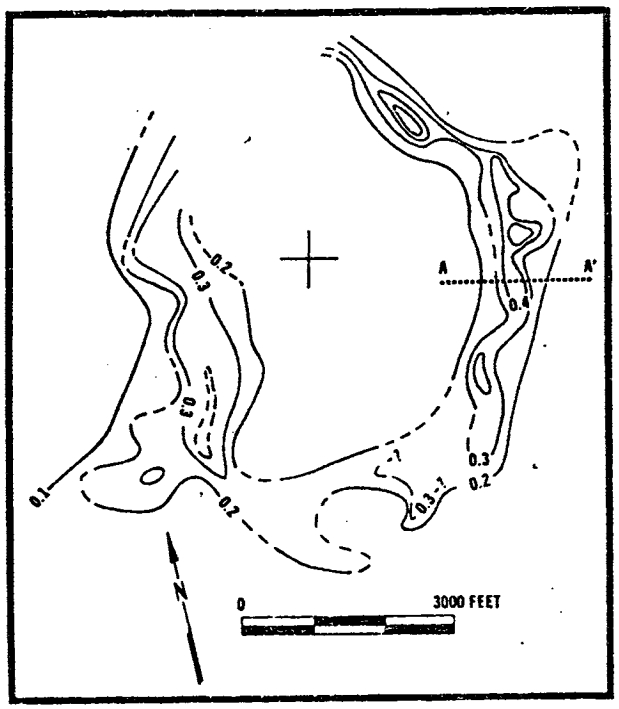

FIG. 4. Contoured copper distribution in the quartzose Precambrian rocks at Ray. Contour interval is 0.1 percent copper.

Slide 5

Slide 4

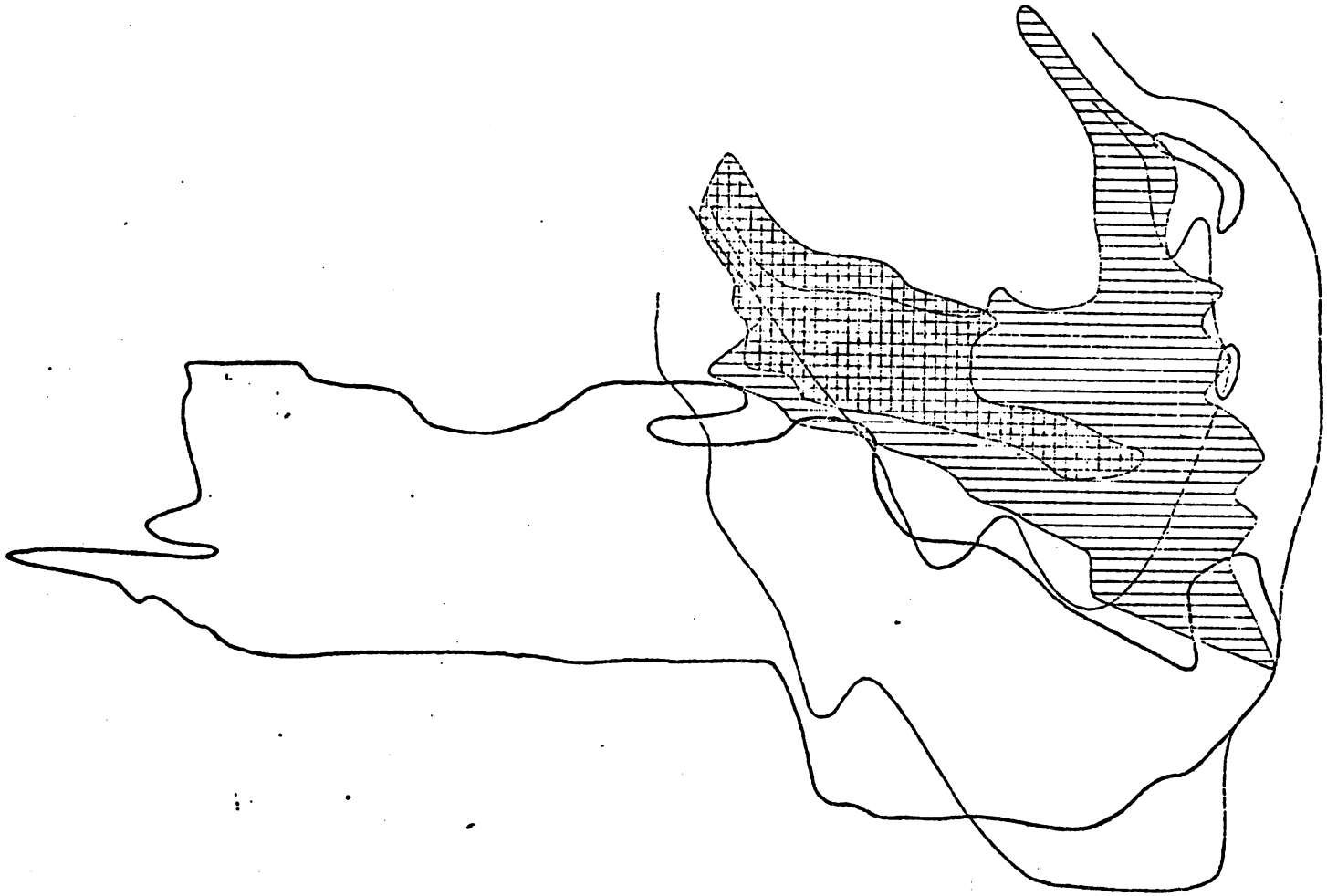

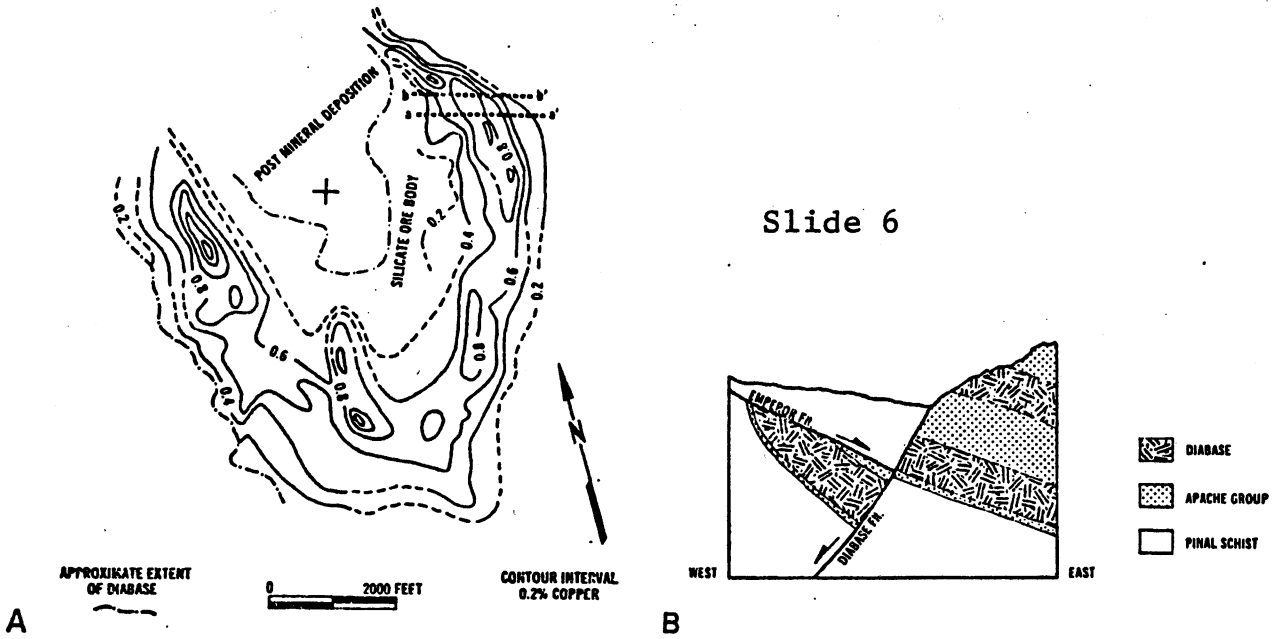

FIG. 6A. Plan view of the hypogene copper distribution in the lower diabase sill at Ray, Arizona. The contours indicate the average grade for the entire thickness of the lower sill at a given point without reference and elevation.

FIG. 6B. Generalized cross section (not to scale) illustrating the extent of the lower diabase sill beneath the Emperor Fault.

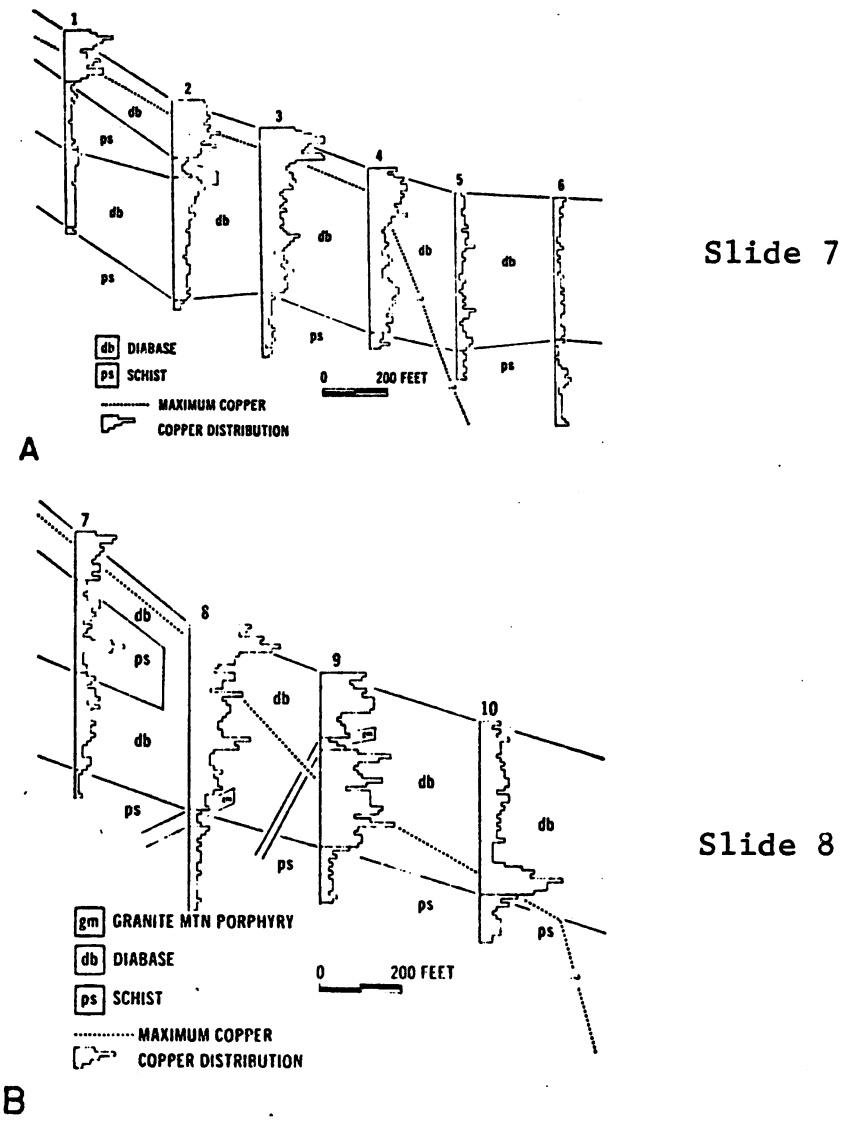

FIG. 7A. Hypogene copper distribution in drill holes along section a-a' (Fig. 6A). Note the high copper concentration at the top of the sill.

FIG. 7B. Hypogene copper distribution in drill holes along section b-b' (Fig. 6A). Note the high copper concentration in the lower part of the sill in holes 9 and 10.

Slide 9

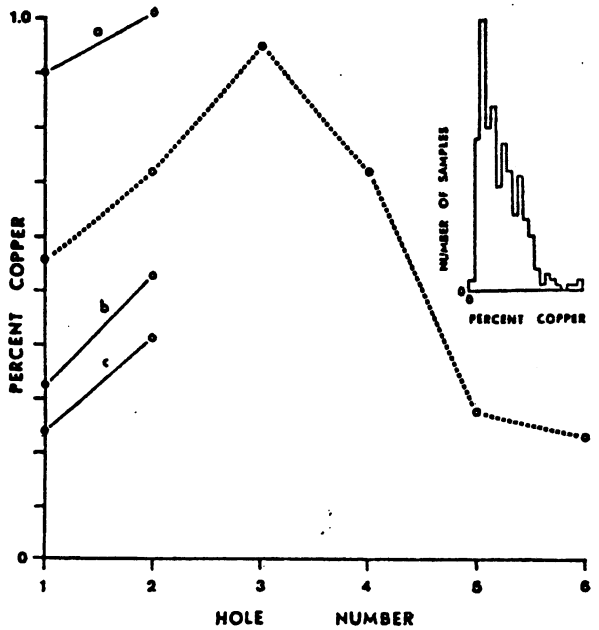

A

Slide 10

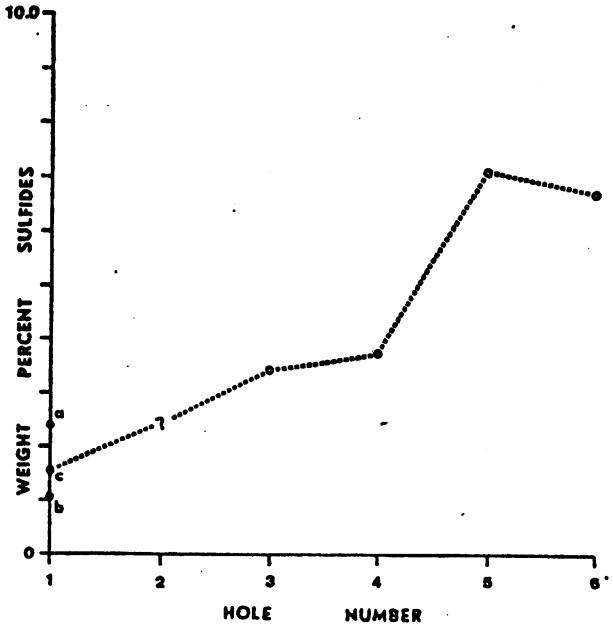

B

Slide 11

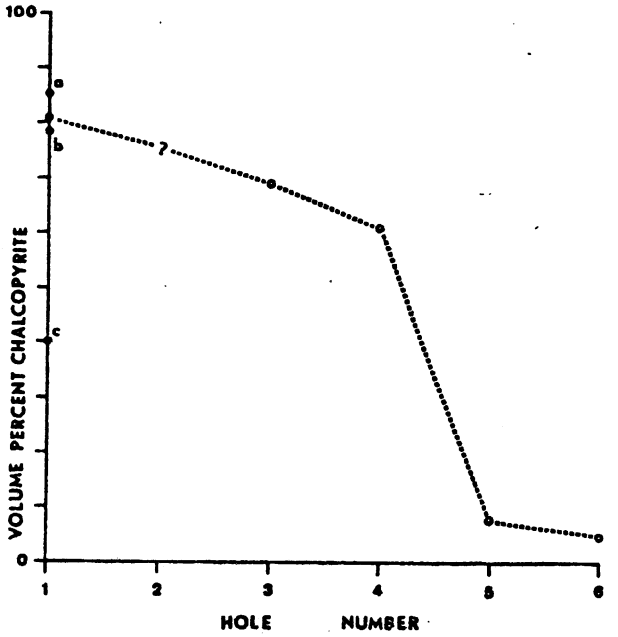

C

Slide 12

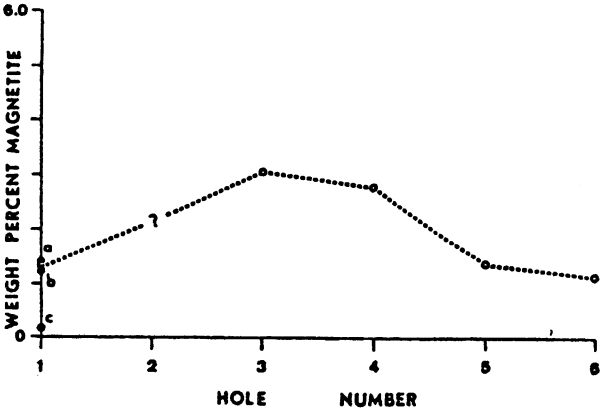

D

FIG. 8A. Total copper distribution along section a-a′. Lines a and b represent upper and lower diabase, while c is a schist lens. Classes in histogram are in units of 0.10 percent copper.

FIG. 8B. Weight percent sulfides in the rock along section a-a′. Points a and b are diabase, while point c is a schist lens and the average of a and b. Dashed line connects data points for the diabase.

FIG. 8C. Volume percent chalcopyrite in the sulfides. Point a and b are diabase and point c is schist. Note the drop in chalcopyrite in the schist.

FIG. 8D. Weight percent magnetite in the rock. Points a and b are diabase and point c is schist. Compare this curve to Figure 8A.

JEK

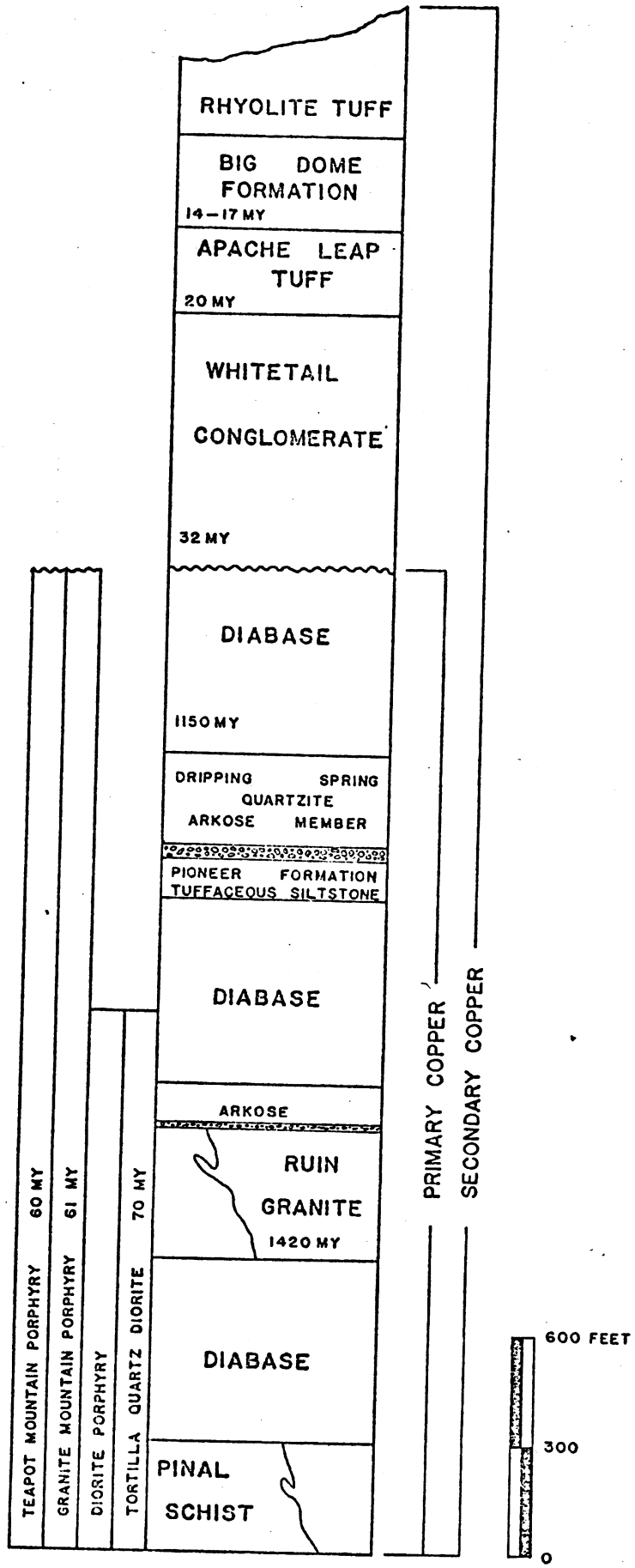
RHYOLITE TUFF
BIG DOME FORMATION
14–17 MY
APACHE LEAP TUFF
20 MY
WHITETAIL CONGLOMERATE
32 MY
DIABASE
1150 MY
DRIPPING SPRING QUARTZITE
ARKOSE MEMBER
PIONEER FORMATION
TUFFACEOUS SILTSTONE
DIABASE
ARKOSE
RUIN GRANITE
1420 MY
DIABASE
PINAL SCHIST
TEAPOT MOUNTAIN PORPHYRY 60 MY
GRANITE MOUNTAIN PORPHYRY 61 MY
DIORITE PORPHYRY
TORTILLA QUARTZ DIORITE 70 MY
PRIMARY COPPER
SECONDARY COPPER
600 FEET
300
0

Slide 1

J
D
7

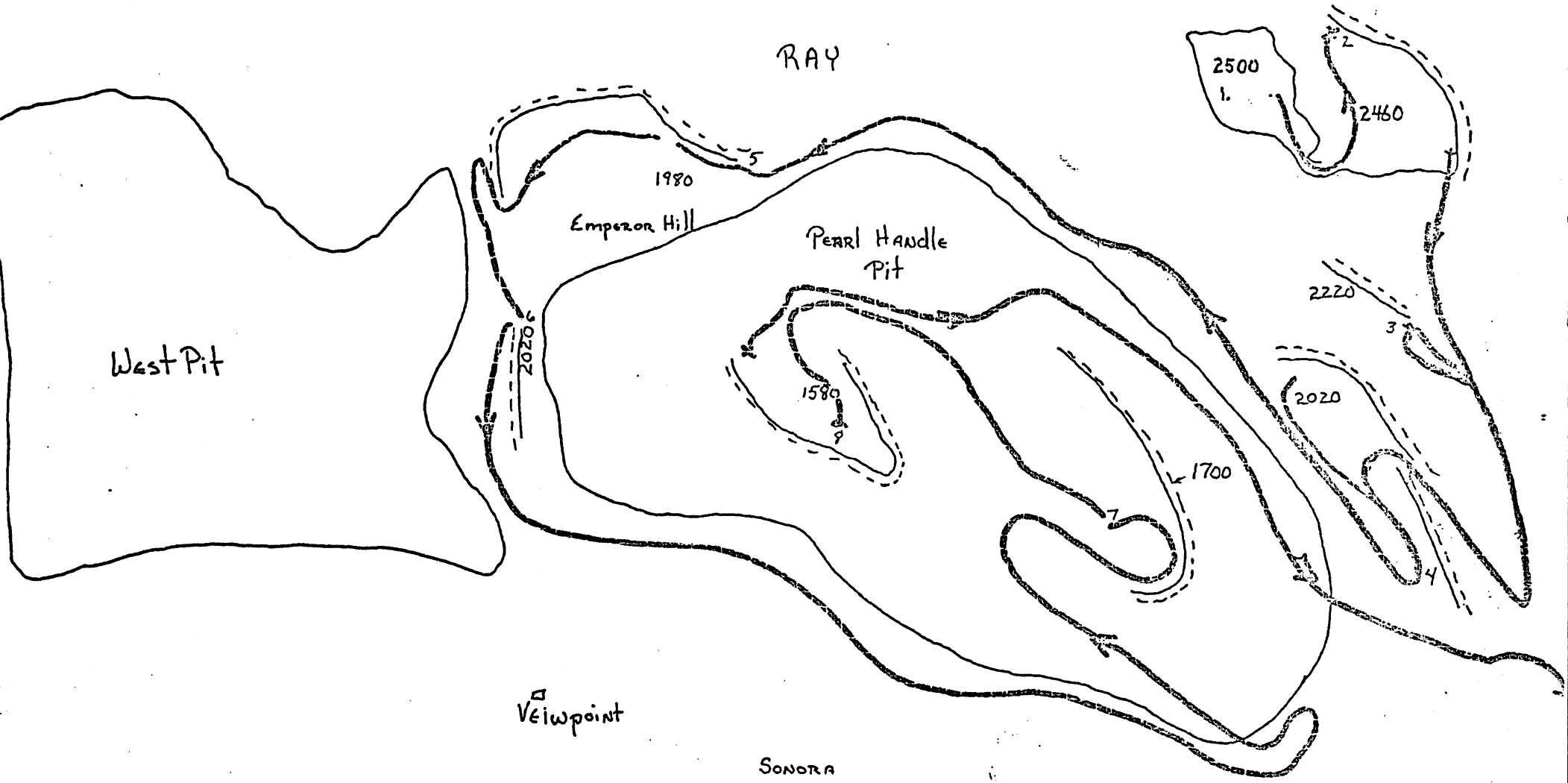

Granite Mt.

JDC
JEK

STRUCTURAL GEOLOGY OF THE RAY MINE
RECENT DEVELOPMENTS

by

Stefan A. Hoelscher
Geologist
Ray Mines Division
Kennecott Copper Corporation

Presented at the
Arizona Conference - AIME
Mining Geology Division Meeting
Ray Mine, Arizona
April 16, 1977

TABLE OF CONTENTS

	Page
Introduction	1
Diabase Fault.	3
Emperor Fault.	5
Emperor Hill	11
Table (Diabase Fault).	17
References Cited	18

INTRODUCTION

The Ray Mine stands apart from most porphyry copper deposits for the complexity of its structural geology. The complexity is exemplified in the professional literature by the history of the Diabase Fault over the life of the mine, as shown on the attached table. The dip of the fault was thought to be easterly from the 1916 publication by Spurr until the 1966 publication by Metz and Rose, when the dip became westerly. Movement on the fault was considered in the literature to be east side down until the 1971 publication of the Sonora Quadrangle by Cornwall, Banks and Phillips, when this sense of movement was reversed. The interpretation of displacement along the Diabase Fault ranges from a few hundred feet in the 1919 publication by Ransome to a "proven minimum" of 2,000 feet in Metz and Rose's 1966 publication.

In 1974 John Witner and the writer redefined the location of the Emperor Fault in the West Pit area and proposed a model to explain the nature and age of the fault's main movement. As part of an in-company slope stability investigation of the West Pit south wall, we concluded, in agreement with work by Wray in 1971, that the trace of the Emperor Fault does not form a complete circle in the Pearl Handle Pit; rather, it

crosses the south side of Emperor Hill. The 1974 report finds that the Emperor Fault separates the oxidized West Pit north wall from the unoxidized West Pit south wall. A large fault interpreted as the Emperor was mapped up the West Pit west wall and projects over Granite Mountain to the southwest.

On Emperor Hill the geology has been redefined by careful pit mapping in conjunction with prospect hole logging. An east-west trending horst block exposes the diabase/Apache Group sequence on the surface of the Emperor Hill area. North and south of the horst, the diabase/Apache Group sequence is structurally covered by schist in the upper plate of the Emperor Fault. The western portion of the horst block is lower plate schist down-section from the diabase/Apache Group sequence.

An apparent breccia pipe occurs at, and just south of, the extreme western end of the horst block. This structure involves clasts of Pioneer Formation, Scanlan Conglomerate, Pinal Schist and diabase.

DIABASE FAULT

The most obvious fault systems at the Ray Mine are the Diabase and Emperor Faults. Several other significant faults are documented in the mine area, including the Bishop, Empress, North End, Sun, West End, Consuelo and School Faults. In the silicate orebody there is at least one additional unnamed fault with several hundred feet of displacement.

The Diabase Fault is a moderately to steeply westerly dipping normal fault, characterized by several tens of feet of gougy, broken and brecciated rock and up to a few feet of strong gouge. In the Pearl Handle Pit, the hanging wall of the Diabase Fault contains the downthrown diabase/Apache Group sequence, which is overlain by schist in the upper plate of the Emperor Fault. The diabase/Apache Group sequence is underlain by basement Pinal Schist. The pre-Tertiary footwall rocks in the same area consist of the diabase/Apache Group sequence.

In the northern corner of the Pearl Handle Pit the normal displacement is about 800 feet, west side down. Southeastward in the mine area the displacement increases to more than 2,000 feet. The Diabase Fault in the Pearl Handle Pit terminates the Emperor Fault to the east; east of the

Diabase Fault, the Emperor Fault is upthrown and eroded away. The hypogene orebody occurs mostly in diabase within the lower Apache Group rocks, which are offset along the Diabase Fault.

EMPEROR FAULT

The Emperor Fault is commonly characterized by several feet of dense, dark gouge and up to tens of feet of gougy, broken and brecciated rock. On the whole, the fault dips about 10 to 30 degrees easterly in the Pearl Handle Pit and northerly in the West Pit. The upper plate, consisting of schist, some porphyry and minor diabase, overlies schist, some porphyry and the diabase/Apache Group sequence in the mine area.

In the Pearl Handle Pit, the Emperor Fault is downthrown in the hanging wall of the Diabase Fault and eroded away in the footwall. A minimum displacement of about 3,000 feet along the Emperor Fault is indicated where schist overlies the diabase/Apache Group sequence. The large amount of schist in the upper plate of the Emperor Fault dictates a westerly source area for that plate.

Geologic pit maps prior to 1975 show the trace of the Emperor Fault as a circle in the Pearl Handle Pit with a ridge of upper plate rocks between Sonora-Barcelona and the two pits. The first step toward the present interpretation of the Emperor Fault was taken by Wray in a 1971 in-company report. Wray mapped the fault correctly in the south Emperor Hill and Sonora-Barcelona areas. In the Barcelona area, the Emporor Fault plane is exposed on original ground forming the dip slope. This is the western termination of the ridge

of upper plate rocks in the Sonora area. In the area between south Emperor Hill and the West Pit floor, Wray shows a sharp southwestward bend in the Emperor Fault trace. The southwestward trace is currently believed to be an unrelated fault.

The Emperor Fault in the northern Pearl Handle Pit is very near the contact between hematitic leached cap and unoxidized, enriched sulfide-bearing rocks. In this area the Emperor Fault is near the "red-to-gray" contact. The 1967 Ray series 1,000-scale color aerial photography shows the red-to-gray contact crossing south Emperor Hill and tracing across the floor of the West Pit to the west wall. There a large fault fitting the description and general attitude of the Emperor was mapped continuously down the recently mined upper half of the west wall, and was visible down the lower half of the west wall to the lake at the floor of the West Pit. This is believed to be the westernmost expression of the Emperor Fault in the mine area.

The red-to-gray rule-of-thumb for locating the Emperor Fault is not applicable west of the West Pit floor nor south of the Pearl Handle Pit extension. In these areas the hematitic oxidation decreases in the upper plate of the Emperor Fault to an irregular oxidation contact. In the Pearl Handle Pit extension there is ore grade (+0.4% Cu) primary as well as secondary sulfide mineralization in both plates of the Emperor Fault.

On Emperor Hill the proximity of the Emperor Fault to the oxidation, or red-to-gray, contact is somewhat variable. In drill core from one recent Emperor Hill hole, the main gouge zone precisely separates leached cap from high-grade (+1.0% Cu) secondary sulfide enrichment. In a second recent hole 250 feet from the first hole, there is 400 feet of high-grade secondary sulfide enrichment with mostly weak oxidation above the fault and more than 100 feet of high-grade secondary sulfide enrichment below the fault, as one continuous ore intercept. On south Emperor Hill, where the 2020 level intersects the Emperor Fault, the main gouge zone is 25 feet below the oxidation contact.

Two older diamond drill holes on south Emperor Hill intersect the Emperor Fault at the depths predicted using the new trace of the fault across Emperor Hill and the mapped 30-degree dip. Hole 881 intersects seven feet of greenish-gray gouge 44 feet below the first sulfides and eight feet above the oxidation contact. Hole 882 encounters a 33-foot gouge zone starting 103 feet below the first sulfides and very near the oxidation contact. A 1977 hole was drilled 450 feet south of hole 881 and south of the new trace of the northward dipping Emperor Fault. The new hole drilled through rocks believed to be upper plate according to the old Emperor Fault interpretation and lower plate according to the new interpretation. This hole proved the new interpretation to be correct. No substantial fault was inter-

sected, and the schist facies encountered from the surface is a more mafic, sometimes mottled facies characteristic of the lower plate in the Emperor Hill area. The same mottled lower plate facies was intersected below the Emperor Fault in hole 881, and a more mafic schist was logged in the lower plate portion of hole 882. It is recognized that the observed schist facies changes may, at least partly, be produced by supergene leaching effects.

This writer agrees with Wray's 1971 in-company report description of the Emperor Fault as a gravity slide rather than a thrust fault. A causative mechanism was proposed in Witner and the writer's 1974 in-company report that would date the main movement of the Emperor Fault. The Granite Mountain Porphyry, with age dates of 60 and 63 million years (Banks and others, 1972), is commonly described in the literature as mushrooming out above the Emperor Fault. In some areas of the mine, the mushrooming concept yields to the likelihood of Granite Mountain Porphyry offset along the Emperor Fault.

The largest stock of Granite Mountain Porphyry in the Ray area centers at Granite Mountain, three miles southwest of the Pearl Handle Pit. The intrusion of this stock would have uplifted the area, causing a gravity slide that moved to the northeast over the Ray Mine area with a shallow northeasterly dip. Further uplift on Granite Mountain to the west

and downfaulting along the Diabase Fault to the east steepened the dip on the Emperor Fault. This mechanism would set the age of the main movement along the Emperor Fault at 60 to 63 million years ago. Since the slide movement would have occurred during the time of Granite Mountain Porphyry intrusion, porphyry masses may have intruded the upper plate both slightly before and after the main movement. Consequently, some porphyry masses would be offset while others would not.

The drilling data, consisting of more than 1,000 diamond drill holes and several hundred churn drill holes, gives no indication of major post mineral displacement along the Emperor Fault. There is hypogene mineralization, some of which is ore-grade (+0.4% Cu), in both plates of the Emperor Fault in the same area. The flat secondary sulfide enrichment blanket clearly crosses the gently dipping Emperor Fault in the Pearl Handle Pit-Emperor Hill area. At the intersection of the enrichment blanket with the Emperor Fault, secondary sulfide ore is commonly found in both plates of the fault within a single drill hole.

It is likely that the Emperor Fault has experienced recurrent minor movements since the episode of major movement. Sulfides in the fault are sheared and thin sheets of native copper are found that exhibit obvious shearing effects. On the other hand, an undisrupted one-half inch thick chalcocite vein occurs in hole 1075 six inches below the Emperor Fault main gouge zone. Between the 1740 and 1780 levels of the

northern Pearl Handle Pit, substantial amounts of Emperor Fault gouge-mylonite with obvious fluxion structure were collected for the native copper content. Unsheared seams of native copper invade the gouge-mylonite along seams of fluxion structure, demonstrating an absence of post native copper movement.

In plan view, central to the horseshoe-shaped hypogene ore zone (Phillips and others, 1974), there are three apophyses of Granite Mountain Porphyry outcropping at about 2500 feet elevation. A review of the diamond drilling data and correlation of the geologic sections and cross-sections adds significance to the central Granite Mountain Porphyry apophyses. The data are permissive if not indicative of a coalescence at depth of the apophyses into the largest stock of Granite Mountain Porphyry in the mine. The main body of this stock appears to be about 2,000 feet wide at sea level. The central relationship of this stock to the geometric hypogene copper zoning suggests strongly that this central Granite Mountain Porphyry stock is the parent intrusive for the Ray orebody. Since only apophyses of porphyry occur at the present surface, it seems likely that the level of erosion at Ray is high in the sulfide system and relatively little hypogene ore has been lost.

EMPEROR HILL

Pre-1976 geologic pit maps show an island of Dripping Spring Quartzite in a sea of schist on north Emperor Hill. The Dripping Spring Quartzite block is about 1,000 feet long and 500 feet wide. It is commonly depicted with faulted boundaries and speculation existed that this was an allochthanous megabreccia slide block from the Dripping Spring Mountains. The area was known to be complexly faulted, but was poorly understood due to the presence of schist on both sides of most faults.

An intensive pit mapping program was undertaken by the writer in late 1975 in order to unravel the structural complexity of the Emperor Hill area. Detailed pit mapping was conducted on a daily to semi-weekly basis in conjunction with prospect hole logging. The following geologic picture emerged.

Six major faults were traced across Emperor Hill in order to clarify the geologic setting. According to the previous interpretation, the surface on Emperor Hill was in the upper plate of the Emperor Fault. The present study reveals a horst block of lower plate rocks in the area of the previously mapped Dripping Spring Quartzite block. The quartzite is part of the diabase/lower Apache Group sequence exposed beneath the Emperor Fault in the Pearl Handle

Pit. The Emperor Fault was uplifted and eroded away in the horst block area.

From east to west, in plan view, the Emperor Hill portion of the horst block consists of Quaternary alluvium, 400 feet of Dripping Spring Quartzite, 450 feet of diabase, 100 feet of Pioneer Formation, 10 feet of steeply to moderately eastward dipping Scanlan Conglomerate, 900 feet of Pinal Schist, 200 feet of an apparent breccia pipe, and mine dump. The east-west trending horst block is adjoined to the south by schist in the upper plate of the Emperor Fault, where drilling information shows the Emperor Fault to be a few hundred feet deep. The area north of the horst block is geologically complex and poorly understood. Immediately north of the horst block diabase/Apache Group sequence, the same diabase/Apache Group sequence is overlain by several hundred feet of schist. This schist blanket was eroded away in the Tertiary basin northeast of the exposed horst block.

The northern horst block bounding fault dips 90 to 70 degrees southward. Although it is locally referred to as the north branch of the North End Fault, it is interpreted to be the same fault as the North End Fault in the West Pit. In the horst block area, the expression of the fault ranges from one foot of breccia with a hematitic silty matrix to several feet of gouge and gougy rock.

The southern horst block bounding fault dips steeply to moderately southward, with steeper dips to the east and more moderate dips to the west. Although this fault is

called the south branch of the North End Fault in the horst block area, it is interpreted to be the western portion of the Diabase Fault. The horst block, therefore, resulted from the union of two steep faults with opposite senses of movement.

The expression of the south branch of the North End Fault normally consists of one or more feet of gouge and up to tens of feet of gougy rock; however, in the southwestern horst block area, the fault becomes quite tight. There is little doubt that the tight fault mapped in this area is the same fault, since it separates a sericitic schist facies to the south from an arkosic/mafic schist facies to the north, as does the larger fault.

Stratigraphic relationships put some time constraints on the ages of movement of the horst bounding faults. The south branch of the North End Fault, or western Diabase Fault, was covered on the original surface by a small patch of Whitetail Conglomerate and Apache Leap Tuff. The concealed fault trace bisected the Tertiary cover. Movement along this fault was therefore pre-mid Tertiary. It is interesting for comparison to note that in the Pearl Handle Pit extension, a small block of Apache Leap Tuff on Pinal Schist was mined in the hanging wall of the Diabase Fault.

The minimum displacement along the western Diabase Fault, based on the depth of the Emperor Fault and the current topography, is around 300 feet. However, the original topography

on Emperor Hill contributes an additional 600 feet to the likely minimum displacement along the western Diabase Fault.

The eastern North End Fault shows a minimum displacement on the order of a few hundred feet where Apache Leap Tuff is faulted against Big Dome Formation northeast of Hagen's Dam. However, there may have been additional movement prior to the development of the Tertiary basin.

The upper plate of the Emperor Fault south of the horst block contains an important fault associated with a thin diabase sill. This is the Empress Fault, which was first mapped in earlier mine exposures. The Empress Fault and its associated diabase sill were folded into a syncline on the northeastern side of the Bishop Fault. The Empress Syncline is probably the result of drag folding along the western Diabase Fault. Southwest of the Bishop Fault, at a farther distance from the western Diabase Fault, only the "south limb" of the Empress Fault has been found. The offset of the Empress Fault along the moderately westerly dipping Bishop Fault is the same as that of the underlying Emperor Fault--30 feet, west side down. In addition, the attitude of the Empress Fault is exactly conformable to that of the Emperor Fault on the southwest side of the Bishop Fault. Genetically, the Empress Fault is probably an imbricate structure relating to movement along the Emperor Fault. The lack of any indication from earlier mapping that the Empress Fault folds also tends to confirm the drag folding hypothesis.

The Empress Fault is generally characterized by up to a few feet of dense limonitic gouge and many feet of strongly sheared diabase. The thickness of the diabase sill associated with the Empress Fault averages around 10 to 20 feet. Like the Emperor Fault, the Empress Fault dips about 30 degrees to the northwest in the hanging wall of the Bishop Fault. A peculiar feature of the Empress Fault is that the gouge zone sometimes occurs at the upper diabase contact, sometimes at the lower diabase contact, and sometimes bisects the diabase or occurs anywhere within the diabase sill. The 1977 geologic pit map shows that a small patch of apparent Whitetail Conglomerate covers the Empress Fault, indicating a pre-mid Tertiary age of movement.

On Emperor Hill, the Bishop Fault is a comparatively small fault, expressed by only a few inches or less of hematitic gouge. This westerly dipping normal fault shows 30 feet of post Emperor/Empress Faults movement. A generally moderate west-northwesterly schistosity dip is retained across the Bishop Fault.

The last significant feature to be recognized as a result of the Emperor Hill pit mapping program is an apparent new breccia pipe near the western end of the horst block. Like the Calumet Breccia Pipe, this pipe is probably related to the post ore (60 million year old) Teapot Mountain Porphyry. An old diamond drill hole in the pipe intersects several Teapot Mountain Porphyry dikes.

The breccia pipe is located within and just south of the westernmost end of the horst block. Surface mapping indicates fragments of Pinal Schist, Scanlan Conglomerate, Pioneer Formation, and diabase are involved in the brecciation. The surface of the pipe is commonly intensely limonitic. The lateral distance to the nearest Apache Group rocks within the horst block is 750 feet. It is not clear at this time what the nature of movement was within the pipe in order to accomplish the substantial apparent lateral offset of Apache Group rocks. Little drilling information is available since this is a poorly mineralized area.

DIABASE FAULT

Date	Author(s)	Paper	Structure	Dip	Movement	Displacement
1916	J. E. Spurr	The relation of ore deposition to faulting: Econ. Geol., v.11.	"Ray Fault"	Easterly	East side down	1000-2000 ft.
1919	F. L. Ransome	The copper deposits of Ray and Miami, Arizona: USGS PP 115.	"Mineral Creek-Ray Fault"	Easterly	East side down	100-600 ft.
1952	O. M. Clarke	Structural control of ore deposition at Ray, Arizona: AGS Guide for Field Trip Excursions in Southern Arizona	"Ray Fault"	Easterly	East side down	1000-2000 ft.
1966	R. A. Metz, A. W. Rose	Geology of the Ray copper deposit, Ray, Arizona: Geology of the Porphyry Copper Deposits, Southwestern North America	"Diabase Fault"	Westerly	East side down	"Proven minimum" 2000 ft.
1968	R. A. Metz, C. H. Phillips C. R. Caviness	Recent developments in the geology of the Ray area: AGS Southern Arizona Guidebook III	"School-Ray-Diabase Fault"	Westerly	East side down?	More than 1500 ft.
1971	H. R. Cornwall, N G. Banks, C. H. Phillips	Geologic Map of the Sonora Quadrangle, Pinal and Gila Counties, Arizona	"Diabase Fault"	Westerly	West side down	1200 ft.
1974	C. H. Phillips, N. A. Gambell, D. S. Fountain	Hydrothermal alteration, mineralization, and zoning in the Ray deposit: Econ. Geol., v.69, no. 8	"Diabase Fault"	Westerly	Either east or west side down	More than 1500 ft.
1977	S. A. Hoelscher	Structural geology of the Ray mine - recent developments: Spring Meeting AIME Mining Geology Division	"Diabase-North End (South Branch)Fault"	Westerly	West side down	Less than 800 ft, to more than 2000 ft.

REFERENCES CITED

Banks, N. G., Cornwall, H. R., Silberman, M. L., Creasey, S. C., and Marvin, R. F., 1972, Chronology of intrusion and ore deposition at Ray, Arizona--Part I, K-Ar ages: Econ. Geol., v. 67, p. 864-878.

Phillips, C. H., Gambell, N. A., and Fountain, D. S., 1974, Hydrothermal alteration, mineralization and zoning in the Ray deposit: Econ. Geol., v. 69, p. 1239-1246.

JEK

Jour. Research U.S. Geol. Survey
Vol. 4, No. 1, Jan.–Feb. 1976, p. 91–117

HALOGEN CONTENTS OF IGNEOUS MINERALS AS INDICATORS OF MAGMATIC EVOLUTION OF ROCKS ASSOCIATED WITH THE RAY PORPHYRY COPPER DEPOSIT, ARIZONA

By NORMAN G. BANKS, Menlo Park, Calif.

Abstract.—The contents of Cl, F, and H_2O+ (calculated) in some hydrous igneous minerals in intrusive rocks of Laramide age (70–60 m.y.) near Ray, Ariz., appear to be related to the age and the chemistry of the whole-rock samples. Apatite and biotite in younger, more silicic rocks contain more F but less Cl and H_2O+ than apatite and biotite in older, more mafic rock; the same relations hold for F and H_2O+ in sphene. Correlations of the abundance of Cl, F, and H_2O+ in hornblende with rock chemistry and age are not as strong as for apatite, biotite, and sphene; igneous(?) epidote does not contain Cl and F in amounts detectable by electron microprobe analysis. The contents of Cl, F, and H_2O+ in whole-rock samples decrease with increasing differentiation index and decreasing age. Data for a single pluton of variable composition mirror the results for a suite of different plutons and dikes. The data are satisfactorily although not exclusively explained by postulating that the melts each contained progressively less Cl, F, and H_2O and that the hydrous minerals consumed most of the Cl, F, and H_2O in the magmas. The data may also be explained by postulating that (1) the stocks evolved Cl-bearing water during their ascent and crystallization, or that (2) Cl and H_2O were concentrated during differentiation of the stocks but the minerals failed to record their buildup. Both alternative explanations find problems with and require special conditions to satisfy field, chemical, and experimental data. If many of the special conditions are not met, a nearby batholithic parent to the stocks is not a favorable source of the mineralized fluids at Ray. Propylitic alteration of biotite results in Cl-poor chlorites and may have provided some Cl to hydrothermal fluids; biotite may have also supplied some F to propylitizing fluids through alteration.

This study provides data on the concentrations of Cl, F, and H_2O in the intrusive bodies and their hydrous minerals related in time and space with the porphyry copper deposit at Ray, Ariz. These and accompanying whole-rock petrochemical data allow interpretation of the magmatic behavior of Cl, F, and H_2O prior to deposition of ore. Microprobe and wet-chemistry analyses for Cl, F, and H_2O+ of mineral grains and whole-rock samples of least altered Laramide intrusive rocks, of mineral grains in least altered Precambrian igneous rocks (Ruin Granite, 1.4 b.y.; diabase, 1.2 b.y.), and of hydrothermal biotite from the deposit are reported. The igneous minerals studied are apatite, biotite, hornblende, sphene, and epidote; secondary minerals include chlorite, epidote, sphene, phengite, and hydrogarnet(?).

The samples used in the microprobe studies were collected at sites indicated in figure 1 and include 7 of at least 12 rock types intruded in the vicinity of the Ray deposit during a 10-m.y. period (70–60 m.y. ago; Banks and others, 1972; Banks and Stuckless, 1973). Ages, differentiation indices, textures, the Fe-Mg silicates present, and percentage of alteration of selected minerals in the Laramide igneous rocks are listed in table 1. Whole-rock chemical and petrologic data have been obtained on one or more samples of each of the 12 rock types. At least 11 of these rock types are cut by sulfide veinlets; part of this veining occurs outside of presently commercial ground.

The deposit, located about 120 km north of Tucson and 120 km east of Phoenix, Ariz. formed about 60 m.y. ago (Banks and Stuckless, 1973). The main hosts of the hypogene sulfides (pyrite, chalcopyrite, and molybdenite) are schist, Ruin Granite (a quartz monzonite), quartzite, and diabase, all of Precambrian age. The center of mineralization occurs near the west-central edge of the Sonora quadrangle (fig. 1).

Acknowledgments.—The manuscript was improved by many fruitful discussions with N. J Page and the helpful reviews by W. J. Moore, N. J Page, H. D. Holland, D. R. Wones, and H. R. Cornwall. The manuscript also benefited from reviews of some of the sections by R. O. Fournier and C. L. Christ. Part of the modal data used for material balance estimates in this report was contributed by H. R. Cornwall. R. Dockter aided in data compilation and drafting. Oliver Ingamels (now with Climax Molybdenum Co., Golden, Colo.) provided the scapolite standard (No. 63–1805) for the Cl analyses.

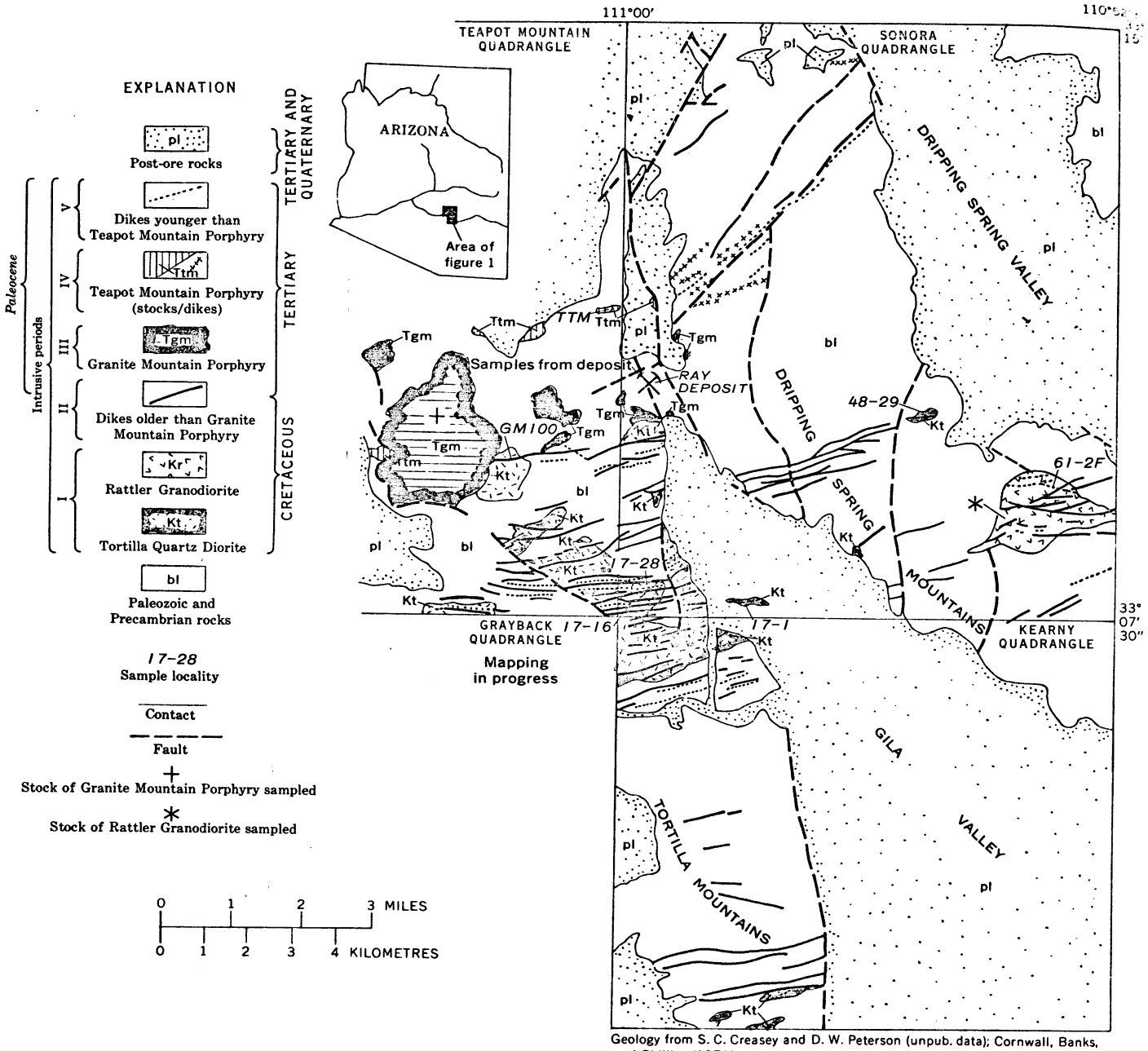

Geology from S. C. Creasey and D. W. Peterson (unpub. data); Cornwall, Banks, and Phillips (1971); and H. R. Cornwall and M. H. Krieger (1975)

FIGURE 1.—General geology and sample locations.

BACKGROUND GEOLOGY AND PETROLOGY OF LARAMIDE IGNEOUS ROCKS

Laramide igneous bodies near Ray were intruded in roughly five periods (fig. 1) that may or may not represent a nearly continuous sequence. One or more major plutons, representing five rock types, were emplaced during each of the first four intrusive periods. The samples for microprobe study came from four of these five major rock types. The excepted rock type represents a granodiorite stock of intrusive period II (63 m.y. old) in the Grayback quadrangle (not shown in fig. 1). Rhyodacitic to quartz latitic dikes were emplaced in intrusive periods II, IV, and V. Samples of the dikes for microprobe study came from two rock types of period II (samples 17–16 and GM100, table 1) and one type of period V (sample 61–2F, table 1).

Bulk compositions of the major Laramide plutons are progressively more felsic (increasing differentiation index) with decreasing age of the intrusive type: these ages were determined on the basis of geologic

TABLE 1.—*Sample data, Laramide rocks*

Rock sample [1]	Rock differentiation index [2]	Texture	Mafic silicates present			Percentage of mafic minerals altered [3]	Percentage of plagioclase altered [4]
			Pyroxene	Hornblende	Biotite		
Tortilla Quartz Diorite (71–70 m.y.) [5]							
17–28	51.4	Intersertal	×	×	×	Trace	16.0
17–1	51.9	----do	×	([6])	×	19.5	5.0
48–29	53.2	----do	×	×	--	10.0	45.0
Rattler Granodiorite (70 m.y.)							
46–99B	48.4	Hypidiomorphic-seriate	×	×	×	1.3	6.6
60–113D†	64.7	Porphyritic	-----	×	×	11.3	3.8
60–108	72.3	Hypidiomorphic-seriate	Trace	×	--	Trace	1.0
60–114†*	72.2	Porphyritic	-----	×	×	2.4	3.0
61–25†	72.4	----do	-----	×	×	8.2	3.5
60–91	72.5	Seriate porphyritic	-----	×	×	11.0	11.2
60–111	72.7	Chilled	-----	--	×	2.0	0.6
60–124*	72.8	Hypidiomorphic-seriate	-----	×	×	13.3	10.0
60–98	75.2	----do	-----	×	×	1.7	3.6
46–11G	75.4	----do	-----	×	×	9.6	10.5
60–131	76.4	Seriate porphyritic	-----	--	×	8.3	7.1
60–130	76.9	Hypidiomorphic-seriate	-----	--	×	9.0	6.3
60–132*	77.7	----do	-----	--	×	17.7	7.1
60–96A	87.3	Aplitic	-----	--	×	72.5	26.7
46–11A	93.3	----do	-----	--	×	72.2	35.9
T16–630‡	71.5	Seriate porphyritic	-----	×	×	----	---
Granite Mountain Porphyry (61–60 m.y.)							
RB5	79.7	Granitoid	-----	--	×	46.0	39.5
GM14	80.5	Seriate porphyritic	-----	--	×	12.5	12.1
GM12	81.8	Porphyritic	-----	--	×	13.6	11.3
GM18	81.9	Granitoid	-----	Trace	×	5.7	9.0
GM6G	83.5	Seriate porphyritic	-----	--do-	×	9.2	2.3
GM1A	[7] 94.7	Aplitic	-----	--	×	100.0	41.0
GM2A	94.7	----do	-----	--	×	85.7	21.0
GM4V	---	Porphyritic	-----	--	×	16.7	2.5
Teapot Mountain Porphyry (61–60 m.y.)							
Ttm†	83.6	Porphyritic	-----	×	×	100.0	68.0
Rhyodacite dikes [8]							
17–16†	[9] 74.0	Porphyritic	-----	×	×	43.2	58.8
GM100†	[9] 80.0	----do	-----	×	×	42.0	52.3
61–2F†	81.0	----do	-----	×	×	86.3	7.8

† Samples with phenocrystic magnetite and hydrous phases.
* No mineral analyses.
‡ No modal analysis.
[1] A numeral 2 or 3 preceding the sample numbers in the following tables indicates that the probe mount is a duplicate or triplicate sample.
[2] Modified from Thornton and Tuttle (1960): uses quartz plus albite plus K-feldspar from molecular catanorm rather than the CIPW norm.
[3] Percentage of the Mg-Fe minerals in the rock converted to secondary minerals.
[4] Percentage of the plagioclase in the rock converted to secondary minerals.
[5] Ages from Banks and Stuckless (1973); Banks and others (1972).
[6] Fibrous amphibole reaction rims on pyroxene.
[7] Aplite assumed to have approximately same differentiation index as sample GM2A.
[8] Ages as follows: Sample 17–16 (<69, >63 m.y.); sample GM 100 (63 m.y.); sample 61–2F (questionable, either 70 m.y. or <60 m.y.).
[9] Rock analysis from the same dike type but not the same dike used for the mineral analyses.

relations and potassium-argon and fission-track ages (table 1). Compositions of the dike rocks are not all intermediate between those of rock types that they crosscut and that crosscut them. However, standard petrochemical plots of whole-rock normative minerals, major elements, and trace elements indicate that the magmas of both the dikes and the stocks of Laramide age near Ray developed along smooth chemical trends (Banks and others, 1972). The results are compatible with, although not proof of, either consanguinity or a common-source partial melting origin of the igneous suite. Various facies of the Rattler Granodiorite almost duplicate in one intrusive mass the chemical, textural and mineralogical variations that occur in the entire suite studied (table 1). This allows comparison of the behaviors of Cl, F, and H_2O in one magma with their behaviors in a series of magmas intruded in the 10-m.y. period. Stratigraphic reconstructions indicate that during Laramide time the presently exposed rocks were at depths ranging from not more than 1.5 km to at least 3 km. Concordance of apatite fission-track ages with other mineral ages places a maximum depth for the exposed rocks and deposit at 5 km during and since Laramide time (Banks and Stuckless, 1973). Depths of

emplacement of the individual plutons studied may have differed by 1.5 km or more.

Several petrochemical observations suggest, although admittedly do not prove, that the stocks and dikes did not saturate early in their crystallization history or evolve much water. The Mg content of the biotite decreases slightly with increasing differentiation index of the sample and, more strikingly, with decreasing sample age (fig. 2). This reducing trend may represent undersaturation of the melt in regard to water (Wones and Eugster, 1965). Additionally, (1) the percentage of aplites in the stocks is low; (2) there is a paucity of pegmatitic aplites; (3) metamorphic aureoles around the intrusive bodies, both stocks and dikes, are very restricted and in some places are virtually absent even in carbonate terrane; (4) miarolitic features or cavities have not been identified in field exposures or thin sections of the Laramide stocks; and (5) J. T. Nash (written commun., 1971, 1972) and M. J. Logsdon (oral commun., 1973) find that the fluid inclusions in quartz in the rocks are sparse, two phase, relatively dilute, and homogenize at temperatures below 450°C.

Another petrologic observation that might indicate the degree of saturation of the magmas at their emplacement is the amount of melt crystallized prior to the first formation of the hydrous minerals. For example, at their depths of emplacement, the melts should have contained about 2.5–3.0 wt percent H_2O before

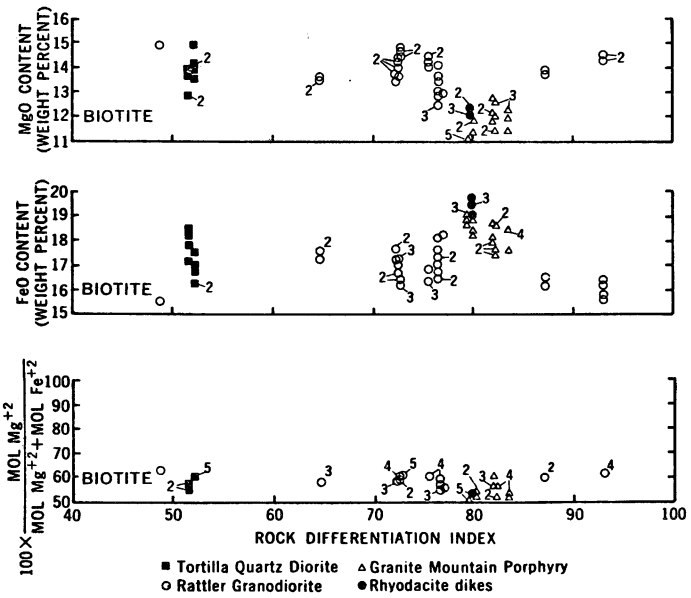

Figure 2.—Variation of MgO, FeO, and $\frac{100 \times \text{mol } Mg^{+2}}{\text{mol } Mg^{+2} + \text{mol } Fe^{+2}}$ in biotite with rock differentiation index. All Fe in biotite is assumed to be in the reduced state for plotting.

biotite formed (D. R. Wones, oral commun., 1973; Wones and Dodge, 1966). Thus, if biotite first formed in a stock when it was 50 percent crystallized, the magma presumably had less than 1.5 wt percent initial H_2O. However, as described below, not only is it difficult to determine with surety when the hydrous minerals first began forming in the magmas, but also the petrologic relations can be interpreted to indicate that a given mineral began forming at different times in the same magma.

In the porphyritic variants of the Rattler Granodiorite and in the rhyodacite dikes and Teapot Mountain Porphyry (flagged by daggers in table 1), anhedral (fig. 3*A*) to euhedral (fig. 3*B*) phenocrysts of hornblende, biotite, and anhydrous minerals are set in either an aplitic or felty groundmass composed mainly of quartz, K-feldspar, and, in some samples, also plagioclase, opaque minerals, hornblende, or biotite. Accessory apatite occurs as subhedral to euhedral grains and as inclusions, mostly in biotite. Sphene rims magnetite phenocrysts, is intergrown with biotite and hornblende, or locally is found as separate, subhedral to anhedral medium-sized grains. Provided that growth rate of the hydrous minerals did not greatly exceed the growth rate of the anhydrous minerals, these relations suggest that the hydrous minerals began forming in the magma before the groundmass, which makes up 30–50 percent of the rocks in this group of samples. However, in the other samples of the Rattler Granodiorite (not flagged by daggers in table 1) and in all samples of the Tortilla Quartz Diorite and Granite Mountain Porphyry (including porphyritic varieties), the hydrous minerals are interstitial to plagioclase (forming roughly 50 percent of the rocks) and are spatially associated with interstitial aplitic to oikocrystic K-feldspar and quartz (fig. 3*D–H*; fig. 4*A*). In the more felsic samples of this group, some of the larger K-feldspar and quartz grains (perhaps another 20–30 percent of the rocks) formed with the plagioclase and therefore also predate the hydrous minerals. Hornblende, biotite, and sphene display euhedral faces against each other and interstitial quartz or K-feldspar (fig. 4*A*, *F*), but they only rarely are euhedral against plagioclase. These relations indicate that at least the outer parts of the hydrous mineral grains are coeval with the interstitial quartz and K-feldspar and postdate main-stage growth of plagioclase and some quartz and K-feldspar but do not rule out the possibility that the cores of the grains began forming during plagioclase growth. Rare small inclusions of apatite, biotite, and hornblende in the early plagioclase might suggest the second possibility but might also be interpreted to be replacement features associated with fractures and crystal dislocations lo-

cated outside of the thin sections. Alternatively, rather than indicating favorable conditions for hydrous minerals throughout the magma, the small inclusions might have resulted from local concentrations of the required components that were rejected by the growing anhydrous plagioclase.

Although these petrographic relations suggest that the hydrous minerals may have formed earlier in some magmas or parts of magmas than in others, textural relations indicate that these minerals continued to form late during crystallization in both sample groups. Some hornblende and biotite in the first sample group include aplitic groundmass material in their edges (fig. 3*A*, *B*) and some in their centers, indicating, as does the presence of hydrous minerals in the groundmass (fig. 3*C*), that at least part of the growth of the hydrous minerals accompanied crystallization of the groundmass. In the samples of the second group, the hydrous minerals show crosscutting, interstitial, and coeval relations with the interstitial anhydrous minerals (fig. 4*B*, *C*) and replace the early-formed plagioclase (fig. 4*D*) and, in the more mafic samples, also pyroxene (fig. 4*E*). These relations and the presence of biotite, apatite, and sphene in the late-stage aplitic differentiates of all the stocks indicate that hydrous phases continued to form until only a small amount of liquid remained. All the hydrous minerals become less abundant with increasing differentiation index of the sample (fig. 5), and the modal amount of a given hydrous mineral is not detectably different when samples of like whole-rock composition from the two sample groups are compared.

Paragenetic relations between the different hydrous phases appear to vary somewhat with rock chemistry. In the more mafic samples, at least part of the hornblende appears intergrown with biotite, whereas in the more felsic Granite Mountain Porphyry, the hornblende occurs only as very rare needles (for example, sample GM18, tables 1, 5) in quartz that may predate biotite. Sphene in the mafic samples is interstitial to hornblende and biotite but in more felsic rocks appears coeval with these minerals (fig. 4*F*). For the most part, however, the frequency of mutual inclusion, intergrowth, replacement, and proximity coupled with similar physical relations with precursor and coeval anhydrous phases indicate that the formation of biotite, hornblende, apatite, and sphene was largely coeval (figs. 3*D*, *H*; 4*D*–*F*). Rare grains of interstitial epidote thought to be igneous or to be replaced interstitial glass are the exception and appear always to postdate the other hydrous phases, except perhaps sphene in the mafic samples. The epidote is sometimes chemically distinguishable from epidote formed at the expense of biotite and plagioclase in the same thin section, and igneous minerals in contact with it appear unaltered (fig. 4*G*, *H*). Compared to the other hydrous minerals, apatite is commonly euhedral (fig. 4*D*, *E*; 3*H*) and seems not to include apparently coeval hydrous anhydrous silicate (it does include zircon and opaque minerals) or even plagioclase in occurrences where it appears to replace that mineral.

Crystal growth relations of the interstitial hydrous minerals, quartz, and K-feldspar appear to be complex. A given hydrous mineral grain may have a euhedral face in contact with an interstitial grain of a given anhydrous mineral, whereas the other face or other grain of the hydrous mineral in the same or different thin section of the same pluton may replace the K-feldspar and quartz or be intergrown with them (fig. 4*A*). The same relations occur between different hydrous minerals and also between interstitial quartz and K-feldspar. Also, replacement and overgrowth features occur between like-mineral grains. These relations indicate that the conditions governing mineral stabilities fluctuated repeatedly over short distances during formation of the interstitial material. They may also suggest equilibrium crystallization where continual reconstitution of the crucial components for growth of a given phase (among them Cl, F and H_2O) was caused by rejection of the components by other nearby phases.

ANALYTICAL RESULTS

Methods

The mineral analyses were done with an ARL (Applied Research Lab.) model EMX–SM electron microprobe using an ADP crystal for Cl and an RAP crystal for F, an excitation voltage of 15 kV, sample currents of 2.5×10^{-8} or 3×10^{-8} A on brass, integration times (terminated on a fixed beam current) of about 40 s, and scapolite (2.57 wt percent Cl) and fluorapatite (3.83 wt percent F) as standards. The electron beam was fully focused. Buildup of carbon contamination and noticeable loss of volatile components were avoided by moving the beam with magnetic deflectors to sweep areas about 4–10 μm^2. At the termination of each counting interval, the sample was moved under the beam about 1 μm. If the grain shape and size did not allow this type of analysis, the sample was moved manually under a fully focused or defocused (2–3 μm) beam about every 10 s. The X-ray intensity data (counts), obtained by averaging 4-10 (usually 8) observations per analysis, were corrected by computer. Except for apatite, observation points were distributed over an area of about 10×10 μm. Data collection for apatite was similar to the above except that the data points

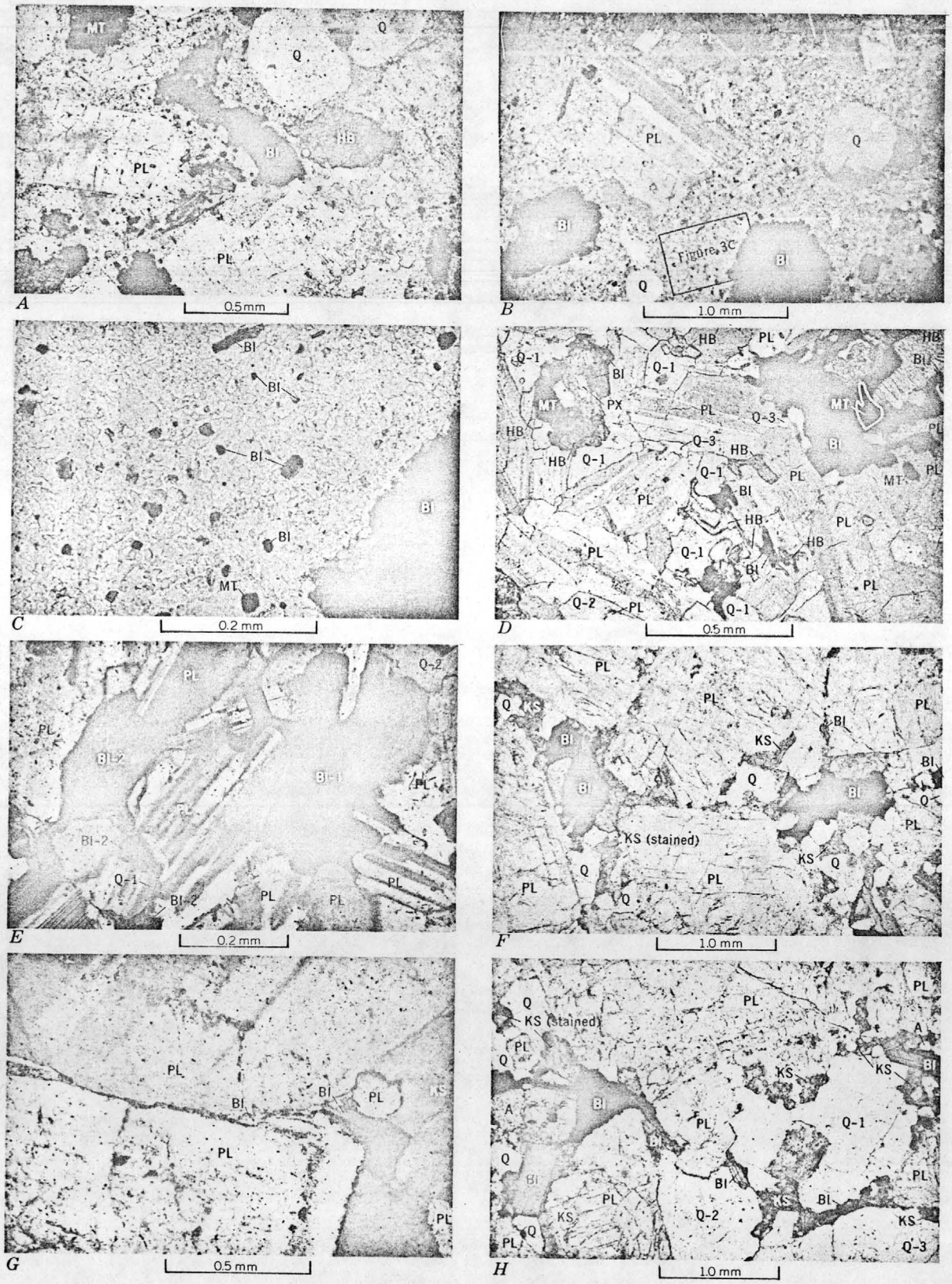

were distributed in two ways: (1) Equal numbers at centers and edges of the grain, or (2) as steps across a grain. Computer corrections included drift, background, and matrix corrections (mass absorption, secondary fluorescence, and atomic number effects: Beeson, 1967; Beaman and Isasi, 1970). Major-element

data used in the computer corrections were gathered during 6–15 counting intervals (of about 20 s each) using (where appropriate) biotite, apatite, rhodonite, hornblende, rutile, hematite, orthoclase and plagioclase as standards.

Precision of the microprobe analyses is considered to be about ±10 percent of the amount present for F and slightly better for Cl. Detection levels were established at three times the square root of the background counts (Birks, 1963). The average Cl and F contents of biotite in one sample determined by microprobe analysis agree within 17 percent of the amount determined by wet-chemical analysis (sample 261–25, table 4). This is good agreement considering the inhomogeneity of this sample with respect to Cl and F and considering the correction factors involved in using scapolite and apatite for Cl and F analysis of biotite. The values of H_2O+ reported in tables 2–6 are calculated by difference by assuming ideality for each mineral phase and using the computer program of Jackson and others (1967) to obtain the required normalizing factors. The H_2O+ data are less precise than the Cl and F data because the precision of the normalizing factor is influenced by sample homogeneity of six to nine elements rather than one. This and the variation in the major-element contents between mineral grains resulted in different calculated H_2O+ contents for some of the mineral grains in tables 3–6, although the grains have similar Cl and F contents. The H_2O+ content, by analysis, of one biotite (grain CHEM, sample 261–25, table 4) is lower than that obtained by calculation and thus also is less than that required for ideality. It is not known whether this is real or resulted from excessively high temperatures used in drying the separate.

Supplementary analyses of whole-rock Cl, F, and H_2O+ were done by wet-chemical methods. The Cl and F analyses were done on dry-rock powders and their water-leached splits. The water leaching removes Cl contributed by salts precipitated on fractures by ground water. The modal data were determined by combined observations of thin sections and stained rock slabs so that the effects of porphyritic texture and large grain size were minimized.

FIGURE 3.—Textural relations of minerals in Laramide rocks at Ray, Ariz. (A, apatite; BI, biotite; KS, K-feldspar; HB, hornblende; MT, magnetite; PL, plagioclase; Q, quartz. Numbers indicate different outcrops of individual, optically continuous grains.) *A*, Sample 60–114, porphyritic facies of Rattler Granodiorite. Phenocrysts of euhedral to subhedral plagioclase, subhedral to anhedral quartz and magnetite, and anhedral biotite and hornblende in groundmass of plagioclase, K-feldspar, quartz, and biotite. *B*, Sample 61–25, porphyritic facies of Rattler Granodiorite. Phenocrysts of subhedral to euhedral plagioclase, biotite, hornblende (not shown), and magnetite and rounded quartz in groundmass of plagioclase, K-feldspar, biotite, and magnetite. *C*, Inset of figure 3*B* showing biotite in groundmass. *D*, Sample 17–28, Tortilla Quartz Diorite. Subhedral plagioclase with interstitial hornblende, biotite, and quartz. *E*, Sample 17–28, Tortilla Quartz Diorite. Detail of interstitial biotite and quartz. *F*, Sample 60–131, seriate porphyritic facies of Rattler Granodiorite. Quartz, K-feldspar (stained) and biotite interstitial to euhedral to subhedral plagioclase. *G*, Sample RB–5, Granite Mountain Porphyry. Euhedral plagioclase with biotite and interstitial oikocrystic K-feldspar (stained). *H*, Sample 60–131, seriate porphyritic facies of Rattler Granodiorite. Euhedral apatite and anhedral biotite, quartz, and K-feldspar (stained) interstitial to euhedral to subhedral plagioclase.

Comparative Cl, F, and H_2O+ contents of the minerals

The Cl, F, and H_2O+ contents of the minerals are summarized in table 2 and presented separately in tables 3–9. Cl and F generally show a preference for apatite over coexisting biotite, hornblende, sphene, and epidote (see also Stormer and Carmichael, 1971), whereas H_2O+ shows a preference for the silicates over apatite. F is dominant over Cl in all the igneous minerals (see also Stormer and Carmichael, 1971, and Taborszky, 1962).

Biotite contains more H_2O+ and F, and usually more Cl by weight than coexisting hornblende, sphene, and interstitial epidote. Correns (1956) and Gillberg (1964) found similar relations between the halogen contents of coexisting biotite and hornblende, and the data of Dodge and others (1968, 1969) for rocks of the Sierra Nevada batholith and Dodge and Ross (1971) for granitic rocks in the Coast and Transverse Ranges, Calif., show that coexisting biotite contains more H_2O+ and F by weight and slightly less or the same amount of Cl than coexisting hornblende. Hornblende, like biotite, generally contains more Cl, F, and H_2O+ by weight than coexisting sphene, whereas sphene contains less H_2O+ and more F than interstitial epidote. In terms of atomic percent, biotite in a given sample contains Cl^-, F^-, and OH^- in about the same relative proportions as hornblende and sphene (ranging from 0 to 2 percent for Cl^-, from 2 to 14 percent for F^-, and from 86 to 96 percent for OH^-) but contains less Cl^- and F^- than apatite (ranging from 0 to 20 percent Cl^-, 32 to 98 percent F^-, and 2 to 48 percent OH^- apatite).

Hydrothermal biotite contains significantly different amounts of Cl and F compared with igneous biotite in equivalent rocks from outside the Ray deposit (table 2; in table 4 compare T123 with samples of Granite Mountain Porphyry). In addition to differences in Cl and F contents, hydrothermal biotite from Granite

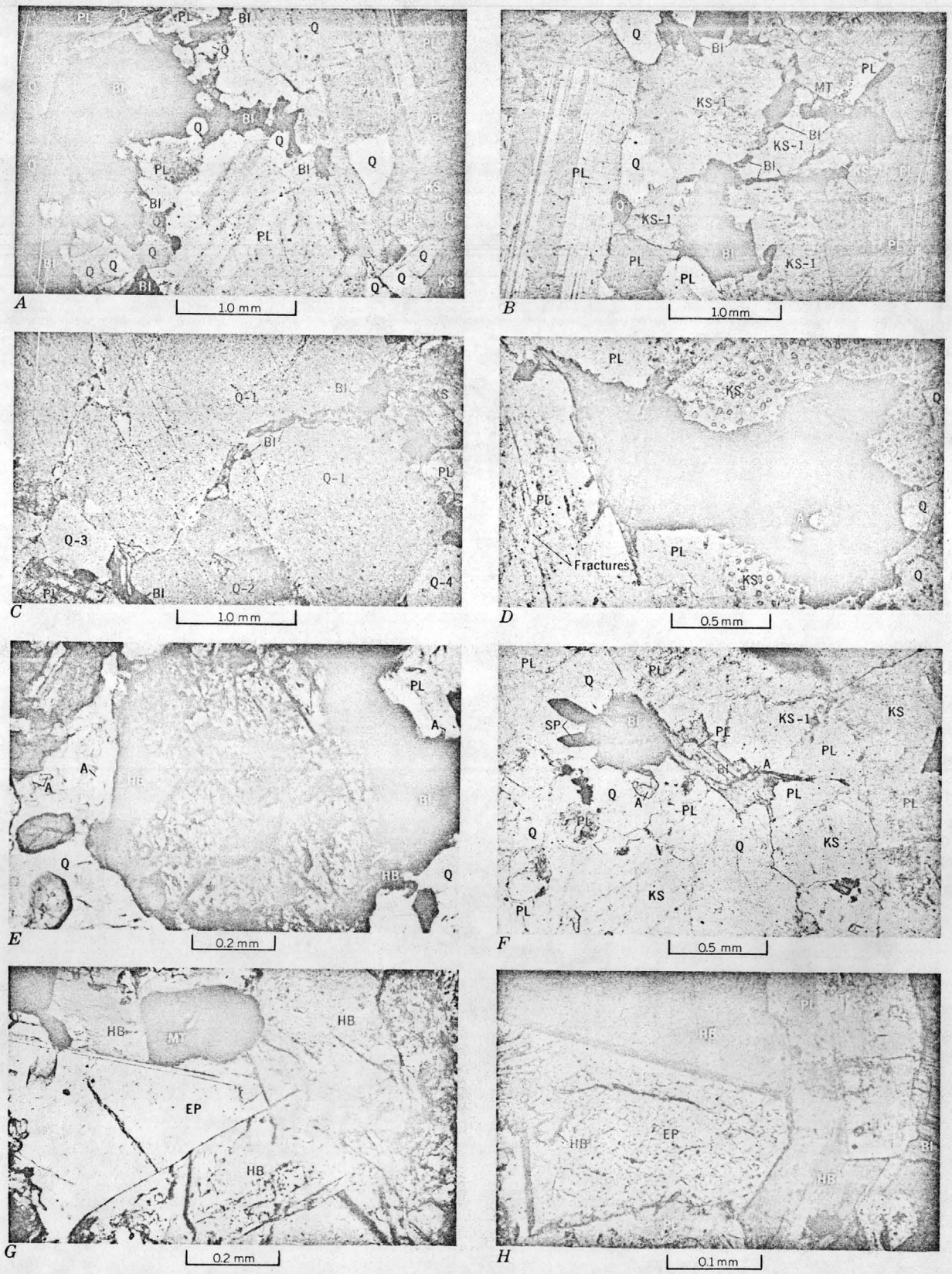

Mountain Porphyry differs from igneous biotite by containing more Mg (66 versus 55 mole fraction phlogopite). Roegge and others (1974) found approximately the same amount of Cl (0.07–0.09 wt percent)

as that of sample T123 in another sample of hydrothermal biotite from the Granite Mountain Porphyry at Ray.

The F content of the chlorite in the Laramide rocks correlates with greater than 99-percent confidence with the F content of its biotite precursor. Similarly, both biotite and its derivative chlorite in the Ruin Granite contain more F than the biotite and chlorite in the Laramide rocks (table 2). Positive correlations also were found between the contents of the major and other minor elements in the chlorites and their precursor biotites from the Laramide rocks (Banks, 1974). There is no correlation between the contents of F in the epidote, sphene, and hydrogarnet(?) analyzed and the content of F in the host biotite.

Analyses of four phengites are given in table 8, although the results are not summarized in table 2. Two are alteration products of plagioclase, and two are alteration products of chlorite. Additionally, an intensely altered area of plagioclase (2GM14, grain 4SPA) containing unidentified fine-grained clay minerals, too

◀ FIGURE 4.—Textural relations of minerals in Laramide rocks at Ray, Ariz. (A, apatite; BI, biotite; EP, epidote; HB, hornblende; KS, K-feldspar; MT, magnetite; PL, plagioclase; PX, pyroxene; SP, sphene; Q, quartz. Numbers indicate outcrops of individual, optically continuous grains.) *A*, Sample 60–130, hypidiomorphic-seriate facies of Rattler Granodiorite. Euhedral plagioclase, interstitial anhedral K-feldspar, and anhedral to euhedral quartz, and biotite. Note euhedral face of biotite against quartz at left side of photograph. *B*, Sample 60–130, same sample as 3*A*. Biotite cutting and interstitial to interstitial K-feldspar. *C*, Sample 60–132, hypidiomorphic-seriate facies of Rattler Granodiorite. Biotite cutting oikocrystic quartz. *D*, Sample RB5, Granite Mountain Porphyry. Biotite and K-feldspar (stained) interstitial to and replacing plagioclase. Apatite in biotite. *E*, Sample 17–28, Tortilla Quartz Diorite. Biotite and hornblende rimming pyroxene. Apatite in interstitial quartz. *F*, Sample, RB5, Granite Mountain Porphyry. Sphene, apatite, and biotite with interstitial quartz and K-feldspar. *G*, *H*, Sample 48–29, Tortilla Quartz Diorite. Epidote interstitial to unaltered hornblende and plagioclase.

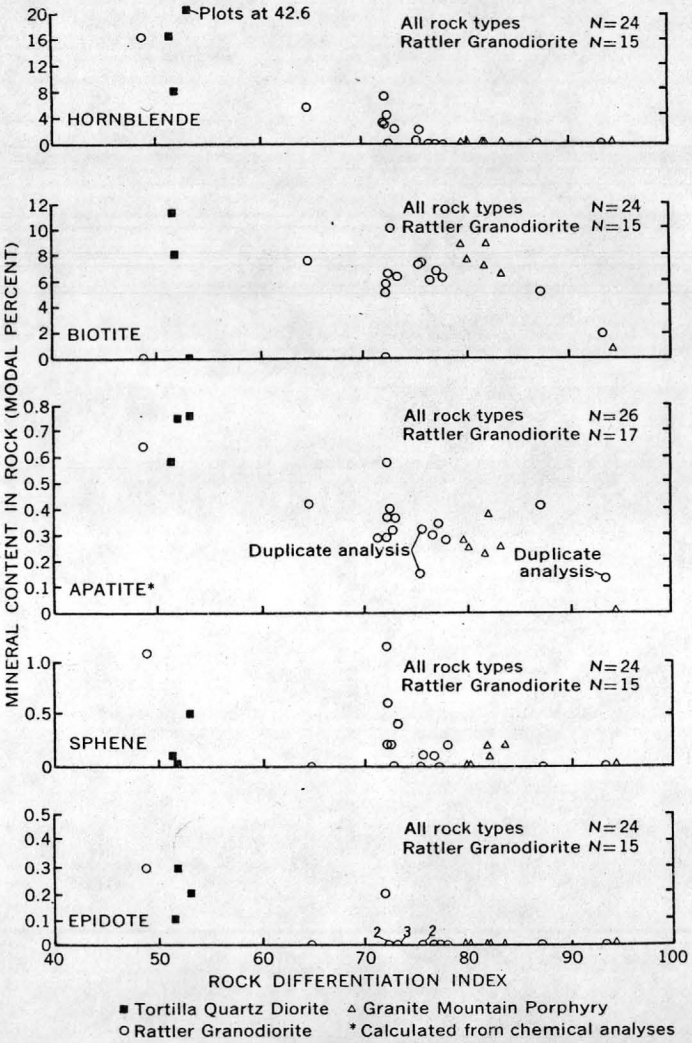

FIGURE 5.—Variation of mineral modal abundance with rock differentiation index.

TABLE 2.—*Ranges of* Cl, F, *and* H_2O+ *contents in the hydrous minerals*

	Igneous minerals					Alteration minerals				
	Apatite	Biotite	Hornblende	Sphene	Epidote	Chlorite	Sphene	Epidote	Hydrogarnet?	Hydrothermal biotite
Laramide rocks:										
Cl	0.02–1.4	0.02–0.26	0.02–0.17	<0.02–0.02	<0.02	<0.02–0.04	-------	<0.02	<0.02	0.06
F	1.2 –3.6	.10–0.86	.11–0.58	.08– .30	<.04	<.04– .30	0.18–2.5	<.04–0.11	.60–1.8	1.7
*H_2O+	.06–1.09	3.52–3.94	1.76–2.00	†.99–1.12	1.86–1.88	.04– .30	-------	----------	---------	3.22
Ruin Granite:										
Cl	.11	.10–0.13	--------	----------	----------	<.02	-------	----------	---------	--------
F	3.3	1.7 –1.8	--------	----------	----------	.37– .44	-------	----------	---------	--------
*H_2O+	--------	--------	--------	----------	----------	----------	-------	----------	---------	--------
Precambrian diabase:										
Cl	.83	.24	--------	----------	----------	----------	-------	----------	---------	0.05–0.09
F	2.1	<.04	--------	----------	----------	----------	-------	----------	---------	1.4
*H_2O+	--------	--------	--------	----------	----------	----------	-------	----------	---------	3.42–3.43

* Calculated by difference assuming ideal [Cl, F, OH].
† Calculated assuming all O_1 oxygen sites occupied by Cl, F, and OH.

TABLE 3.—Cl, F, *and* H_2O+ *contents in igneous apatite from Laramide intrusive rocks near the Ray porphyry copper deposit, Arizona*

Rock type	Probe sample	Grain No.	Grain Occurrence [1]	Contents (weight percent) [2]Cl	[2]F	[3]H_2O+
Tortilla Quartz Diorite.	217–28	1A	H	0.67±0.04	2.4±0.1	0.47
		5A	P	.61± .04	1.6± .1	.88
		5AA	P	.64± .07	2.0± .1	.68
	217–1	1A	P	.97± .07	1.7± .1	.73
		5A	P	1.0 ± .09	1.9± .1	.63
		7A	M	.67± .05	2.1± .1	.67
	248–29	1A	P	.53± .03	1.6± .1	.87
		2A	P	.42± .01	1.5± .1	.94
		3A	P	.46± .04	1.2± .2	1.09
Rattler Granodiorite.	46–99B	T17A	H	.80± .02	1.9± .01	.69
		T16A	PL	.64± .02	2.4± .1	.53
		T19A	M	1.3 ± .002	1.9± .04	.51
		T20A	P	1.4 ± .02	1.5± .05	.72
	60–113D	T22A	P	.73± .02	2.3± .1	.52
		T21A	P	.73± .02	2.2± .1	.54
	60–108	1A	P	.14± .01	2.7± .1	.48
		3A	P	.29± .04	2.6± .1	.47
		6A	P	.25± .02	2.5± .1	.53
	61–25	T14A	P	.42± .02	2.8± .1	.37
		T15A	GM	.35± .02	2.8± .1	.39
	60–91	1A	P	.34± .02	2.2± .2	.65
		2A	B	.36± .01	2.3± .2	.60
		6A	P	.47± .05	2.2± .1	.59
	60–111	2A	P	.75± .05	2.1± .1	.60
	60–98	1A	M	.47± .05	2.3± .2	.57
		3A	B	.45± .02	2.5± .1	.47
		6A	P	.47± .01	2.6± .1	.43
	246–11G	6A	P	.25± .03	2.5± .2	.50
		6AA	P	.23± .02	2.6± .2	.48
		7A	B	.45± .01	2.5± .2	.46
	60–131	M1A	P	.62± .02	2.4± .1	.46
		M2A	GM	.58± .03	2.5± .2	.42
	60–130	3A	B	.34± .04	2.7± .1	.40
	260–96A	2A	B	.52± .07	2.2± .2	.59
		3A	B	.54± .01	2.1± .1	.61
		3AA	B	.60± .03	2.1± .1	.62
	46–11A	1A	P	.25± .01	2.3± .2	.63
		3A	B	.20± .02	2.6± .2	.50
		4A	P	.30± .02	2.8± .1	.37
	T16–630	3A	P	.34± .04	2.2± .2	.65
		7A	B	.57± .02	2.3± .1	.55
Rhyodacite dike.	17–16	1A	P	.28± .13	2.4± .2	.58
		M1A	P	.37± .17	2.4± .4	.54
		M2A	P	.14± .06	2.8± .1	.41
Rhyodacite dike.	GM100	7A	B	.11± .02	2.3± .3	.67
		XA	P	.09± .02	2.4± .2	.63
		YA	P	.08± .04	1.2± .2	1.21
Granite Mountain Porphyry.	RB5	2A	B	ND	3.0± .1	.36
		3A	B	ND	3.0± .1	.36
		3AA	B	ND	3.2± .1	.26
	GM14	T33A	B	ND	3.0± .1	.39
		T33B	B	ND	3.1± .1	.32
	GM12	2A	B	ND	2.8± .2	.45
		3A	B	ND	3.3± .2	.21
		4A	B	ND	3.3± .2	.21
	GM18	2A	P	ND	3.2± .2	.28
		7A	P	ND	3.0± .3	.36
		8A	P	ND	2.9± .1	.42
	2GM6G	1MA	P	.03± .01	3.2± .1	.24
		2MA	B	ND	3.6± .2	.06
		5A	P	ND	3.3± .2	.22
	2GM1A	1A	P	ND	3.5± .3	.13
		1AA	P	ND	3.0± .5	.29
		2A	P	ND	3.0± .1	.36
	2GM2A	5A	PL	ND	2.9± .1	.41
		5AA	PL	.02± .01	3.4± .1	.15

TABLE 3.—Cl, F, *and* H_2O+ *contents in igneous apatite from Laramide intrusive rocks near the Ray porphyry copper deposit, Arizona*—Continued

Rock type	Probe sample	Grain No.	Grain Occurrence [1]	Contents (weight percent) [2]Cl	[2]F	[3]H_2O+
Teapot Mountain Porphyry.	2TTM	1A	B	.13± .02	2.6± .2	.51
		2A	GM	.09± .02	3.3± .1	.20
		5A	B	.12± .01	2.6± .2	.53
		5AA	GM	.11± .01	2.8± .1	.42
Rhyodacite dike.	61–2F	T18A	GM	.77± .03	1.4± .1	.91
		T10A	P	.16± .02	1.7± .1	.92

[1] Grain occurrence: P, phenocryst or large grain; H, inclusion in hornblende; B, inclusion in biotite; M, inclusion in magnetite; Pl, inclusion in plagioclase; and GM, groundmass.

[2] Microprobe analysis. Precision calculated from standard counting error from mean of 6 to 10 data points. ND, not detected at 0.02 wt percent Cl.

[3] Calculated assuming ideal [Cl, F, OH].

TABLE 4.—Cl, F, *and* H_2O+ *contents in Laramide igneous and hydrothermal biotite in and near the Ray porphyry copper deposit, Arizona.*

Rock type	Probe sample	Grain No.	Contents [1] (weight percent) [2]Cl	[2]F	[3]H_2O+
Tortilla Quartz Diorite.	217–28	2BIC	0.13±0.01	0.27±0.01	3.87
		2BIE	.14± .01	.26± .01	3.85
		5BIC	.15± .01	.26± .03	3.80
		5BIE	.13± .02	.25± .05	3.81
	217–1	1BIC	.15± .02	.14± .03	3.89
		1BIE	.15± .02	.16± .02	3.94
		5BI	.17± .01	.19± .04	3.89
		4BIC	.12± .02	.23± .02	3.88
		4BIE	.14± .01	.20± .03	3.94
Rattler Granodiorite.	246–99B	*3BIC	.18± .003	.27± .04	3.80
		*3BIE	.19± .003	.30± .06	3.78
	260–113D	3BIC	.23± .01	.34± .05	3.77
		3BIE	.26± .03	.41± .04	3.74
		*4BI	.23± .01	.37± .02	3.75
	261–25	1BIC	.15± .004	.46± .03	3.71
		1BIE	.14± .003	.47± .09	3.73
		3BIC	.14± .003	.54± .05	3.62
		CHEM	[4] .12	[5] .42	3.3
	60–91	2BIC	.13± .01	.34± .03	3.83
		2BIE	.12± .01	.29± .02	3.83
		4BIC	.12± .01	.32± .03	3.85
		4BIE	.10± .01	.31± .05	3.88
		5BIC	.13± .01	.31± .04	3.81
		5BIE	.12± .01	.36± .05	3.80
	60–111	2BI1C	.18± .01	.39± .03	3.82
		2BI1E	.19± .01	.41± .04	3.80
		2BI2C	.20± .02	.40± .03	3.78
		2BI2E	.19± .01	.36± .03	3.82
		1BIC	.17± .01	.37± .05	3.85
	246–11G	3BIC	.12± .01	.49± .03	3.74
		3BIE	.14± .01	.46± .04	3.75
		4BIC	.13± .01	.48± .05	3.74
		4BIE	.11± .01	.50± .06	3.78
	60–131	1BIC	.13± .01	.38± .03	3.79
		1BIE	.13± .01	.35± .03	3.82
		2BIC	.12± .01	.40± .03	3.81
		2BIE	.11± .01	.38± .04	3.82
		3BI	.14± .01	.43± .02	3.76
		4BIC	.13± .01	.45± .03	3.82

TABLE 4.—Cl, F, *and* H_2O+ *contents in Laramide igneous and hydrothermal biotite in and near the Ray porphyry copper deposit, Arizona*—Continued

Rock type	Probe sample	Grain No.	Contents [1] (weight percent)		
			[2]Cl	[2]F	[3]H_2O+
Rattler Granodiorite—Con.		4BIE	.14± .01	.42± .05	3.80
		5BI	.18± .01	.43± .03	3.73
	60–130	2BI	.16± .01	.40± .03	3.79
	260–96A	3BIC	.15± .01	.45± .04	3.80
		3BIE	.16± .01	.46± .03	3.78
	246–11A	1BIC	.14± .01	.60± .03	3.68
		1BIE	.14± .01	.61± .05	3.66
		5BIC	.16± .01	.62± .04	3.63
		5BIE	.15± .01	.62± .05	3.63
	T16–630	1BI	.10± .01	.31± .03	([6])
		3BI	.11± .001	.28± .03	([6])
		4BI	.11± .01	.34± .04	([6])
		5BI	.10± .01	.29± .03	([6])
		9BI	.12± .01	.36± .05	([6])
Rhyodacite dike.	2GM100	1BIC	.15± .004	.16± .03	3.81
		1BIE	.09± .01	.25± .01	3.79
		3BIC	.07± .003	.20± .04	3.85
		3BIM	.09± .02	.23± .04	3.83
		3BIE	.06± .01	.25± .07	3.83
Granite Mountain Porphyry.	RB5	6BIC	.04± .02	.56± .03	3.67
		6BI1E	.05± .01	.50± .02	3.69
		6BI2E	.04± .002	.52± .03	3.68
		7BIC	.04± .01	.58± .06	3.65
		7BIE	.03± .01	.59± .03	3.67
	2GM14	2BI	.02± .01	.67± .07	3.61
		2BIA	.02± .01	.61± .04	3.67
		6BI	.02± .01	.63± .04	3.59
	GM12	4BI	.05± .01	.61± .07	3.64
		2BI	.03± .01	.69± .05	3.61
		3BI	.05± .01	.61± .05	3.63
		3BIA	.02± .01	.63± .03	3.65
	GM18	MBIC	.04± .01	.75± .05	3.59
		MBIE	.04± .003	.72± .05	3.61
		M1BIC	.03± .01	.82± .05	3.57
		M1BIE	.02± .004	.81± .04	3.62
		M2BIC	.03± .01	.62± .06	3.66
		M2BIE	.04± .01	.54± .12	3.70
	GM6G	3BIA	.02± .006	.66± .06	3.58
		4BIA	.03± .006	.69± .04	3.60
	2GM6G	4BI	.03± .01	.76± .13	3.52
	2GM4V	1BIA	.02± .004	.77± .06	3.59
		3BIA	.03± .006	.86± .04	3.58
		3BIB	.04± .01	.82± .05	3.55
	GM2A	1BI	.02± .01	.72± .18	3.60
Mineralized diabase.	P70–22	1BI	.05± .02	1.4 ± .1	3.43
		1BIA	.09± .03	1.4 ± .2	3.42
Mineralized Granite Mountain Porphyry.	T123	BI1	.06± .005	1.7 ± .1	3.22
		BI2	.06± .003	1.7 ± .1	3.22

* Inclusion in hornblende.
[1] Precision calculated from standard counting error from the mean of 5 to 10 data points collected within a 10×10 μm area.
[2] Microprobe analysis.
[3] Calculated assuming ideal [Cl, F, OH].
[4] Cl by chemical analysis; J. Budinsky, analyst.
[5] F and H_2O+ by chemical analysis; M. Cremer, analyst.
[6] Incomplete analysis; H_2O+ was not calculated.

TABLE 5.—Cl, F, *and* H_2O+ *contents in hornblende from Laramide intrusive rocks near the Ray porphyry copper deposit, Arizona*

Rock type	Probe sample	Grain No.	Contents [1] (weight percent)		
			[2]Cl	[2]F	[3]H_2O+
Tortilla Quartz Diorite.	217–28	2H	0.08±0.007	0.16±0.03	1.92
		3H	.07± .007	.16± .02	1.94
		4H	.09± .012	.13± .04	1.94
		4HA	.07± .007	.11± .06	1.95
	248–29	1H	.02± .004	.12± .03	1.96
		2HC	.03± .009	.14± .03	1.99
		2HE	.02± .005	.14± .02	2.00
		3H	.03± .004	.15± .03	1.97
Rattler Granodiorite.	246–99B	1HC	.10± .007	.19± .05	1.93
		1HE	.07± .005	.17± .02	1.93
		2H	.08± .006	.16± .03	1.94
		3HC	.08± .006	.22± .02	1.91
		3HM	.08± .006	.22± .02	1.91
		3HE	.09± .012	.14± .02	1.98
	60–113D	MHC	.09± .010	.24± .02	1.89
		MHE	.13± .008	.24± .02	1.90
		M1HC	.17± .013	.21± .01	1.87
		M1HE	.14± .007	.22± .03	1.88
		M2HC	.17± .006	.23± .02	1.85
		M2HE	.12± .010	.23± .03	1.88
	60–108	1H	.09± .009	.48± .06	1.76
		4HC	.05± .007	.58± .03	1.77
		4HE	.09± .005	.48± .02	1.79
		6HC	.06± .004	.45± .05	1.83
		6HE	.09± .005	.54± .04	1.79
	T16–630	4H	.05± .008	.14± .05	([4])
		6H	.03± .007	.14± .03	([4])
		8H	.04± .007	.21± .03	([4])
	261–25	MH	.08± .010	.30± .03	1.84
		4H	.04± .013	.27± .02	1.93
		5HC	.07± .002	.26± .01	1.80
		5HE	.06± .002	.31± .01	1.83
	60–91	MH	.10± .013	.21± .02	1.85
		4MHC	.05± .004	.22± .04	1.93
		4MHE	.05± .002	.18± .01	1.91
		1MH	.03± .06	.22± .02	1.95
	60–98	MHC	.04± .008	.24± .03	1.86
		MHE	.04± .021	.24± .02	1.90
		1MH	.05± .010	.27± .04	1.86
	246–11G	3H	.04± .016	.30± .04	1.89
		5HC	.06± .017	.28± .03	1.91
		5HE	.06± .038	.26± .04	1.93
		7HC	.04± .010	.29± .02	1.91
		7HE	.04± .001	.26± .02	1.93
Rhyodacite dike.	17–16	MHC	.14± .012	.17± .03	1.87
		MHE	.15± .009	.17± .02	1.87
		M1H	.15± .015	.15± .04	1.89
		2HC	.13± .010	.17± .05	1.88
		2HE	.15± .011	.17± .03	1.89
Rhyodacite dike.	GM100	MH	.03± .005	.12± .03	1.98
		M1H	.08± .024	.14± .02	1.90
		M2H	.04± .010	.13± .03	1.97
Granite Mountain Porphyry.	GM18	T1HC	.06± .007	.38± .03	1.79
		T1HE	.08± .005	.39± .04	1.77

[1] Precision for Cl and F calculated from standard counting error from the mean of 5 to 10 data points collected within a 10×10 μm area.
[2] Microprobe analysis.
[3] Calculated assuming ideal [Cl, F, OH].
[4] Incomplete analysis; H_2O+ was not calculated.

TABLE 6.—Cl, F, *and* H_2O+ *contents in igneous (?) epidote and igneous sphene from Laramide intrusive rocks near the Ray porphyry copper deposit, Arizona*

Rock type	Probe sample	Grain No.	Contents (weight percent) [1]Cl	[1]F	[2]H_2O+
Epidote analyses					
Tortilla Quartz Diorite.	217–1	6PE [3]	ND	ND	1.88
Rattler Granodiorite.	246–99B	MPE [3]	ND	ND	1.86
Sphene analyses					
Tortilla Quartz Diorite.	217–1	6PS [3]	0.02±0.007	0.09±0.02	1.10
	217–28	2PS [4]	ND	.09± .04	1.12
Rattler Granodiorite.	246–99B	4PS [4]	ND	.08± .02	1.12
	246–11G	MPSC [4]	ND	.12± .02	1.07
		MPSE [4]	ND	.12± .03	1.07
		7PS [5]	ND	.16± .03	1.06
	261–25	MPS [4]	ND	.12± .02	1.08
	T16–630	2PS [4]	ND	.08± .02	([6])
		10PS [4]	ND	.09± .01	([6])
Granite Mountain Porphyry.	RB5	5PSC [4]	ND	.25± .03	1.03
		5PSE [4]	ND	.24± .02	1.02
	2GM14	4PS [5]	ND	.30± .03	.99

[1] Microprobe analysis. Precision calculated from standard counting error from the mean of 5 to 10 data points within a 10×10 μm area. ND, not detected at 0.02 wt percent Cl, 0.04 wt percent F.
[2] Calculated assuming ideal [Cl, F, OH].
[3] Interstitial to feldspar and Fe-Mg silicates.
[4] Phenocryst or large grain.
[5] Included in biotite.
[6] Incomplete analysis; H_2O+ not calculated.

TABLE 7.—Cl *and* F *contents in chlorite derived from biotite in Laramide igneous rocks in and near the Ray porphyry copper deposit, Arizona*

Rock type	Probe sample	Grain No.	Contents [1] (weight percent) [2]Cl	[2]F
Tortilla Quartz Diorite.	217–28	5CL	ND	ND
Rattler Granodiorite.	246–99B	1CLA	ND	ND
		1CLB	0.03±0.012	0.10±0.02
		2CLA	ND	ND
		2CLB	ND	ND
	260–113D	3CLA	.04± .001	.05± .001
		3CLB	.03± .004	.08± .02
		4CLA	.03± .003	.13± .03
		4CLB	ND	.08± .03
	261–25	2CLA	ND	.07± .02
		2CLB	ND	.16± .07
	246–11G	2CLA	ND	.09± .03
		2CLB	ND	.11± .01
		4CL	ND	.11± .001
	260–96A	3CL	ND	.12± .001
	246–11A	1CLA	.03± .007	.30± .04
		1CLB	.03± .008	.24± .03
		5CLA	.02± .008	.15± .03
		5CLB	.02± .006	.27± .02
	T16–630	1CL	ND	.12± .03
		5CL	ND	.09± .01
		8CL	ND	.13± .05
		10CL	ND	.10± .04
Granite Mountain Porphyry.	2GM14	2CL	ND	.12± .03
		6CL	ND	.13± .03
		6CLA	ND	.10± .03
	GM12	3CL	ND	.14± .02
		3CLA	ND	.13± .02
		4CL	ND	.14± .04

TABLE 7.—Cl *and* F *contents in chlorite derived from biotite in Laramide igneous rocks in and near the Ray porphyry copper deposit, Arizona*—Continued

Rock type	Probe sample	Grain No.	Contents [1] (weight percent) [2]Cl	[2]F
Granite Mountain Porphyry—Continued	GM6G	3CLA	ND	.09± .03
		4CLA	ND	.16± .03
	2GM6G	4CL	ND	.06± .04
		6CL	ND	.07± .06
		6CLA	ND	.10± .06
	2GM4V	1CL	ND	.16± .03
		1CLA	ND	.19± .04
		3CL	ND	.23± .04
	2GM2A	3CL	ND	.18± .09
		4CL	ND	.16± .05
		5CL	ND	.16± .11
	2GM1A	2CL	.03± .009	.23± .08
		2CLA	.03± .013	.27± .13
		2CLB	.03± .008	.26± .13
Mineralized diabase.	P70–22	1CL	.05± .016	.27± .13

[1] Precision calculated from standard counting error from the mean of 4 to 10 data points within a 10×10 μm area.
[2] Microprobe analysis. ND, not detected at 0.02 wt percent Cl, 0.04 wt percent F.

TABLE 8.—Cl *and* F *contents in minerals formed from biotite, plagioclase, pyroxene, and chlorite in Laramide intrusive rocks near the Ray porphyry copper deposit, Arizona*

Rock type	Probe sample	Grain No.	Contents [1] (weight percent) [2]Cl	[2]F
Epidote after biotite				
Tortilla Quartz Diorite.	217–1	6SE	ND	ND
Rattler Granodiorite.	260–113D	2SE	ND	0.11±0.05
		5SE	ND	.07± .02
	261–25	1SE	ND	.09± .08
	246–11G	2SE	ND	.05± .02
Granite Mountain Porphyry.	RB5	4SE	ND	.06± .01
	2GM6G	1SE	ND	.04± .03
Sphene after biotite				
Tortilla Quartz Diorite.	217–1	3SS	ND	0.51±0.05
Rattler Granodiorite.	246–99B	1SS	ND	1.4 ± .2
	261–25	1SS	ND	.18± .01
	246–11G	2SS	ND	2.2 ± .1
		3SS	ND	1.3 ± .2
		6SS	ND	1.0 ± .03
	246–11A	4SS	ND	1.1 ± .1
	T16–630	1SS	ND	.74± .15
		8SS	ND	1.2 ± .07
		10SS	ND	.66± .05
Granite Mountain Porphyry.	RB5	4SS	ND	1.7 ± .2
		5SS	ND	1.5 ± .2
	GM12R	4SS	ND	.20± .02
		3SS	ND	.50± .03
	2GM14	6SSA	ND	.66± .09
		6SSB	ND	.49± .10
	GM6G	2D	0.09±0.02	2.5 ± .3
	2GM6G	6SSA	ND	.44± .04
		6SSB	ND	.65± .03

TABLE 8.—Cl *and F contents in minerals formed from biotite, plagioclase, pyroxene, and chlorite in Laramide intrusive rocks near the Ray porphyry copper deposit, Arizona*—Continued

Rock type	Probe sample	Grain No.	Contents [1] (weight percent) [2]Cl	[2]F
Phengite and clay analyses				
Tortilla Quartz Diorite.	217–1	MSP [3]	0.03±0.03	ND
Granite Mountain Porphyry	2GM14	4SPA [3]	ND	ND
	GM12R	4SPA [3]	ND	0.04±0.05
	GM2A	4P [4]	ND	.55± .02
		5P [4]	ND	.45± .08
Hydrogarnet(?) after biotite				
Tortilla Quartz Diorite.	217–28	4M	ND	0.69±0.10
Rattler Grano-diorite.	260–113D	3M	ND	1.8 ± .1
	T16–630	5M	ND	1.4 ± .1
		9M	ND	1.6 ± .1
Fibrous amphibole analysis				
Tortilla Quartz Diorite.	217–1	MFHB [5]	0.02±0.008	0.11±0.03

[1] Precision calculated from standard counting error from the mean of 5 to 10 data points within a 10×10 μm area.
[2] Microprobe analysis. ND, not detected at 0.02 wt percent Cl, 0.04 wt percent F.
[3] Alteration product of plagioclase.
[4] Alteration product of chlorite.
[5] Reaction rim on pyroxene.

TABLE 9.—Cl *and* F *contents in igneous and alteration minerals from Precambrian intrusive rocks near the Ray porphyry copper deposit, Arizona*

Rock type (Sample No.)	Mineral	Grain No.	Contents [1] (weight percent) [2]Cl	[2]F
Ruin Granite (PCR).	Biotite	2BI	0.13±0.01	1.7 ±0.07
		3BI	.12± .01	1.7 ± .09
		3B12	.11± .004	1.7 ± .04
		M1BI	.10± .01	1.8 ± .15
	Chlorite	2CL	ND	0.44± .01
		3CL	ND	.43± .03
		4CL	ND	.37± .04
	Apatite	3A	.11± .02	3.3 ± .14
		3A2	.11± .01	3.3 ± .09
Diabase (DBA–32).	Biotite	MBI	.24± .04	ND
	Apatite	7A	.83± .06	2.1 ± .28

[1] Precision calculated from standard counting error from the mean of 5 to 8 data points in a 10×10 μm area.
[2] Microprobe analysis. ND, not detected at 0.02 wt percent Cl, 0.04 wt percent F.

fine to resolve, and also one grain of fibrous amphibole formed from pyroxene are included in table 8. Cl occurs near or below detection level in the clay, phengites, and amphibole; only the intensely altered area in the plagioclase, the phengite derived from chlorite, and the amphibole contain detectable amounts of F.

Intrasample variations and zoning

The igneous minerals in the Laramide rocks studied have not been homogenized with respect to the halogens (or other constituents; author, unpub. data) by exchange with magma, magmatic fluid, or postmagmatic fluid. Measurably different abundances of one or both halogens occur between like-mineral grains in the same sample (40 percent of the samples for apatite, 25 percent for biotite, and 35 percent for hornblende) and zoning of major and (or) minor elements is found in apatite, biotite, and hornblende as well as in plagioclase. Analytically distinguishable zoning of Cl or F, or both, occurred in 11 of 34 apatite grains and in 9 of 16 hornblende grains studied for zoning, whereas zoning of the halogens in biotite was seldom detected (compare grain numbers ending in C, centers, and E, edges; table 4). Neither the zoning or abundance of Cl or F in the igneous minerals seems related to the amount of plagioclase or mafic minerals altered in a sample (table 1), proximity of altered grains to the one analyzed, or the potential susceptibility of a grain to exchange by virtue of its size or inclusion in other minerals. (See mineral occurrence data in table 3, and in footnotes of tables 4 and 6.) However, although the minerals have not been homogenized with respect to the halogens, there are no firm trends in the variations (figs. 6 and 7). This suggests that if the observed abundances and variations retain an imprint of those obtained from the magma, then the conditions controlling uptake of Cl, F, and H_2O by the minerals from the magma were complex. Not enough data were collected for epidote or sphene to make conclusions regarding zoning of Cl and F.

Intersample variations with rock chemistry, Laramide rocks

The abundances of Cl, F, and H_2O+ in the igneous minerals vary measurably between samples, and these variations appear to be related to greater or lesser degree to variations in whole-rock chemistry (as indicated by differentiation indices, D.I., of the samples). The abundance of Cl in apatite and biotite correlates negatively with rock D.I. (fig. 8), the abundance of F in apatite, biotite, sphene, and perhaps hornblende correlates positively with rock D.I. (fig. 9; tables 6 and 1 for sphene), and the abundance of calculated H_2O+ in apatite, biotite, sphene, and perhaps hornblende correlates negatively with rock D.I. (fig. 10; tables 6 and 1 for sphene). Correlations of the mineral contents of Cl, F, and H_2O+ with rock D.I. for the samples from the Rattler Granodiorite generally mirror but are not as strong as those for the entire sample suite. Table 10

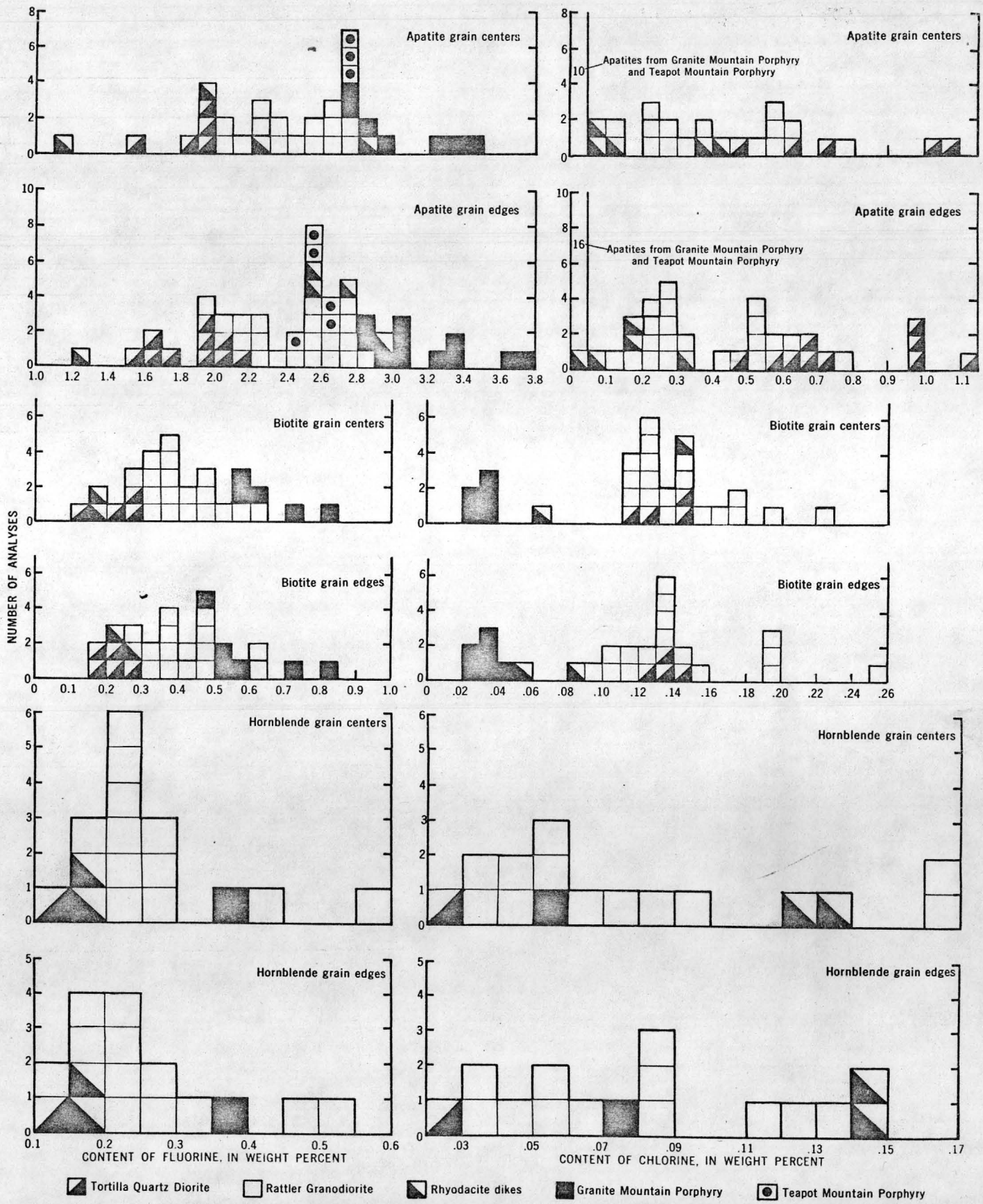

FIGURE 6.—Frequency distribution of F and Cl contents in centers and edges of apatite, biotite, and hornblende grains, Laramide rocks.

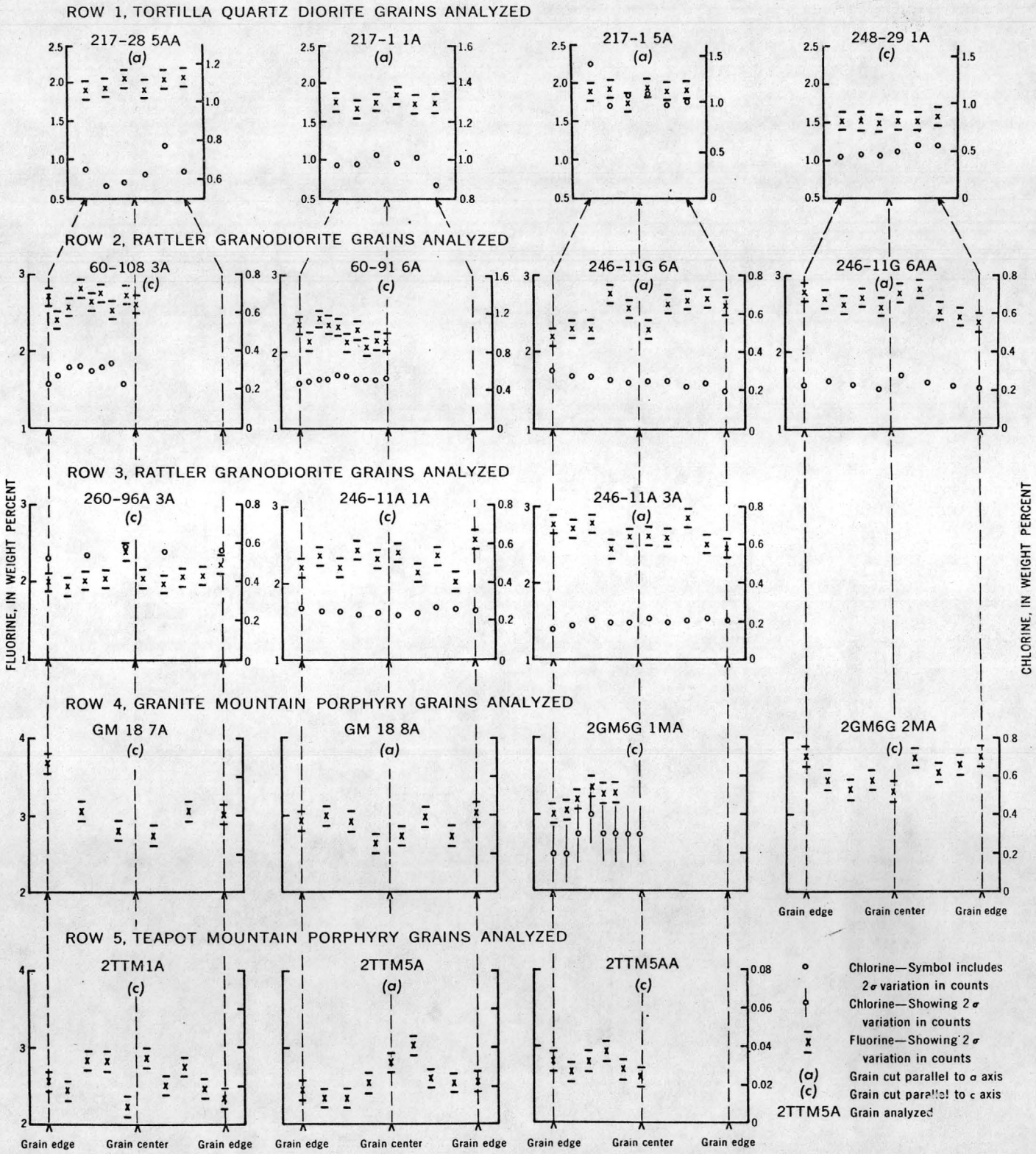

Figure 7.—Distribution of Cl and F in individual apatite grains in Tortilla Quartz Diorite, Rattler Granodiorite, Granite Mountain Porphyry, and Teapot Mountain Porphyry.

presents statistical data for figures 8–10. The Pearson correlation assumes that the samples are representative of a larger population, whereas the Spearman rank correlation simply ranks the sample data without any weighting of the samples. Thirty percent of the trends considered have correlation coefficients exceed-

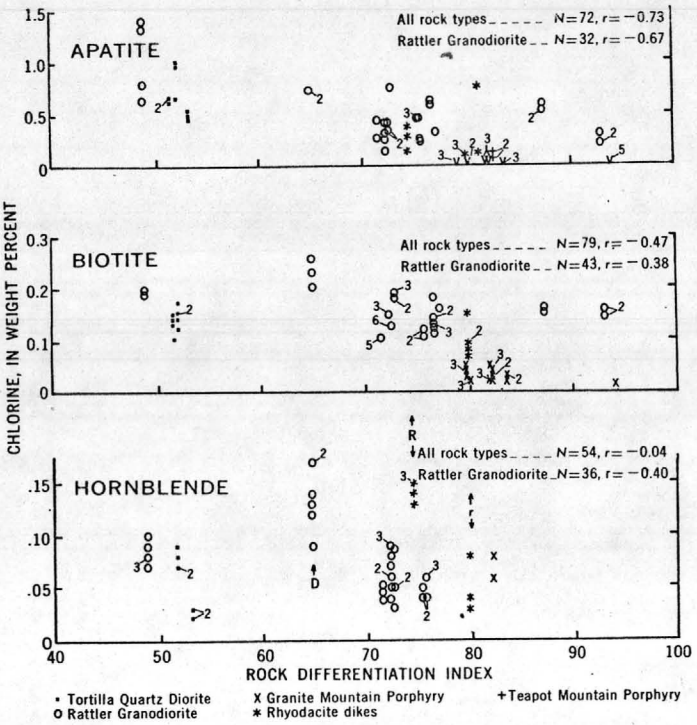

Figure 8.—Variations of Cl content of mineral with rock differentiation index.

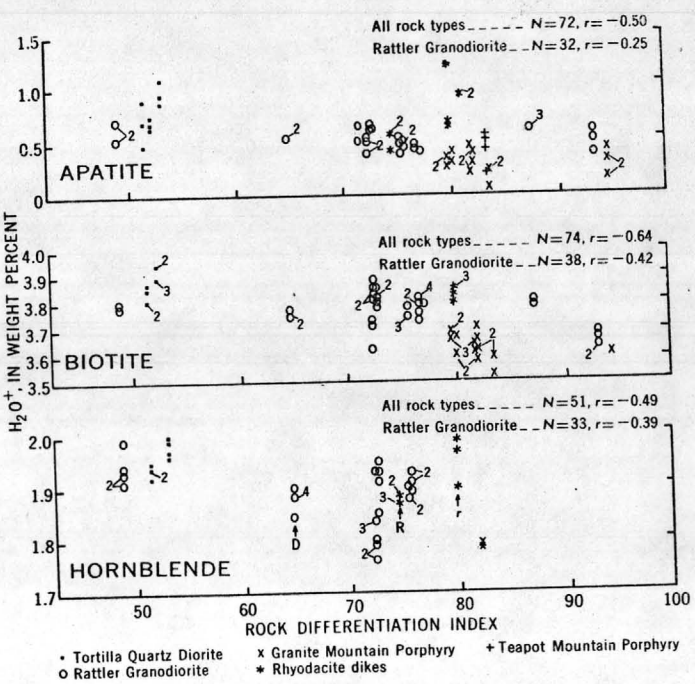

Figure 10.—Variations of calculated H_2O+ content of mineral with rock differentiation index.

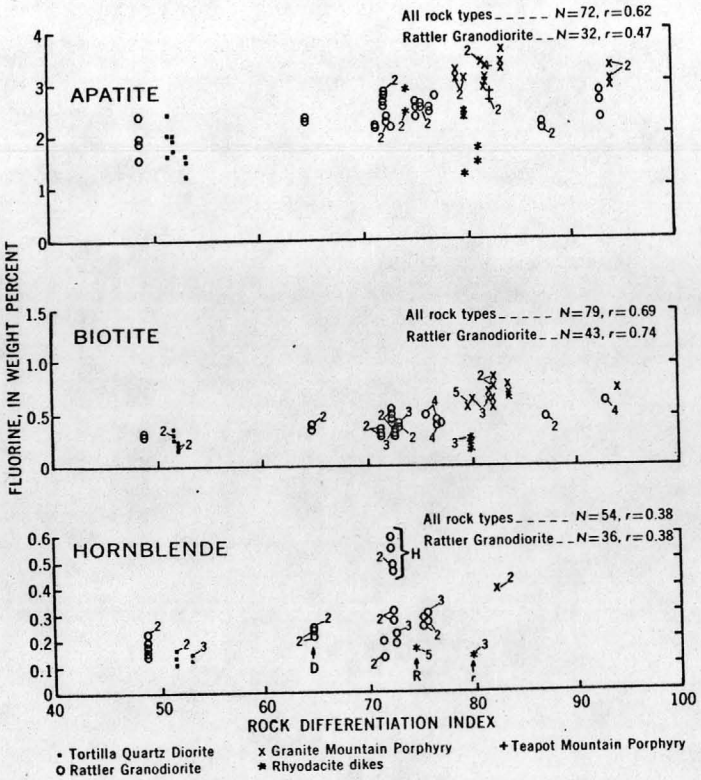

Figure 9.—Variations of F content of mineral with rock differentiation index.

ing |0.65| and are thought to have geological significance. Fifty-five percent of the trends have correlation coefficients that exceed |0.50|, and all but one of those with coefficients less than |0.65| have the same slope as the trends with high correlation coefficients.

The positive association of the abundance of F and a negative or lack of association of the abundance of Cl and H_2O+ in the minerals with increasing differentiation index of the host rock is not unique to the Ray igneous suite. Goldschmidt (1954) found that the F content of igneous minerals increases as the host rock becomes more felsic. The Cl and H_2O+ contents are higher and the F contents lower in apatites from mafic rocks than in apatite from more felsic rocks (A. Kind, cited by Correns, 1956; Taborszky, 1962). Nash (1972a, b) reported that the F content of apatite increased with differentiation of the Iron Hill complex and Shonkin Sag laccolith, and his data indicate that the Cl content of apatite either remained the same or decreased as the host rocks became more differentiated in both intrusive suites. Lee and Van Loenen (1970) found that the F content of biotite increases with decreasing CaO content of hybrid rocks of the southern Snake Range, Nev., and the data of Ivanov (1971), Dodge and Moore (1968), Dodge and others (1968, 1969), Dodge and Ross (1971) suggest the same for F content of biotite from igneous rocks of central Chukatka, Russia, the Sierra Nevada batholith, and the

TABLE 10.—*Statistical data for* Cl, F, *and* H_2O+ *contents of minerals and rocks plotted against differentiation index (figures 8–12)*

Rock type	Mineral	Cl, F, and H_2O+ in mineral	Pearson correlation			Spearman rank correlation			
			r	*N*	Confidence level	Coefficient	*t* test	Degrees of freedom	Confidence level
Data from figure 8									
All	Apatite	Cl	−0.73	72	>99	−0.69	−8.0	70	>99
	Biotite	Cl	−.47	79	>99	−.51	−5.2	77	>99
	Hornblende	Cl	−.04	54	--	−.18	−1.35	52	>85
Rattler Granodiorite	Apatite	Cl	−.67	32	>99	−.40	−2.45	30	>95
	Biotite	Cl	−.28	43	<95	.01	.05	41	--
	Hornblende	Cl	−.40	46	>95	−.60	−4.43	34	>99
Data from figure 9 [a]									
All	Apatite	F	0.62	72	>99	0.59	6.2	70	>99
	Biotite	F	.69	79	>99	.74	9.7	77	>99
	Hornblende	F	.54	54	>99	.34	2.57	52	>95
	Sphene	F	.66	12	>95	.94	8.2	10	>99
Rattler Granodiorite	Apatite	F	.47	32	>99	.29	1.64	30	>90
	Biotite	F	.74	43	>99	.65	5.5	41	>99
	Hornblende	F	.38	36	>95	.48	3.23	34	>99
	Sphene	F	.58	7	<95	.89	([b])	([b])	([b])
Data from figure 10 [a]									
All	Apatite	H_2O+	−0.50	72	>99	−0.52	−5.1	70	>99
	Biotite	H_2O+	−.64	74	>99	−.66	−7.6	72	>99
	Hornblende	H_2O+	−.49	51	>99	−.31	−2.25	49	>99
	Sphene	H_2O+	−.87	10	>95	−.98	−1.59	8	>85
Rattler Granodiorite	Apatite	H_2O+	−.25	32	<95	−.24	−1.32	30	>85
	Biotite	H_2O+	−.42	38	>99	−.17	−1.01	36	>80
	Hornblende	H_2O+	−.39	33	>95	−.04	−2.13	31	>95
	Sphene	H_2O+	−.97	5	>95	−.92	([b])	([b])	([b])

Rock type	Figure part	Cl, F, and H_2O+ in mineral	Pearson correlation			Spearman rank correlation			
			r	*N*	Confidence level	Coefficient	*t* test	Degrees of freedom	Confidence level
Data from figure 11									
All	*A*	Cl	−0.75	20	>99	−0.81	−5.9	18	>99
Rattler Granodiorite	*A*	Cl	−.70	11	>95	−.55	−1.98	9	>90
All	*B*	F	−.39	20	<95	−.29	−1.30	18	>80
Rattler Granodiorite	*B*	F	−.57	11	>95	−.66	−2.54	9	>95
Data from figure 12									
All	*A*	H_2O+	−0.36	27	<95	−0.39	−2.10	25	>95
	B	H_2O+	−.44	22	>95	−.34	−1.62	20	>90
	C	H_2O+	−.80	20	>99	−.70	−4.18	18	>99
Rattler Granodiorite	*A*	H_2O+	−.16	18	--	−.27	−1.13	16	>80
	B	H_2O+	−.40	13	<95	−.27	−9.2	11	>99
	C	H_2O+	−.83	11	>99	−.61	−2.30	9	>95

[a] Sphene not included in figures 9 and 10. [b] Small sample set.

California Transverse and Coast Ranges. In addition, the Cl and H_2O+ contents of biotite and hornblende in the Sierra Nevada batholith (data of Dodge and others, 1968, 1969), intrusive rocks of the Coast and Transverse Ranges (data of Dodge and Ross, 1971), and of Scandinavian granites (Gillberg, 1964) either correlate negatively or do not correlate with increasing host rock acidity.

Intersample variations with sample age, Laramide rocks

Minerals from the oldest Laramide stocks at Ray (Tortilla Quartz Diorite, Rattler Granodiorite) generally contain more Cl and H_2O+ and less F than minerals from the younger stocks (Granite Mountain Porphyry, Teapot Mountain Porphyry). This correlation between the age of a pluton and the Cl, F, and H_2O+ content of its minerals is expected because the contents of these components in the minerals appear related to rock chemistry and, in general, there is a negative correlation between rock differentiation index and the age of the rock type. There are five exceptions: (1) Apatite from the Teapot Mountain Porphyry contains about the same or a little more Cl and H_2O+ and perhaps less F than apatite in the older Granite Mountain Porphyry; (2) hornblende in sample 17–16 (*R* in figs. 8–10) contains more Cl than hornblende in

the Tortilla Quartz Diorite which it cuts; (3) biotite in sample GM100 (*r* in figs. 8–10) contains less F and more H_2O+ than the older Rattler Granodiorite; (4) apatite in sample 61–2F (asterisk symbols in figs. 8–10 plotted at greater than 80 differentiation index), which may be the youngest intrusive type studied, contains less F and more Cl and H_2O+ than apatite from the Granite Mountain Porphyry; and (5) hornblende and biotite in sample 60–113D (*D* in figs. 8–10), which was intruded as a late dike in the Rattler Granodiorite but prior to aplite development (Cornwall and others, 1971), contain more Cl than do the hornblende and biotite from the samples cut by the dike.

Four of the five exceptions involve minerals from dikes that probably were more susceptible than the stocks to gain and loss of Cl, F, and H_2O+ by diffusion and contamination. Moreover, for most of the exceptions, only one or two rather than all three components are present in a given mineral in amounts anomalous for the age of the sample, and in several of the exceptions, one of the other coexisting minerals does not show the anomaly.

Intersample variations with rock texture and modal abundance, Laramide rocks

Porphyritic texture is sometimes attributed to the buildup and release of volatiles from a cooling magma (pressure quenching, Jahns and Tuttle, 1963). Thus one should perhaps expect the hydrous minerals in porphyritically textured rocks to have different halogen and water contents compared to like minerals in nonporphyritic rocks. However, the halogen and water contents of the igneous minerals are not consistently related to the texture (even porphyritic texture) of the rock. (Compare rock textures in table 1 with data in tables 3–5 or figures 8–10).

Competition for the available water and halogens in the magmas also might be expected to affect the amount of water and halogens incorporated by the minerals, and this might be detected by comparing the compositions of like minerals from samples from the same rock type having like differentiation index but different modal composition. However, a consistent pattern does not emerge from such comparisons. For example, hornblende in sample 48–29 (Tortilla Quartz Diorite) contains three times less Cl and is three times as abundant as the hornblende in sample 17–28, but the F contents of the hornblende in the two samples are not appreciably different. Similarly, samples 61–25 and 60–91 of the Rattler Granodiorite have almost identical differentiation indices as those of samples 60–108 and 60–111 and contain half the amount of biotite (about 6 percent) as that in sample 60–111, which contains no hornblende, and half the amount of hornblende (about 4 percent) as that of sample 60–108, which contains no biotite. Thus because there are about two times fewer sites for halogens in sample 60–108, one would expect to find more halogens in hornblende of sample 60–108 than in hornblende of samples 61–25 and 60–91; hornblende of sample 60–108 contains comparably more F but not more Cl. Likewise one would perhaps expect a little less of the halogens in the biotite of sample 60–111 compared to that in biotite of samples 61–25 and 60–91. However, biotite in sample 60–111 contains a little more Cl, and about the same amount of F as biotite in samples 61–25 and 60–91.

Cl, F, and H_2O variations with changes in mineral chemistry

The uptake of the halogens and water by the hydrous minerals may be affected by the substitution of other elements in the minerals. This possibility, although considered secondary compared to the variations linked to changes in magma chemistry and age (figs. 8–10), was investigated by comparing variations of halogen abundances with variations in the abundances of other elements in (1) individual grains (zoning) and in (2) all like-mineral grains from the same stock or rock type and from all rock types. For the first comparison, the number and type of correlation (positive, negative, or none) were tabulated for all grains that were studied for zoning in each rock type. No trends emerged from these data for apatite, biotite, and hornblende (summarized in table 11). The data for sphene and epidote were not sufficient for this type of comparison. For the second comparison, correlation matrices were constructed to check for coupled substitution between Cl and F and other elements in the minerals. In these data, trends did emerge for certain elements in apatite, biotite, and hornblende (tables 12–14). However, the correlations do not determine whether Cl, F, and H_2O+ vary in abundance in response to substitution of the other elements in the minerals (with the possible exception of Cl with Mg and Fe in hornblende) or whether the abundance of the halogens and water as well as the other elements in the minerals all changed in response to changes in the magma(s). For example, the MgO content of biotite correlates positively with the Cl content of biotite, but because Cl and MgO of biotite both vary negatively in abundance with the differentiation index of the samples, it is unclear whether Cl varies in abundance mainly because of coupled substitution with Mg or mainly because of changes in the magma. In view of the zoning studies and the similar correlations between Cl abundance in other minerals and rock chemistry, the changes

in magma are considered most likely. The same is probable for the other correlations between the abundance of an element in biotite, apatite, or hornblende and the abundance of Cl, F, or H_2O+ in the mineral because they either are not consistent from rock type to rock type, are not significant, or are matched by appropriate negative or positive correlations with rock differentiation index.

TABLE 11.—*Comparative zoning of halogens and oxides in apatite, biotite, and hornblende*

[Data are number of correlations tabulated for all grains studied]

	Halogen and oxide: Detectably and sympathetically zoned		Detectably and antipathetically zoned		Halogen only or oxide only detectably zoned		Halogen or oxide not detectably zoned	
	Cl	F	Cl	F	Cl	F	Cl	F
Apatite:								
SiO_2	1	1	1	0	11	15	35	35
CaO	0	0	0	0	4	7	47	44
Na_2O	0	2	0	1	16	14	35	34
P_2O_5	0	0	0	0	4	7	47	44
Biotite:								
SiO_2	0	0	2	1	5	7	22	21
Al_2O_3	1	0	0	0	11	12	17	17
FeO*	1	1	2	1	7	10	19	17
MgO	0	1	3	2	14	12	13	14
MnO	2	0	1	2	5	4	21	23
TiO_2	2	1	0	2	10	10	17	16
K_2O	3	2	1	1	4	7	21	19
Hornblende:								
SiO_2	0	1	3	3	9	4	4	8
Al_2O_3	4	3	0	2	9	7	3	4
FeO*	1	2	2	2	9	7	4	5
MgO	0	1	2	0	3	9	6	6
CaO	0	0	1	0	6	7	9	9
TiO_2	5	3	0	3	7	5	4	5
Na_2O†	2	0	1	0	3	5	1	5
K_2O†	2	2	0	3	6	3	1	1

* All Fe calculated as FeO.
† Fewer correlations for Na_2O and K_2O.

TABLE 12.—*Partial correlation matrices of apatite chemistry and rock differentiation index*

[Italic figures represent correlation at less than 95-percent confidence level. *N*, number of observations in a population]

	SiO_2	CaO	Na_2O	P_2O_5	D.I.
Tortilla Quartz Diorite (*N*, 9)					
Cl	*0.38*	*0.23*	*0.28*	*0.22*	*0.33*
F	*.21*	*.32*	*.15*	*.13*	*.26*
D.I.	*−.13*	*.44*	.97	.72	1.00
Rattler Granodiorite (*N*, 30)					
Cl	*−0.09*	−0.37	*−0.08*	*0.37*	−0.67
F	*.09*	*.16*	*.00*	*.31*	.47
D.I.	*.25*	*.06*	.52	−.59	1.00
Granite Mountain Porphyry (*N*, 17)					
Cl	*−0.12*	*−0.20*	*0.01*	*−0.35*	*0.29*
F	*.03*	.50	*−.03*	*−.24*	*.04*
D.I.	*.26*	*−.01*	*.36*	*−.34*	1.00
All rock types (*N*, 70)					
Cl	*0.08*	*−0.12*	*0.12*	*0.20*	−0.73
F	*−.03*	*−.12*	*−.06*	*−.20*	.62
D.I.	*.09*	*−.13*	.29	*−.10*	1.00

TABLE 13.—*Partial correlation matrices of biotite chemistry and rock differentiation index*

[Italic figures represent correlation at less than 95-percent confidence level, *N*, number of observations in a population]

	SiO_2	Al_2O_3	FeO*	MgO	MnO	TiO_2	K_2O	D.I.
Tortilla Quartz Diorite (*N*, 9)								
Cl	*−0.08*	*−0.40*	*0.05*	*0.03*	*−0.35*	*0.23*	*0.16*	*0.41*
F	*−.32*	*.55*	*.37*	*−.43*	.74	*−.65*	*−.47*	−.85
D.I.	*.55*	*−.46*	−.76	*.61*	−.91	.88	*.65*	1.00
Rattler Granodiorite (*N*, 35)								
Cl	*−0.18*	*−0.08*	*0.01*	*0.11*	*−0.10*	*−0.26*	*0.21*	*−0.28*
F	*−.26*	*−.22*	*−.19*	*.12*	*.06*	*.22*	.50	.74
D.I.	*.04*	*.20*	*−.18*	*−.13*	*−.24*	.43	−.43	1.00
Granite Mountain Porphyry (*N*, 27)								
Cl	*−0.17*	*−0.10*	0.38	*−0.24*	*0.17*	*0.23*	*0.14*	−0.32
F	*.43*	*.05*	−.75	.65	−.65	*−.17*	*.22*	.56
D.I.	.38	*.25*	−.66	.47	−.76	*−.26*	*.29*	1.00
All rock types (*N*, 78)								
Cl	0.42	−0.59	−0.52	0.77	−0.65	0.42	*0.04*	−0.47
F	−.30	.49	*.06*	−.46	.54	−.39	*−.10*	.69
D.I.	−.28	.60	.24	−.47	.53	−.53	*−.06*	1.00

* All Fe calculated as FeO.

TABLE 14.—*Partial correlation matrices of hornblende chemistry and rock differentiation index*

[Italic figures represent correlation at less than 95-percent confidence level. *N*, number of observations in a population]

	SiO_2	Al_2O_3	FeO*	MgO	CaO	TiO_2	Na_2O	K_2O	D.I.
Tortilla Quartz Diorite (*N*, 8)									
Cl	0.94	−0.97	0.96	−0.91	0.85	−0.96	−0.95	---	−0.96
F	*.16*	*−.12*	*−.07*	*.08*	*−.01*	*−.12*	*−.01*	---	*−.07*
D.I.	−.17	.99	−.99	.96	−.92	.99	.98	---	1.00
Rattler Granodiorite (*N*, 28) [1]									
Cl	−0.66	0.76	0.49	−0.59	*−0.35*	0.46	0.40	0.59	−.40
F	*.28*	*−.32*	*−.10*	*.19*	.49	−.46	−.72	*.28*	.38
D.I.	.48	−.55	*−.13*	*−.27*	*.32*	−.81	*−.24*	*−.11*	1.00
All rock types (*N*, 46) [2]									
Cl	−0.35	0.32	0.50	−0.52	*−0.17*	0.03	−0.15	0.59	*−0.04*
F	*.28*	−.31	*−.13*	*.20*	*.14*	−.36	*.04*	*.28*	.54
D.I.	*.24*	−.32	.29	*−.14*	*.19*	−.70	*−.31*	*−.11*	1.00

* All Fe calculated as FeO.
[1] *N* for Na_2O is 6, *N* for K_2O is 22.
[2] *N* for Na_2O is 24, *N* for K_2O is 22.

Cl, F, and H_2O+ contents of the rocks

The amounts of Cl and H_2O+ (figs. 11*A*, 12*C*) contributed to the rocks by the hydrous igneous minerals decrease with decreasing age and increasing differentiation index of the rock, whereas the amount of F contributed decreases only in the aplitic differentiates of the stocks (fig. 12*B*; table 10). These figures were constructed using the mineral analyses, measured rock specific gravities, assumed mineral specific gravities, and modal abundances of the minerals (including their pseudomorphic alteration products) and ignoring the secondary hydrous phases formed in the anhydrous silicates. The trends therefore do not necessarily reflect the actual amount of original Cl, F, or H_2O+ in

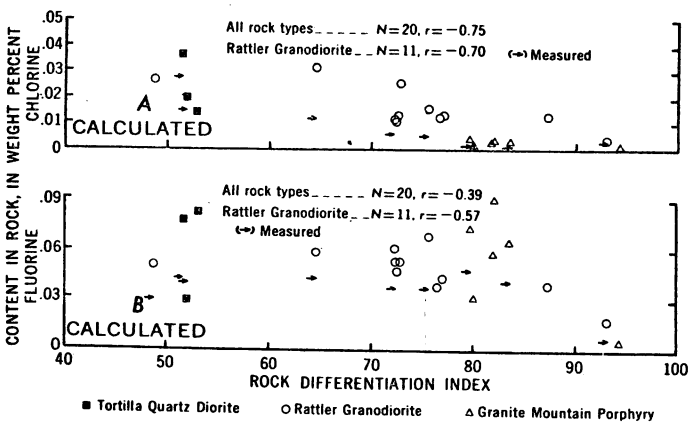

Figure 11.—Variation of Cl and F contents of rock samples with differentiation index. Symbols represent calculated values; arrows represent measured amount in water-leached rock powders.

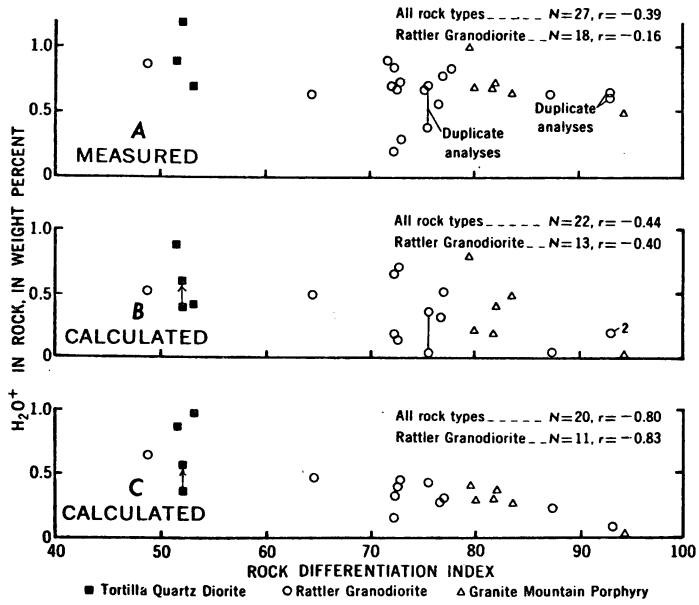

Figure 12.—Variation of H_2O+ contents of rock sample with rock differentiation index. *A*, Measured. *B*, Corrects *A* by removing effects of alteration products. *C*, Calculated from rock and mineral densities, mineral analyses, and modal abundance of originally unaltered igneous minerals.

the magmas because of the possibilities (1) that some of the alteration products of the igneous minerals are deuteric and thus drew halogens and water from the melt or (2) that halogens or water were either gained by or lost from the magma or rock, although for F experimental work suggests that little F would leave the magmas via an aqueous phase (Burnham, 1967).

Also plotted, as horizontal arrows, in figures 11*A* and 11*B* (data in table 15) are whole-rock analyses of Cl and F in finely ground, water-leached splits (to remove salts deposited from ground water) of a few

Table 15.—Cl *and* F *contents of some Laramide igneous rocks near Ray porphyry copper deposit*

Rock type	Sample No.	Contents (weight percent) Cl (a)	Cl (b)	Cl (c)	F (a)	F (b)	F (c)
Tortilla Quartz Diorite.	17–28	0.058	0.028	0.037	0.039	0.042	0.077
	17–1	.048	.015	.020	.037	.040	.029
Rattler Grandiorite.	46–99B	----	----	0.027	0,026	0.030	0.050
	60–113D	0.035	0.015	.035	.039	.042	.060
	T16–630	.023	.012	----	.049	.052	----
	61–25	.036	.006	.013	.037	.036	.064
	46–11G	.019	.005	.016	.032	.036	.068
	46–11A	.050	.003	.004	.006	.007	.018
Granite Mountain Porphyry.	RB5	0.033	<0.001	0.004	0.049	0.052	0.070
	GM6G	.14	<.001	.003	.039	.040	.066

[a] Chemical analysis by R. Moore and J. Budinsky.
[b] Whole-rock split ground to −325 mesh, leached with distilled water, dried at 90°C, and reanalyzed. A slight increase in the amount of F may reflect contamination by laboratory dust not completely compensated by blanks run simultaneously. Analysts, R. Moore and J. Budinsky.
[c] Amount of Cl and F in the rock contributed by original igneous minerals (calculated using modal data and electron-microprobe mineral analyses).

selected samples. These measured values confirm the trends (or lack of them) in figure 11 determined by calculation. However, the measured values are less than the calculated values for the halogen contents of the rock (except for F of sample 17–1, table 15). This discrepancy is expected for Cl because the OH-bearing alteration minerals of biotite contain less Cl than the biotite (fig. 13), and the loss of Cl cannot be wholly compensated by the Cl that might occur in alteration products of the feldspars (table 8). On the other hand, because the F content of some of the biotite alteration products is considerably greater than the host biotite (fig. 13), the higher values of F^c versus F^b (see footnote explanations in table 15) were not expected. It is not known if the higher values (F^c in table 15) are

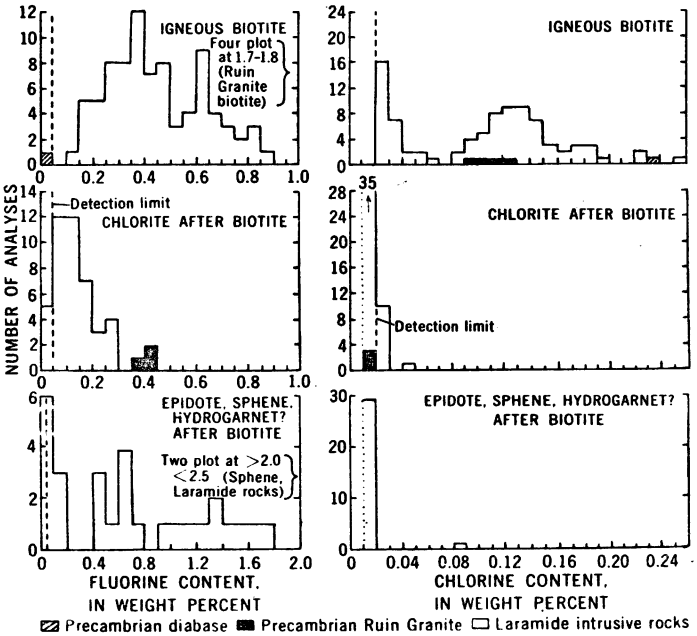

Figure 13.—Frequency distribution of F and Cl of biotite and biotite alteration products.

artifacts of different analytical procedures, or whether part of the biotite's F (like the Cl) was removed from the rock during conversion of the biotite to alteration minerals.

Rock powders of all the samples were analyzed for H_2O+ (fig. 12*A*), and although these values also correlate negatively with rock differentiation index, the correlation is poorer than for the calculated values of H_2O+ (fig. 12*C*, table 10). The poor correlation between figures 12*A* and 12*C* is somewhat improved by removing (by calculation) the effects of the hydrous alteration products in the samples (fig. 12*B*), and part of the remaining wide scatter in the points (fig. 12*B*) may be attributed to the more inhomogeneous distribution of the hydrous alteration products (containing as much as 12 percent H_2O+ by weight) compared to the hydrous igneous minerals (containing no more than 4 percent H_2O+ by weight). The arrow between the two filled squares (Tortilla Quartz Diorite, fig. 12*B*, *C*) represents the original H^2O+ content of sample 17–1, assuming that the fibrous amphibole (table 8) is (1) not igneous and replaces pyroxene (lower position) or (2) igneous or replacing hornblende (upper position). The statistics (table 10) were calculated assuming the former.

Simonen (1948), working with another consanguineous rock sequence, notes that more mafic rocks are richer in Cl than more silicic ones, and the data in Dodge and others (1968) show that rock Cl and F contents generally decrease with increasing differentiation index of the samples from the Sierra Nevada batholith. Thus, the findings at Ray are not unique. On the other hand, many conflicts are found in the literature. Correns (1956) found no correlation between the halogen contents and SiO_2 contents of rocks when comparing samples from widely separated localities, where Goldschmidt (1954) and Simonen (1948) suggest that rock F contents increase with magmatic evolution of igneous series. Kuroda and Sandell (1953) and Correns (1956) found no correlation between rock composition and Cl content, whereas Behne (1953) suggests that felsic rocks contain more Cl than basic ones. It is suspected that some of these conflicts and exceptions to the findings at Ray may result in part from comparison of data compiled for rocks of differing origins, conditions of emplacement, and degrees of alteration. For example, the data in Simonen (1948) for petrochemically related rocks show, like the Ray rocks, little or no relation between rock chemistry and F content. Similarly, if plots like figure 11*A* and *B* had been made comparing the calculated Cl and F contents of the Ruin Granite at Ray (a Precambrian quartz monzonite) with those of the Granite Mountain Porphyry (an Early Tertiary granodiorite), there would have resulted a strong positive correlation of the contents of Cl and F in the rock with increasing SiO_2 content of the rocks. Clearly, because the Ruin Granite was emplaced as a batholith 1.4 b.y. prior to the Granite Mountain Porphyry (a stock), such plots would exceed their intended use. Thus the likelihood of constructing misleading geochemical trends for minor elements seems large if, in addition to a lack of time-space proximity of the rocks compared, the data are not corrected for the halogens and water introduced or lost during incipient alteration of the rock (fig. 13) or the halogens present in fluid inclusions and in salts deposited from ground water along microfractures (see table 15).

APPLICATION TO PETROLOGIC MODELS

The preceding data indicate that the abundances of the halogens and water in the igneous minerals studied have not been uniformly homogenized nor are they detectably controlled by changes in chemistry of the minerals, proximity or degree of local alteration, or potential susceptibility of a grain to exchange with the magma(s) or aqueous fluids. On the other hand, changes in abundance of Cl, F, and calculated H_2O+ in the igneous hydrous minerals appear to be related to changes in the age and chemistry of the parent magma(s). Similar trends are observed for minerals in other consanguineous igneous suites. These facts suggest that the hydrous igneous minerals studied at Ray probably retain an imprint of magmatic events and that the changes in the halogen and water contents of the minerals are more likely the result of changes in or initial differences between the magma(s) than the result of postmagmatic events. This interpretation is consistent with the resistance of fluorapatite to exchange with chloride-rich aqueous fluids (Ekström, 1973).

Given the interpretation that the changes in mole fractions of Cl, F, and H_2O ($X_{Cl,\,F,\,H_2O}$) in the minerals probably reflect magmatic processes during development of the igneous suite at Ray, it is of interest to petrology and current ideas about ore genesis if the data lead to the determination of how $X_{Cl,\,F,\,H_2O}$ varied in the melt(s) as the magmas became younger and more differentiated. Unfortunately, such a determination requires experimental data not yet available concerning the activity coefficients of Cl^-, F^-, and OH^-, how the activity coefficient of each ion changes relative to the others with respect to temperature and pressure, and if and how the partition coefficients (between melt and mineral) of each ion change with temperature and pressure. Additionally, subjective deci-

sions must be made as to whether the exposed plutons represent (1) sequential differentiates of one batholith while it was emplaced in the upper crust, (2) differentiates of several common source batholiths while they were emplaced in the upper crust, (3) as in 1 but occurring in the lower crust or upper mantle, (4) as in 2 but occurring in the lower crust or upper mantle, or (5) sequential or separate partial melts from a common source area.

It seems obvious that with so many possible variables, strong defense of any unique explanation for the data would be unwise. If explanations 2, 4, or 5 apply to Ray, then data need not be necessarily considered petrologic indicators of processes in differentiation of magma. However, the data for one magma (Rattler Granodiorite) are consistent with those for the entire igneous suite and, as cited earlier, with similar data for other igneous suites. Thus it seems at least reasonable to postulate that the trends observed in figures 8–10 could result from differentiation of a single magma and that evaluation of the magmatic behavior of Cl, F, and H_2O is warranted. The following discussion concerns only explanation 1 above because of its significance to one current theory of ore genesis—that both ore and ore fluid components for porphyry copper deposits have their source in calc-alkaline magma emplaced in the upper crust.

A long list of literature, reviewed in part by Lowell and Guilbert (1970), notes a time-space relation between intermediate calc-alkaline intrusive rocks and "disseminated" or porphyry copper ore deposits; this relation has generally been interpreted as causal. In the classical magmatic hypothesis of ore deposits, the calc-alkaline magmas are considered the vessels that transported the copper and sulfur to or near to the deposits, and there the magmas produced the mineralization through differentiation. However, in the Laramide plutons associated with Ray and also in those elsewhere in Arizona (Rehrig and Heidrick, 1972), mineralization is associated with a regional tectonic fracture system rather than with observed radial, concentric, and sheeting joints associated with cooling of the plutons. Thus, if the mineralizing fluids evolved according to the classical magmatic model, they must have come from deeper sources than the exposed plutons; that is, explanation 1 above, in which water is first concentrated through crystal differentiation in and later released from a nearby batholith. To facilitate transport of the ore and to explain the NaCl in fluid inclusions in porphyry deposits, the fluids released should preferably be rich in chloride (see for example, Helgeson, 1964; Garrels, 1941; Roedder, 1971).

This presumed late buildup of Cl and H_2O was not recorded by the minerals in the exposed plutons associated with Ray (figs. 8–10, table 10). Thus, either the classical magmatic hypothesis does not apply to the Ray deposit, or it must be postulated that the minerals did not record the required processes in the batholith. Three models that might explain the data are presented below. The first two outline the processes and list the special conditions that apply if the rocks studied here are related to a nearby batholith that produced mineralizing fluids. The third model does not assume a classical magmatic origin for the Ray deposit.

Changes imposed on the stocks

If the classical magmatic hypothesis applies to Ray and if figures 8–10 depict directly how X_{Cl, F, H_2O} varied in the melts of the exposed stocks, then the processes in the stocks did not follow those in the parent batholith. Because the stocks were emplaced at shallower depths than the batholith, it seems a reasonable postulate that they evolved water before the batholith did. Experimental studies (Koster van Groos and Wyllie, 1969; Wyllie and Tuttle, 1964) indicate that in a degassing melt, Cl would leave with H_2O while most of the F would tend to remain in the melt (Burnham, 1967; Munoz and Eugster, 1969). Thus evolution of water from the ascending and crystallizing magmas of the exposed stocks would increase the activity of F in the melts of the stocks relative to the fugacity of water and the activity of chlorine while the batholith could continue to maintain and concentrate chlorine and water. However, several lines of evidence have already been discussed that are not consistent with the assumption that the exposed stocks saturated early in their crystallization history or evolved much water. To review, these are that: (1) biotite does not show a magnesium enrichment with decreasing age or with progressive differentiation of the stocks, (2) the percentage of aplites in the stocks is low, (3) pegmatitic aplites are sparse, (4) metamorphic aureoles around the intrusive rocks, both stocks and dikes, are restricted and in some places are virtually absent even in carbonate terrane, (5) miarolitic features or cavities have not been identified in field exposures or thin section samples of the Laramide stocks, and (6) the fluid inclusions in quartz in the rocks are sparse, two phase, and homogenize at temperatures considerably below the granite minimum. Also problematical to the postulate that evolution of Cl-bearing water explains the correlations of X_{Cl, F, H_2O} in the minerals with rock chemistry and age are ex-

perimental data (Munoz and Ludington, 1974; Munoz and Eugster, 1969). These data suggest that evolution of water at magmatic temperature from the stocks in amounts proportional to those required of the parent batholith to form the Ray deposit should have resulted, but did not (table 4), in (1) homogenization of F contents of biotite in individual samples and stocks and (2) higher F contents in the high-temperature igneous rather than in the lower temperature hydrothermal biotite. The fact that neither expectation is met requires that the igneous biotite had little contact with the water evolved at magmatic temperature and that the ore fluids had chemical parameters different from the water evolved from the stocks. In addition, the increase in F content of the biotites with increasing differentiation (fig. 9) is opposite to the trend expected because with vapor phase present, each of the following factors should have resulted in a decrease in the F content of biotite: (1) the Mg content of the biotite decreases with differentiation (see Ludington, 1973; Ekström, 1972; Munoz and Eugster, 1969; Munoz and Ludington, 1974; Wones and Eugster, 1965), (2) the F content of the rock decreased or remained the same during differentiation (fig. 11*B*; see also Munoz and Eugster, 1969), and (3) presumably the temperature of the differentiating magma(s) and its evolving vapor phase(s) would be progressively lower (see Munoz and Eugster, 1969). Thus, an additional requirement on the evolving water(s) is that they became progressively enriched in F as the host rock became more felsic despite the observed decrease of F content of the rock (fig. 11*B*) and probable decrease in temperature of the magma. As an alternative to this, it could be postulated that the Tortilla Quartz Diorite and Rattler Granodiorite did not evolve much water whereas the Granite Mountain Porphyry evolved much more water that, for some reason, resulted in higher contents of and homogenization of F in individual biotite grains of the Granite Mountain Porphyry without homogenizing the grains with respect to the other elements or with respect to F contents of biotite in adjacent grains and in other samples from the stock. Finally, at their depths of emplacement, the stock should have saturated at between 2.5 to more than 3.5 wt percent H_2O (Burnham, 1967); this is about the approximate amount required in the melts for biotite to form in the stocks (D. R. Wones, oral commun., 1974; Wones and Dodge, 1966). Thus, if it is postulated that the magmas evolved water while ascending or during the main stage of crystallization, disequilibrium crystallization also must be postulated.

Taken alone, any one of the foregoing requirements and observations does not preclude the possibility that the character of the magmas of the stocks changed through evolution of water and chlorine. However, with so many requirements on the presumed aqueous phase(s) and with the popular desire for simplicity and consistency in interpretation of data, alternative explanations of the trends with age and chemistry indicated in figures 8–10 seem warranted. Another model that maintains the assumptions of the classical magmatic model is given below.

End-stage degassing of the stocks and batholith

This model drops the requirement that the stocks evolved water during their ascent and main-stage crystallization but maintains the requirement of the classical magmatic model that chloride-rich water was produced at or near the end of differentation of the parent batholith (and also of its effluent stocks). However, like the preceding one, this model finds the same problems with the paucity or even negative physical evidence that water in the volumes proportional to those required for the deposit evolved from the stocks at magmatic temperatures. It also requires the same special conditions to explain the lack of magnesium enrichment in biotite from aplites of the stocks and why the biotite did not respond chemically to presence of the evolving magmatic water. In addition, the failure of $X_{Cl,\,H_2O}$ in the minerals to record the buildup of $X_{Cl,\,H_2O}$ in the parent batholith means that to explain figures 8–10, changes in the activities of Cl^-, F^-, and OH^- (or fugacity of H_2O) in the melt do not directly record changes in $X_{Cl,\,F,\,H_2O}$ in the melt. This model cannot be evaluated further without experimental data that indicates that activity of F can in fact increase relative to the activities of both water and chlorine in a differentiating melt while X_F in the melt (probably very close to figure 11*B*) remains roughly constant or decreases and while X_{Cl} and X_{H_2O} in the melt increase.

Magmatic evolution through crystal differentiation

This model postulates that the magmas were undersaturated in water when emplaced at the present levels of exposure, that the precipitation of hydrous minerals controlled the activities of Cl, F, and H_2O in the melt, and, as a consequence of these postulates and the petrologic evidence indicating that the hydrous minerals continued to form late in the crystallization history of the stocks, that the magmas evolved very little water. The paucity of evolved water is consistent with fluid-inclusion data, lack of miarolitic features in

stocks, paucity of pegmatitic dikes, low percentage of aplites, lack of Mg enrichment in the igneous biotite, and restricted skarn development associated with the plutons. It is also consistent with the F chemistry of the biotite. This interpretation of the data does not preclude the possibility that water evolved from the magmas after the hydrous minerals ceased forming, perhaps after other components required for formation of the hydrous minerals were consumed or perhaps in response to local disequilibrium. In fact, the presence of interstitial epidote in the stock suggests that fugacity of H_2O in the stocks did increase locally during the very final stages of crystallization. However, in this model the water evolved was probably small in amount and low in Cl content.

If the magmas were originally undersaturated and evolved only insignificant amounts of water relative to the total volumes of the stocks, then the trends observed between the age and chemistry of the rock and the abundances of Cl, F, and H_2O+ in the minerals (figs. 8–10) must be explained by crystal differentiation, whereby most of the Cl, F, and H_2O originally present in each magma was extracted from the melts by the hydrous minerals. In this model then, changes in activities of Cl^-, F^-, and OH^- (as indicated in figs. 8–10) were proportional to changes of X_{Cl^-, F^-, OH^-} in the melt (as indicated in figs. 11*A*, *B*; 12*C*). Thus, for the Rattler Granodiorite, the first hydroxyl-bearing minerals that separated from the magma tended to incorporate more chlorine relative to water and fluorine, and more water relative to fluorine than hydroxyl-bearing minerals that separated at a later time or from the more differentiated magma. If all the stocks came from the same nearby batholith (questionable that it would remain molten for 10 m.y. in the shallow crust) or deep batholith (where heat input might lengthen the life of the batholith), then the explanation applied to the Rattler Granodiorite applies to the entire igneous suite.

As with the preceding model, there is no direct experimental justification or refutation for this explanation of the data. However, F is much more soluble in silica-rich melts than both H_2O and Cl, and H_2O is more soluble than Cl (Koster van Groos and Wyllie, 1968, 1969; Burnham, 1967). Thus given the assumption that less soluble components would tend to leave the melt prior to more soluble components, this model, although not irrefutably supported, is at least consistent with the experimentally determined relative solubilities of Cl, F, and H_2O in silicate melts.

Failure of the outer edges of the mineral grains consistently to record the postulated progressive depletion of Cl and H_2O in the melts relative to F may be attributed to (1) inhomogeneities in the melt, (2) convective mixing of the grains, or (3) in-place variations of conditions controlling halogen uptake. The first of these alternatives is favored because it seems likely that with several coexisting hydrous phases simultaneously consuming volatiles from the melt in different amounts and at different rates, and with the nearby anhydrous minerals simultaneously rejecting and thus reconcentrating them at different rates, it seems reasonable to postulate that the diffusion rates of all components were not adequate to maintain, on a local scale, a homogeneous melt with respect to Cl, F, and H_2O. The larger intragrain and intrasample variation of Cl and F in apatite relative to the biotite, hornblende, and sphene might also be explained by inhomogeneities in the melts because the demands by apatite for Cl and F in the melt were greater and thus less likely to be fulfilled at a consistent ratio of $Cl:F:H_2O$ compared to those of the hydrous silicates. The two alternative explanations offered above do not seem as likely because one should expect the biotite, hornblende, and sphene to have recorded variations in halogen abundances similar to those observed in the apatite, if either convective mixing or in-place variation of P_{H_2O}, T, or P_{total} were the major cause of the observed intrasample and intragrain variations. Further, it is difficult to visualize mechanisms that would change P_{H_2O}, T, and P_{total} on a millimetre scale or ways in which adjacent grains might have moved over the distances required to cause the observed differences in halogen contents, both within and between grains, in the samples that were possibly 50–80 percent crystallized prior to formation of hydrous minerals.

This model requires that the melts arrived at their level of emplacement not only undersaturated but carrying not much more than 1–0.5 percent H_2O by weight (mafic and felsic stocks, respectively), or in other words, the hydrous minerals could not begin to form in the magmas until about 50 percent of the mafic magmas and about 80 percent of the felsic magmas had crystallized. This is consistent with petrologic observations and interpretations for most of the samples but not with those for the rhyodacite dikes and the porphyritic facies of the Rattler Granodiorite where the presence of phenocrysts suggests the possible onset of hydrous mineral formation when less than 30–50 percent of the magma(s) had crystallized. Thus, if the above model is to explain the data, either some of the magmas (and part of the Rattler Granodiorite magma) had two to three times more water initially, or water was locally concentrated in or introduced into some of the magmas. For example, the porphyritic facies of the Rattler Granodiorite may have gained water from the

rest of the melt because of diffusion of water to cooler parts of the melt (Kennedy, 1955), thereby enriching one part of the melt in water at the expense of the other prior to formation of the groundmass minerals. However, under conditions of small concentration gradients, diffusion of water in melts may be slow (Burnham, 1967), and instead, a convecting or turbulent part of the magma exposed to wet wallrocks may have stripped water from the wallrocks in a manner similar to metallurgic zone refining (Shaw, 1972; Harris, 1957). A final special condition required for this model concerns sample 60–113D (D of figs. 8–10), a dike that intrudes both the porphyritic and nonporphyritic facies of the Rattler Granodiorite prior to development of aplites in the stock. Biotite and hornblende in this dike contain more Cl than biotite and hornblende in rocks cut by the dike. Possible explanations for this relation are (a) turbulent flow in the dike caused "stripping" of Cl and H_2O of meteoric or magmatic origin from the nearly crystallized parts of the stock, (b) the dike represents a late resurgence from an unconsolidated deeper and less differentiated part of the stock or (c) the dike represents an intrusion that was not part of the Rattler Granodiorite magma.

Concluding remarks

The last of the three models discussed in this section is thought to be consistent with more data and to require fewer unprovable special conditions than the first two models, but no one model can be considered the unique explanation of the data, particularly if all stocks and dikes did not originate from a nearby batholith. Although the first two models do not incorporate all the field, chemical, and existing experimental observations as favorably as the last, neither they nor a classical magmatic genesis for Ray can be ruled out with certainty. On the other hand, the data for the Ray rocks neither require nor support the classical magmatic origin of the Ray deposit, and they are similar to those for plutons that are not associated with porphyry copper deposits. Thus a source alternative to an upper crustal batholith might profitably be sought to explain the mineralization at Ray and perhaps other deposits.

BIOTITE AS A PARTIAL OR SUPPLEMENTARY SOURCE OF CHLORINE AND FLUORINE IN THERMAL WATERS

Chlorine

The distribution of Cl between igneous biotite and its propylitic type alteration products at Ray (fig. 13) suggests that natural thermal waters and ore fluids might find a partial or supplementary source of Cl in that released during alteration of biotite to chlorite, epidote, and sphene. For example, upon alteration of 20 percent of the biotite (comprising an average of more than 7 volume percent of the rock), each cubic kilometre of average Laramide igneous rock ($\rho \approx 2.8$ g/cm^3) at Ray, using the average Cl abundance of biotite (1,100 ppm) analyzed here, would release as much as 4×10^{10} g Cl to the altering fluid if the average biotite alteration product contained Cl in amounts just below detection (200 ppm). If the average alteration product contained Cl in amounts considerably below detection levels (contents of 20–30 ppm), 4.8×10^{10} g Cl would be released to the fluids.

This does not imply that the major source of Cl in natural hot waters is altered biotite because much might be trapped in fluid inclusions or in alteration products of the feldspars. For example, if the observed modal phengite and clay (both containing no more than 200 ppm Cl) had developed in the coexisting plagioclase and K-feldspar during the period of biotite destruction, only 1.3×10^{10} to 1.8×10^{10} g/km^3 Cl would still be available for incorporation in fluid inclusions or for further transport in the fluid phase. This does not rule out the possibility that alteration of biotite might be a supplementary or partial source of Cl in hydrothermal fluids, particularly if the hydrous alteration products of plagioclase contain significantly less Cl than that detectable by methods used here (200 ppm) or if the plagioclase alteration occurred at a different time than the biotite alteration.

Fluorine

Chloritization of the igneous biotite in the Laramide rocks at Ray was accompanied by development of anhedral sphene, epidote, and perhaps even the F-bearing hydrogarnet(?) (in decreasing order of abundance). The sphene and hydrogarnet(?) contain F in abundances usually greater than the host biotite (fig. 13, compare tables 4 and 8) suggesting that much of the F in the biotite was immediately reprecipitated. However, if data in table 15 apply, only part of the F originally in the biotite remained in the rock (compare F^b with F^c in table 15). Thus, it seems possible that biotite could also provide some F to waters that cause propylitic alteration, particularly in instances where the calcium content of the waters is low, and epidote and sphene do not form in biotite during the alteration.

REFERENCES CITED

Banks, N. G., 1974, Distribution of copper in biotite and biotite alteration products in intrusive rocks near two Arizona porphyry copper deposits: U.S. Geol. Survey Jour. Research, v. 2, p. 195–212.

Banks, N. G., Cornwall, H. R., Silberman, M. L., Creasey, S. C., and Marvin, R. F., 1972, Chronology of intrusion and ore deposition at Ray, Arizona—Part I, K-Ar ages: Econ. Geology, v. 67, p. 864–878.

Banks, N. G., and Stuckless, J. S., 1973, Chronology of intrusion and ore deposition at Ray, Arizona—Part II, fission-track ages: Econ. Geology, v. 68, p. 657–664.

Beaman, D. R., and Isasi, J. R., 1970, A critical review of computer programs used in quantitative electron microprobe analysis: Anal. Chemistry, v. 42, p. 1540–1568.

Beeson, M. H., 1967, A computer program for processing electron microprobe data: U.S. Geol. Survey open-file rept., 40 p.

Behne, W., 1953, Untersuchungen zur Geochemie des Chlor und Brom: Geochim. et Cosmochim. Acta, v. 3, p. 186–215.

Birks, L. S., 1963, Electronprobe microanalysis: New York, John Wiley and Sons, 253 p.

Burnham, C. W., 1967, Hydrothermal fluids at the magmatic stage, *in* Barnes, H. L., ed., Geochemistry of hydrothermal ore deposits: New York, Holt, Rinehart, and Winston, p. 34–76.

Cornwall, H. R., Banks, N. G., and Phillips, C. H., 1971, Geologic map of the Sonora quadrangle, Pinal and Gila Counties, Arizona: U.S. Geol. Survey Geol. Quad. Map GQ–1021, scale 1:24,000.

Cornwall, H. R., and Krieger, M. H., 1975, Geologic map of the Kearny quadrangle, Pinal County, Arizona: U.S. Geol. Survey Geol. Quad. Map GQ–1188, scale 1:24,000. (In press.)

Correns, C. W., 1956, The geochemistry of the halogens: Physics and Chemistry of the Earth, v. 1, p. 181–233.

Dodge, F. C. W., and Moore, J. G., 1968, Occurrence and composition of biotites from the Cartridge Pass pluton of the Sierra Nevada batholith, California, *in* Geological Survey research 1968: U.S. Geol. Survey Prof. Paper 600–B, p. B6–B10.

Dodge, F. C. W., Papike, J. J., and Mays, R. E., 1968, Hornblendes from granitic rocks of the central Sierra Nevada batholith, California: Jour. Petrology, v. 9, p. 378–410.

Dodge, F. C. W., and Ross, D. C., 1971, Coexisting hornblendes and biotites from granitic rocks near the San Andreas fault, California: Jour. Geology, v. 79, p. 158–172.

Dodge, F. C. W., Smith, V. C., and Mays, R. E., 1969, Biotites from granitic rocks of the central Sierra Nevada batholith, California: Jour. Petrology, v. 10, p. 250–271.

Ekström, T. K., 1972, The distribution of fluorine among some coexisting minerals: Contr. Mineralogy and Petrology, v. 34, p. 192–200.

——— 1973, Synthetic and natural chlorine-bearing apatite: Contr. Mineralogy and Petrology, v. 38, p. 329–338.

Garrels, R. M., 1941, The Mississippi Valley type lead-zinc deposits and the problem of mineral zoning: Econ. Geology, v. 36, p. 729–744.

Gillberg, M., 1964, Halogens and hydroxl contents of micas and amphiboles in Swedish granitic rocks: Geochim. et Cosmochim. Acta, v. 28, p. 495–516.

Goldschmidt, V. M., 1954, Geochemistry, edited by Alex Muir: London, Oxford Clarion Press, 730 p.

Harris, P. G., 1957, Zone refining and the origin of potassic basalts: Geochim. et Cosmochim. Acta, v. 12, p. 195–208.

Helgeson, H. C., 1964, Complexing and hydrothermal ore deposition: New York, MacMillan, 128 p.

Ivanov, V. S., 1971, Composition of biotite in granitoids, as influenced by temperature and chemical activity of potassium: Internat. Geology. Rev., v. 13, no. 5, p. 649–657.

Jackson, E. D., Stevens, R. E., and Bowen, R. W., 1967, A computer-based procedure for deriving mineral formulas from mineral analyses, *in* Geological Survey research 1967: U.S. Geol. Survey Prof. Paper 575–C, p. C23–C31.

Jahns, R. H., and Tuttle, O. F., 1963, Origin of igneous aplites [abs.]: Geol. Soc. America Spec. Paper 73, p. 177–178.

Kennedy, G. C., 1955, Some of the aspects of the role of water in rock melts: Geol. Soc. America Spec. Paper 62, p. 489–503.

Koster van Groos, A. F., and Wyllie, P. J., 1968, Melting relationships in the system $NaAlSi_3O_8$–NaF–H_2O: Jour. Geology, v. 76, p. 50–70.

——— 1969, Melting relationships in the system $NaAlSi_3O_8$–NaCl–H_2O at one kilobar pressure, with petrological applications: Jour. Geology, v. 77, p. 581–605.

Kuroda, P. K., and Sandell, E. B., 1953, Chlorine in igneous rock, some aspects of the geochemistry of chlorine: Geol. Soc. America Bull., v. 64, p. 879–896.

Lee, D. E., and Van Loenen, R. E., 1970, Biotites from hybrid granitoid rocks of the southern Snake Range, Nevada, *in* Geological Survey research 1970: U.S. Geol. Survey Prof. Paper 700–D, p. D196–D206.

Lowell, J. D., and Guilbert, J. M., 1970, Lateral and vertical alteration-mineralization zoning in porphyry ore deposits: Econ. Geology, v. 65, p. 373–408.

Ludington, S. D., 1973, Refinement of the biotite-apatite geothermometer [abs.]: Geol. Soc. America, Rocky Mountain Sec., Abstracts with Programs, v. 5, no. 6, p. 493–494.

Munoz, J. L., and Eugster, H. P., 1969, Experimental control of fluorine reactions in hydrothermal systems: Am. Mineralogist, v. 54, p. 943–959.

Munoz, J. L., and Ludington, S. D., 1974, Fluoride-hydroxyl exchange in biotite: Am. Jour. Sci., v. 274, p. 396–413.

Nash, W. P., 1972a, Apatite-calcite equilibria in carbonatite—chemistry of apatite from Iron Hill, Colorado: Geochim. et Cosmochim. Acta, v. 36, p. 1313–1319.

——— 1972b, Apatite chemistry and phosphorus fugacity in a differentiated igneous intrusion: Am. Mineralogist, v. 57, p. 877–886.

Rehrig, W. A., and Heidrick, T. L., 1972, Regional fracturing in Laramide stocks of Arizona and its relationship to porphyry copper mineralization: Econ. Geology, v. 67, p. 198–213.

Roedder, Edwin, 1971, Fluid inclusion studies on the porphyry-type ore deposits at Bingham, Utah, Butte, Montana, and Climax, Colorado: Econ. Geology, v. 66, p. 98–118.

Roegge, J. S., Logsdon, M. J., Young, H. S., Barr, H. B., Borcsik, M., and Holland, H. D., 1974, Halogens in apatites from Providencia area, Mexico: Econ. Geology, v. 69, p. 229–240.

Shaw, D. M., 1972, Development of the early continental crust—Part 1, use of trace element distribution coefficient models for the Protoarchean crust: Canadian Jour. Earth Sci., v. 9, p. 1577–1595.

Simonen, Ahti, 1948, On the petrology of the Aulanko area in southwestern Finland: Finlande Comm. Géol. Bull. 143, p. 1–66.

Stormer, J. C., and Carmichael, I. S. E., 1971, Fluorine-hydroxyl exchange in apatite and biotite—A potential igneous geothermometer: Contr. Mineralogy and Petrology, v. 31, p. 121–131.

Taborszky, F. K., 1962, Geochemie des apatits in Tiefgesteinen am Beispiel des Odenwaldes: Beitr. Mineralogie u. Petrographie, v. 8, p. 354–392.

Thornton, C. P., and Tuttle, O. F., 1960, Chemistry of igneous rocks—I, Differentiation index: Am. Jour. Sci., v. 258, p. 664–684.

Wones, D. R., and Dodge, F. C. W., 1966, On the stability of phlogopite [abs.]: Geol. Soc. America and associated societies, Ann. Mtg., San Francisco, Calif., 1966, Program, p. 243.

Wones, D. R., and Eugster, H. P., 1965, Stability of biotite; Experiment, theory and application: Am. Mineralogist, v. 50, p. 1228–1272.

Wyllie, P. J., and Tuttle, O. F., 1964, Experimental investigation of silicate systems containing two volatile components—Part III, the effects of SO_3, P_2O_5, HCl, and LiO_2, in addition to H_2O, on the melting temperatures of albite and granite: Am. Jour. Sci., v. 262, p. 930–939.

JDL

JEK

UNITED STATES DEPARTMENT OF THE INTERIOR

GEOLOGICAL SURVEY

IGNEOUS ROCKS AND COPPER MINERALIZATION IN THE RAY PORPHYRY COPPER DISTRICT, ARIZONA

By

Henry R. Cornwall and Norman G. Banks
U.S. Geological Survey, Menlo Park, California 94025

U.S. Geological Survey
Open-file Report 77-255
1977

This report is preliminary and has not been edited or reviewed for conformity with Geological Survey standards and nomenclature.

Table of Contents

	Page
Introduction	1
Laramide plutons	1
Tortilla Quartz Diorite	1
Rattler Granodiorite	2
Tea Cup Granodiorite	2
Granite Mountain Porphyry	3
Teapot Mountain Porphyry	3
Chemical and modal data	4
Depth of intrusion	6
Volatile contents of the magmas	6
Source of copper in the Ray deposit	8
References cited	10

IGNEOUS ROCKS AND COPPER MINERALIZATION IN THE RAY PORPHYRY COPPER DISTRICT, ARIZONA

By Henry R. Cornwall and Norman G. Banks
U.S. Geological Survey, Menlo Park, California 94025

INTRODUCTION

The Ray porphyry copper district is approximately 110 km north of Tucson and 120 km east-southeast of Phoenix in southeastern Arizona. The major disseminated copper deposit at Ray has reserves estimated at 650 million tons[1] of both primary and secondary ore, and occurs mostly in Precambrian Pinal Schist and diabase, but partly in the Granite Mountain Porphyry of Laramide age. The Granite Mountain Porphyry is part of a suite of Laramide igneous plutons and dikes in the Ray area that range in age from 70 to 60 m.y. and in composition from diorite to quartz monzonite. Hydrothermal biotite from the copper deposit at Ray has been dated at 65 m.y. (K-Ar age), and apatite in mineralized diabase has been reset at 60 m.y. (fission-track age). These ages indicate a close temporal and possibly genetic relationship with these Laramide igneous rocks.

LARAMIDE PLUTONS

The Laramide plutons, roughly in order from mafic to silicic and from older to younger are: (1) Tortilla Quartz Diorite, (2) Rattler Granodiorite, (3) Tea Cup Granodiorite, (4) Granite Mountain Porphyry, and (5) Teapot Mountain Porphyry. In addition, there are swarms of east-west-trending dikes, mostly rhyodacite, but ranging from andesite to quartz latite.

Tortilla Quartz Diorite

The Tortilla Quartz Diorite forms a large stock, 5 km long and 3 km wide, 5 km south of the Ray mine. It also crops out as small stocks in the same area, in the southern part of the Kearny quadrangle, the eastern Sonora quadrangle, and in the central El Capitan Mountain quadrangle. It intrudes Precambrian Ruin Granite, Madera Diorite and diabase, and late Paleozoic Escabrosa and Naco Limestones. Where it intrudes these limestones at Elder Gulch in the southern Sonora quadrangle, it is partly surrounded by breccia masses containing fragments of Naco and older rocks. The Tortilla Quartz Diorite is variable in composition and appearance from stock to stock, ranging from pyroxene-hornblende

[1]N. A. Gambell (oral commun., 1976).

diorite to biotite-hornblende quartz diorite, but quartz diorite predominates. It is fine to medium grained, typically with hypidiomorphic-intersertal texture, partly porphyritic, with andesine, hornblende, pyroxene (mostly augite), biotite, and magnetite-ilmenite in an interstitial matrix of quartz and potash feldspar.

Rattler Granodiorite

The Rattler Granodiorite crops out as a pear-shaped body in the southeastern Sonora quadrangle. It is 2.7 km long, east to west, and 0.3 to 1.8 km wide with two offshoots up to 0.9 km long, extending westward from the main body. A second pluton of Rattler Granodiorite crops out 0.8 km to the east in the El Capitan Mountain quadrangle. It is 0.6 km wide and 0.9 km long and is overlapped on the east and north by Tertiary and Quaternary gravels. The granodiorite intrudes Precambrian diabase, siltstone, quartzite, limestone, and dolomite, Cambrian sandstone and siltstone, and Devonian dolomite. It is a composite intrusion ranging from quartz diorite to quartz monzonite with small marginal bodies of melanocratic quartz diorite and late-formed leucocratic aplitic dikes of quartz monzonite.

Texturally the Rattler Granodiorite is fine- to medium-grained hypidiomorphic-seriate to porphyritic. The phenocrysts are most commonly plagioclase (predominantly andesine), but also include quartz, biotite, and hornblende, 1-4 mm long. The groundmass and smaller grains in the seriate rocks consist of the same minerals plus magnetite-ilmenite, interstitial K-feldspar and quartz, and accessory minerals. The accessory minerals in this and the other intrusives of the Ray area are apatite, sphene, zircon, sulfides, and locally primary epidote, allanite, and garnet. The sulfides are pyrite and chalcopyrite plus rare bornite.

Tea Cup Granodiorite

The Tea Cup Granodiorite occupies the western half of the Grayback quadrangle about 10 km southwest of the Ray copper deposit and extends south and west for possibly 35 and 8 km, respectively. It is overlapped on the west and partly on the south by Tertiary and Quaternary gravels. It cuts Precambrian Ruin Granite, diabase, and Pinal Schist. Locally apophyses of the granodiorite and its aplitic facies project out into the host rock for as much as 1,200 m. The Tea Cup Granodiorite ranges from granodiorite to quartz monzonite in composition. It is medium grained and locally contains aplitic dikes and pegmatitic segregations. In some areas these latter rocks and associated granodiorite or quartz monzonite contain two micas, phengite and biotite, and traces to 0.6 percent almandine garnet. Elsewhere the granodiorite and aplite contain only biotite. The texture is hypidiomorphic-seriate, porphyritic, and granitic. Phenocrysts, where present, are plagioclase (oligoclase-andesine), quartz, and locally hornblende up to 12 mm long. The groundmass and smaller grains in the granitic and seriate-textured

rocks are these same minerals plus K-feldspar, biotite, magnetite, and accessory minerals.

Granite Mountain Porphyry

The Granite Mountain Porphyry crops out in eight separate plutons plus half-a-dozen smaller bodies mostly intruded into Precambrian Pinal Schist in the southeastern Teapot Mountain quadrangle and southwestern Sonora quadrangle. The intrusions occupy a zone elongated in an east-northeast direction for 8 km. At the west end the zone is 4 km wide, at the east end 0.6 km wide. The Ray porphyry copper deposit occurs in the eastern part of this zone.

The Granite Mountain Porphyry is mostly granodiorite, but partly quartz monzonite. Textures range from granitic to porphyritic. Phenocrysts are plagioclase (oligoclase and andesine), quartz, and K-feldspar. In addition, the rock contains biotite, magnetite, and accessory minerals.

Laramide dikes and small plugs, ranging in composition from andesite to quartz latite, are closely related temporally and spatially to the larger plutons just described. The oldest are andesitic with a K-Ar age of 90-75 m.y. (unpublished K-Ar and fission-track ages in Hayden and Christmas quads.); the youngest are rhyodacitic and quartz latitic with a probable age of about 60 m.y. They thus range from older to somewhat younger than the larger intrusives. The dikes are steep to vertical, mostly trending east-west to N. 70° E., but locally northwest or northeast and are mostly less than 30 m thick.

The andesites contain phenocrysts of hornblende and labradorite in a groundmass of these minerals plus a little quartz, K-feldspar, ilmenite-magnetite, and accessory minerals.

The rhyodacite porphyries are the most abundant of the dikes, and crosscutting relationships indicate that they were intruded at several periods between 70 and 60 m.y. The rhyodacites have phenocrysts up to 15 mm long of andesine, hornblende, quartz, biotite, and magnetite-ilmenite in a groundmass of the same minerals plus K-feldspar and accessories. The melanocratic rhyodacite is similar but contains more hornblende in the groundmass.

Teapot Mountain Porphyry

The Teapot Mountain Porphyry is one of the youngest Laramide intrusive rocks in the area and forms small plugs and dikes in the Teapot Mountain quadrangle and northeastward in the Sonora quadrangle just north of the zone of Granite Mountain Porphyry plugs. The Teapot Mountain Porphyry is a silicic rock, quartz monzonitic in composition and similar in appearance to the rhyodacite porphyries but distinguished

from them by the presence of large pink K-feldspar phenocrysts.

The quartz latite porphyry, also one of the youngest intrusives in the area, is quite similar to the Teapot Mountain Porphyry but contains more K-feldspar in the groundmass.

CHEMICAL AND MODAL DATA

The triangular diagram pc-qtz-Kspar of the modes for the larger plutons shows that they range from diorite, quartz diorite, and syenodiorite to granodiorite, quartz monzonite, and granite. The sequence is from Tortilla Quartz Diorite to Rattler Granodiorite to Granite Mountain Porphyry to Tea Cup Granodiorite. The most silicic rocks in the quartz monzonite and granite fields are aplitic facies of the plutons.

The triangular diagram pc-qtz-Kspar for the dikes shows a trend similar to the larger plutons with the andesite most mafic, rhyodacites intermediate, and quartz latites most silicic. The dikes are lower in quartz than the plutons. This may be due to a greater abundance of unresolved or not easily discernible aphanitic groundmass in the dikes that contains quartz not seen.

The triangular diagram of normative pc-qtz-Kspar shows a trend similar to the one shown for the modes but more orderly. Nockold's average for quartz monzonite and quartz latite (qtz monzonite field), granodiorite (near qtz monzonite field), and dacite and quartz diorite (near qtz diorite field) are shown for comparison.

The triangular plot of normative Ab-An-Or shows a trend of decreasing An as we go from mafic Rattler Granodiorite to Tortilla Quartz Diorite to main Rattler Granodiorite to Granite Mountain Porphyry and Tea Cup Granodiorite. The lowest in An and richest in Ab+Or are the Teapot Mountain Porphyry and aplitic facies of the other plutons.

Chemical compositional trends of the igneous rocks show an orderly progression from mafic to silicic as is well shown in this slide where individual oxides of the major cations are plotted against the differentiation index (D.I.) modified from Thornton and Tuttle (1960). We determined the D.I. by adding quartz+albite+K-feldspar from molecular catanorms rather than from the CIPW norms, but the two are quite similar.

The andesites, Tortilla Quartz Diorite, and mafic facies of the Rattler Granodiorite, are the most mafic, ranging in D.I. from 48 to 58. The main body to the Rattler Granodiorite is intermediate in composition, ranging in D.I. from 65 to 78. The Granite Mountain Porphyry and Tea Cup Granodiorite are the most silicic of the plutons, ranging in D.I. from 79 to 87. Dikes and small stocks of rhyodacite and Teapot Mountain Porphyry overlap the Rattler Granodiorite and

Granite Mountain Porphyry in D.I. Aplites of the Rattler Granodiorite, Granite Mountain Porphyry, and Tea Cup Granodiorite range in D.I. from 93 to 96 except for one from the Rattler Granodiorite which is 87.

SiO_2 and K_2O show an orderly increase with increasing D.I. the SiO_2 from 55 to 76 percent, and the K_2O from 1.5 to 6 percent. Al_2O_3, total Fe as FeO, MgO, and CaO decrease with increasing D.I. as follows: Al_2O_3, 19 to 13 percent; ΣFe, 9 to 0.5 percent; MgO, 4 to 0 percent; CaO, 8 to 0.3 percent. For all of these constituents, the trends are reasonably orderly except for MgO in an andesite with a D.I. of 55 which has a high MgO content of 5.3 percent. Na_2O ranges from 2.7 to 4.2 percent in these rocks but does not show a trend up or down with increasing D.I.

In considering the trends of the oxides, it should be kept in mind that because the sum of the oxides in an analysis is constant, a large increase in one oxide (commonly SiO_2) causes a proportionate decrease in the sum of the remaining oxides. The true trends of individual oxides are modified by this effect but still convey a general impression of relative increases and decreases, especially where pronounced. This problem has been discussed by Chayes (1967) Krauskopf (1967, p. 398-399), and others.

The Ray igneous rocks are a calc-alkaline suite. Using the criterion of Peacock (1931), the trend line of Na_2O+K_2O crosses the trend line of CaO at about D.I. 60 where the SiO_2 line is at 60 percent. This is in the calc-alkalic (calc-alkaline) range. These rocks also fall in the calc-alkaline field using the criteria of Irvine and Barager (1971).

The Laramide igneous rocks at Ray were intruded in five surges during a 10-m.y. period, 70-60 m.y. ago (see Banks and others, 1972; Banks and Stuckless, 1973; Banks, 1976). One or more major plutons were intruded in each of the first four periods as follows: I, Tortilla Quartz Diorite and Rattler Granodiorite; II, Tea Cup Granodiorite; III, Granite Mountain Porphyry; IV, Teapot Mountain Porphyry. Rhyodacite to quartz latite dikes were intruded during periods II, IV, and V. As is shown by the D.I. trends and the above discussion, the oldest plutons are the most mafic and the progressively younger plutons are successively more silicic. The entire differentiation trend is also seen in successive facies of the Rattler Granodiorite, the pluton that we have been able to study in greatest detail.

The dike rocks follow the D.I. trends of the larger plutons and in general range from more mafic to more silicic with decreasing age; namely, andesite to mafic rhyodacite to rhyodacite to quartz latite, but there are reversals within the rhyodacite group, and andesite dikes cut the granodiorites of periods I and II.

As with the major constituents, the trace elements show similar trends in each pluton during successive stages of differentiation.

This suggests a common source for the magmas probably at considerable depth either in the upper mantle or lower crust.

Using all of our analytical data, we have calculated Spearman Rank correlation coefficients. Part of the matrix is shown in this slide where minor elements are correlated with major elements and with each other. Only positive and negative correlation coefficients greater than 0.6 are shown here. (Number of data pairs: major vs. minor elements 35; minor vs. minor elements 75; coefficients shown significant at 99 percent confidence level.) Minor elements with positive correlations toward each other are: Mn, Co, Sc, Sr, V. These elements also show positive correlations with Al, Ti, Fe, Mg, Ca, and P, and negative correlations with D.I., Si, K, and Pb.

Copper at a lower level correlates positively with Co, Ga, Ni, Ti, Fe, Mg, and P. Copper is erratically distributed in the igneous rocks ranging from less than 2 to 365 ppm. The mean for all the rocks (77 samples) is 74 ppm; for the Granite Mountain Porphyry (21 samples) 80 ppm; for the Rattler Granodiorite (40 samples) 81 ppm. Our studies indicate that less than half of the copper was a primary constituent of the rock.

DEPTH OF INTRUSION

Stratigraphic reconstructions indicate that the depth of cover in the Ray district at the time of the Laramide pluton intrusions was between 1 and 3 km. It is interesting to note that a similar depth range has been estimated for the Bingham stock in the Bingham mining district, Utah, by Gilluly (1932; 1946) and Moore (1973, p. B38). The maximum depths of the upper parts of the Rattler Granodiorite and some of the Tortilla Quartz Diorite intrusives are estimated to have been 1.5 km , and of the Granite Mountain Porphyry and Teapot Mountain intrusives 2.5 km. Concordance of apatite fission-track ages with other mineral ages indicates a maximum depth for these plutons and for the Ray copper deposit of 5 km during and since Laramide time (Banks and Stuckless, 1973). No stratigraphic reconstruction can be estimated for the depth of intrusion of the Tea Cup Granodiorite as it was intruded into older Precambrian rocks of unknown thickness.

VOLATILE CONTENTS OF THE MAGMAS

As has been pointed out by Banks (1976, p. 94), several petrochemical features of the Laramide plutons in the Ray area suggest that they did not saturate early during their crystallization nor evolve much water. The MgO content of the biotite decreases slightly with increasing differentiation index, but markedly with decreasing age of the intrusives. Wones and Eugster (1965) have suggested that such a trend indicates undersaturation of water in the melt. Low volatile contents of the magmas are also indicated by: scarcity of aplites and

pegmatites in the plutons, minor metamorphic aureoles around all of the intrusive bodies, absence of miarolitic cavities, sparsity of fluid inclusions in quartz and the fact that they are dilute, two phase, and homogenize at below 450°C (J. T. Nash, written commun., 1971, 1972; M. J. Logsdon, oral commun., 1973).

The water content of the magmas at their emplacement is also indicated by the point during crystallization at which hydrous minerals first formed. In the rhyodacite dikes, Teapot Mountain Porphyry and a restricted porphyritic variant of the Rattler Granodiorite phenocrysts of biotite and hornblende occur in a fine-grained groundmass that makes up 30-50 percent of the rock, which indicates that the hydrous minerals started to form before the midpoint of crystallization. However, in the Granite Mountain Porphyry, Tea Cup Granodiorite, Tortilla Quartz Diorite, and the main facies of the Rattler Granodiorite, the hydrous minerals are interstitial to plagioclase, which makes up about 50 percent of the rocks, and intergrown with quartz and K-feldspar. Thus in these rocks, which comprise the bulk of the intrusive bodies at Ray, biotite and hornblende probably did not start to form before the midpoint of solidification.

At their depths of emplacement the intrusives at Ray should have contained 2.5-3.0 wt. percent H_2O before biotite started to form (D. R. Wones, oral commun., 1973; Wones and Dodge, 1966). Thus if, as indicated above, biotite first formed after the plutons were 50 percent crystallized, the initial water content of the magma must have been less than 1.5 percent.

Our textural studies also show that hydrous minerals show cross-cutting, interstitial, and coeval relations with the late-forming anhydrous minerals (mainly quartz, K-feldspar, and plagioclase). These relations and the presence of biotite, apatite, and sphene in late-stage aplitic differentiates of all the plutons indicate that hydrous phases continued to form until only a small amount, if any, liquid remained.

Banks (1976) has also studied the halogen contents of igneous minerals in the Laramide intrusives at Ray. He has summarized the results of this study as follows:

> "Apatite and biotite in younger, more silicic rocks contain more F but less Cl and H_2O+ than apatite and biotite in older, more mafic rock; the same relations hold for F and H_2O+ in sphene. * * * The contents of Cl, F, and H_2O+ in whole-rock samples decrease with increasing differentiation index and decreasing age. * * * The data are satisfactorily although not exclusively explained by postulating that the melts each contained progressively less Cl, F, and H_2O and that the hydrous minerals consumed most of the Cl, F, and H_2O in the magmas."

SOURCE OF COPPER IN THE RAY DEPOSIT

The Ray deposit is a major disseminated copper deposit. Since 1911 production has amounted to 1-3/4 million tons of copper, 45,000 oz of gold, and 4.5 million oz of silver. Total reserves are estimated at 650 million tons of ore of which three-fourths is primary, the remainder secondary (N. A. Gambell, oral commun., 1976). The deposit covers an area 3.2 km long in an east-west direction and 2.4 km north-south and is at the intersection of major northwest- and northeast-trending fault zones. It is also in an area of small plugs of Granite Mountain Porphyry, which occupy a zone elongated in an east-northeast direction for 5 km from the main exposed pluton of Granite Mountain Porphyry.

The primary hypogene minerals are pyrite, chalcopyrite, minor bornite and molybdenite, with traces of galena, sphalerite, and tennantite. Primary copper, occurring mainly in chalcopyrite, averages 0.1-0.2 percent in the Pinal Schist (Precambrian) and Granite Mountain Porphyry and forms large bodies of ore grade (more than 0.4 percent Cu) in the Precambrian diabase.

In considering the source of the copper and mineralizing solutions that formed the Ray deposit, several factors should be considered. First, the age of mineralization has been determined by K-Ar dating of hydrothermal biotite intergrown with ore minerals at 65 m.y. (Banks and others, 1972, p. 872, 875), and at 60 m.y. by fission-track determination of reset apatite in the deposit (Banks and Stuckless, 1973). The Granite Mountain Porphyry, which was mineralized by the ore solutions at the deposit, has a K-Ar age of 61 m.y. The Teapot Mountain Porphyry, which crops out as northeast-trending zone of small stocks and dikes 0.8 km north of the Ray deposit, has been dated at 63 m.y. The Tortilla Quartz Diorite dated at 70 m.y. (Banks and others, 1972, p. 871, 874) crops out in a small stock 0.8 km south of the deposit and also in a large pluton 3 km to the southwest.

These stocks and the east-trending rhyodacite dikes in the area are the intrusive rocks most closely related spatially and possibly genetically with the Ray copper deposit. It is possible that ore solutions emanated directly from one of these igneous bodies, or from a common source beneath the area at shallow or great depth. The ore deposit and two of the intrusives (Granite Mountain Porphyry and Teapot Mountain Porphyry) occur near the intersection of major northwest- and northeast-trending fault zones. It is quite likely that these throughgoing intersecting shear zones provided access to the surface from great depth for both magmas and hydrothermal solutions. The hydrothermal solutions could have carried copper from a deep source or have leached it from basement rocks as they migrated upward.

We prefer a model of magmas and copper-bearing hydrothermal solutions ascending from considerable depth--probably from the upper mantle. Derivation of the copper-bearing solutions directly from one

of the nearby plutons does not appear too likely in view of the probable small amounts of volatiles that could have been evolved from most of these as discussed above. If a local source directly from a pluton is postulated, the Granite Mountain Porphyry is probably the most likely one. The small stocks in the area of the copper deposit could be underlain at shallow depth by a larger body from whence the solutions could have emanated.

As discussed above, the distribution of trace copper in the igneous bodies in the Ray area does not give any clues that one or another is a likely source of copper for the deposit, either because it is enriched or depleted in copper. The range of copper content is similar in all the bodies including those far removed from the Ray deposit and goes from several to several hundred ppm, but commonly less than 90 ppm. Our studies indicate that more than half of this copper is secondary, introduced after solidification of the bodies.

REFERENCES CITED

Banks, N. G., 1976, Halogen contents of igneous minerals as indicators of magmatic evolution of rocks associated with the Ray porphyry copper deposit, Arizona: U.S. Geol. Survey Jour. Research, v. 4, no. 1, p. 91-117.

Banks, N. G., Cornwall, H. R., Silberman, M. L., Creasey, S. C., and Marvin, R. F., 1972, Chronology of intrusion and ore deposition at Ray, Arizona--Part I, K-Ar ages: Econ. Geology, v. 67, p. 864-878.

Banks, N. G., and Stuckless, J. S., 1973, Chronology of intrusion and ore deposition at Ray, Arizona--Part II, Fission-track ages: Econ. Geology, v. 68, p. 657-664.

Chayes, Felix, 1967, On the graphical appraisal of the strength of associations in petrographic variation diagrams, *in* Abelson, P. H., ed., Researches in geochemistry, v. 2: New York, John Wiley and Sons, p. 322-339.

Gilluly, James, 1932, Geology and ore deposits of the Stockton and Fairfield quadrangles, Utah: U.S. Geol. Survey Prof. Paper 173, 171 p.

_____1946, The Ajo mining district, Arizona: U.S. Geol. Survey Prof. Paper 209, 112 p.

Irvine, T. N., and Baragar, W. R. A., 1971, A guide to the chemical classification of the common volcanic rocks: Canadian Jour. Earth Sci., v. 6, p. 523-548.

Krauskopf, K. B., 1967, Introduction to geochemistry: New York, McGraw-Hill Book Co., 721 p.

Moore, W. J., 1973, Igneous rocks in the Bingham mining district, Utah: U.S. Geol. Survey Prof. Paper 629-B, 42 p.

Peacock, M. A., 1931, Classification of igneous rock series: Jour. Geology, v. 39, p. 54-67.

Thornton, C. P., and Tuttle, O. F., 1960, Chemistry of igneous rocks--I, Differentiation index: Am. Jour. Sci., v. 258, p. 664-684.

Wones, D. R., and Dodge, F. C. W., 1966, On the stability of phlogopite [abs.]: Geol. Soc. America and associated societies, Ann. Mtg., San Francisco, Calif., 1966, Program, p. 243.

Wones, D. R., and Eugster, H. P., 1965, Stability of biotite; experiment, theory, and application: Am. Mineralogist, v. 50, p. 1228-1272.

PORPHYRY SYMPOSIUM ASSOCIATES

1704 WEST GRANT ROAD TUCSON, ARIZONA 85705

DIRECTORS:
Paul I. Eimon
602-624-7421
John M. Guilbert
602-884-2509
J. David Lowell
602-887-5241
Thomas W. Mitcham
602-623-6316
Kenyon Richard
602-297-5733

Silver Bell Field Trip

Friday, October 31, 1975

Chief Guides: Steve Davis, Exploration Geologist, Tucson Office, Asarco
Jim Gayley, Resident Geologist, Silver Bell, Asarco

STOPS (See attached map)

(1) West end of Oxide Pit. Note pink K-spar in veinlets---sericite alteration of original plagioclase----chloritic alteration of original muscovite. Chalcocite at this point believed to have moved in supergene solutions laterally from areas of good limonite-after-chalcite capping (now mined out to eastward) and deposited beneath poor capping at this locality. Post-mineral andesite dikes show in pit banks just to east of this stop. Potassic alteration is not found in alaskite. In general a potassic zone extends ESE. through the middle of the Oxide pit as a narrow zone with strong, wide phyllic alteration zones on each side. Spotty propylitic alteration occurs outside of phyllic zone.

(2) Bottom level---east center of Oxide pit. Two benches of chalcocite ore below this level. Note the consistent systems of parallel veinlets striking N. to ENE. in pit walls around the NE. side and striking southerly around the S. side. Part of the N. side of the pit (the blackened areas) is a thin (50'?) shell of silicified (not silicated) Paleozoic limestone which contains no Cu. The chalcite ore, now mined out, occurred in monzonite and dacite porphyries up to this shell.

(3) Road cut in main haulage road from El Tiro pits to mill. Note weak propylitic alteration in quartz monzonite porphyry---some of porphyry is almost fresh. The edge of the main zone of phyllic alteration is about 1500' NE. from this point. Ask Tom Mitcham to show you supergene Cu-Mn in weathered rock here.

(4) Midway on power line side road. Note Cu-Mn oxide relationships in alaskite. Alteration here generally weak phyllic and moderate argillic. In some parts of this area potassic alteration as secondary biotite can be seen in outcrops. This point is about the S. edge of the main El Tiro alteration zone. At this stop the alteration is essentially weak across (NE) the entire zone.

(5) Pit bench (final) W. side of E. Extension No. 2 of El Tiro ore body. Actually in tactite capping over ore-grade material which will not be mined. A monzonite stock lies to the W. It is only weakly altered and contains no ore.

(6) Bottom of E. Extension No. 2 of El Tiro pits (Whattaname!) Note spotty tactite ore mixed with marble. Tactite is roughly zoned away from porphyry and across the bedding. Going easterly, the principal order of zonation is garnet, serpentine and diopside. These zones overlap and are mixed. Tremolite and wollastonite have spotty occurrence. This ore may be in Abrigo (?) and extend up into Martin (?).

(7) West of Daisy hilltop. Geothite, hematite and jarosite capping. The system of parallel veinlets is pronounced. This same structural condition of generally NE-striking close-spaced veinlets was mapped in the original outcrops from this point continuously to the S. edge of El Tiro pit. What causes a mass made up of two intrusives---- alaskite and monzonite----to be fractured like that?

(8) West entrance to El Tiro pit. Note the sharp interface between sulphides and leached capping.

(9) Bottom of El Tiro pit. Note weak potassic alteration in monzonite. Here a pebble dike can be seen containing altered limestone clasts which have been carried upward 150'.

The foregoing brief notes were compiled by me; but, for the most part, they consist of the opinions and work done in recent years by Fred Graybeal, Steve Davis, and others. Harold Courtright, Steve Von Fay and I used to be experts on Silver Bell geology, but these young fellows are smarter. If you ask me any questions I'll only give you an, "I-remember-once-when-I-saw-such-and-such-an-exposure-which-indicated-so-and-so----but, now it's either dug out or buried!"

Kenyon Richard

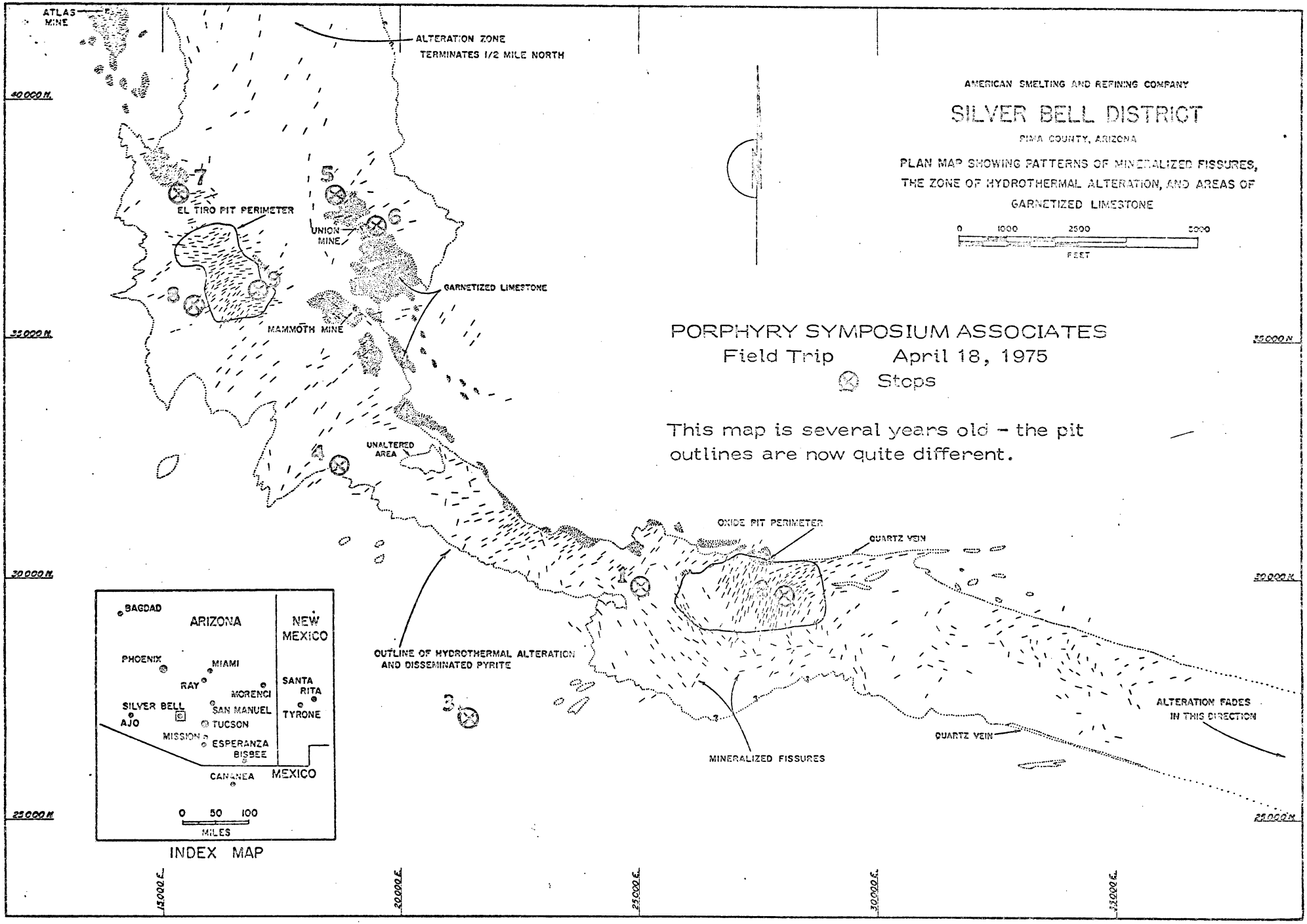
AMERICAN SMELTING AND REFINING COMPANY
SILVER BELL DISTRICT
PIMA COUNTY, ARIZONA
PLAN MAP SHOWING PATTERNS OF MINERALIZED FISSURES, THE ZONE OF HYDROTHERMAL ALTERATION, AND AREAS OF GARNETIZED LIMESTONE
0 1000 2500 5000
FEET
PORPHYRY SYMPOSIUM ASSOCIATES
Field Trip April 18, 1975
Stops
This map is several years old - the pit outlines are now quite different.
ATLAS MINE
ALTERATION ZONE TERMINATES 1/2 MILE NORTH
EL TIRO PIT PERIMETER
UNION MINE
GARNETIZED LIMESTONE
MAMMOTH MINE
UNALTERED AREA
OXIDE PIT PERIMETER
QUARTZ VEIN
OUTLINE OF HYDROTHERMAL ALTERATION AND DISSEMINATED PYRITE
MINERALIZED FISSURES
QUARTZ VEIN
ALTERATION FADES IN THIS DIRECTION
40000 N.
35000 N.
30000 N.
25000 N.
15000 E.
20000 E.
25000 E.
30000 E.
33000 E.
BAGDAD
ARIZONA
NEW MEXICO
PHOENIX
MIAMI
RAY
MORENCI
SANTA RITA
SILVER BELL
SAN MANUEL
AJO
TUCSON
TYRONE
MISSION
ESPERANZA
BISBEE
CANANEA
MEXICO
0 50 100
MILES
INDEX MAP

PORPHYRY SYMPOSIUM ASSOCIATES
Field Trip

This map is several years old – the pit outlines are now quite different.

Stops

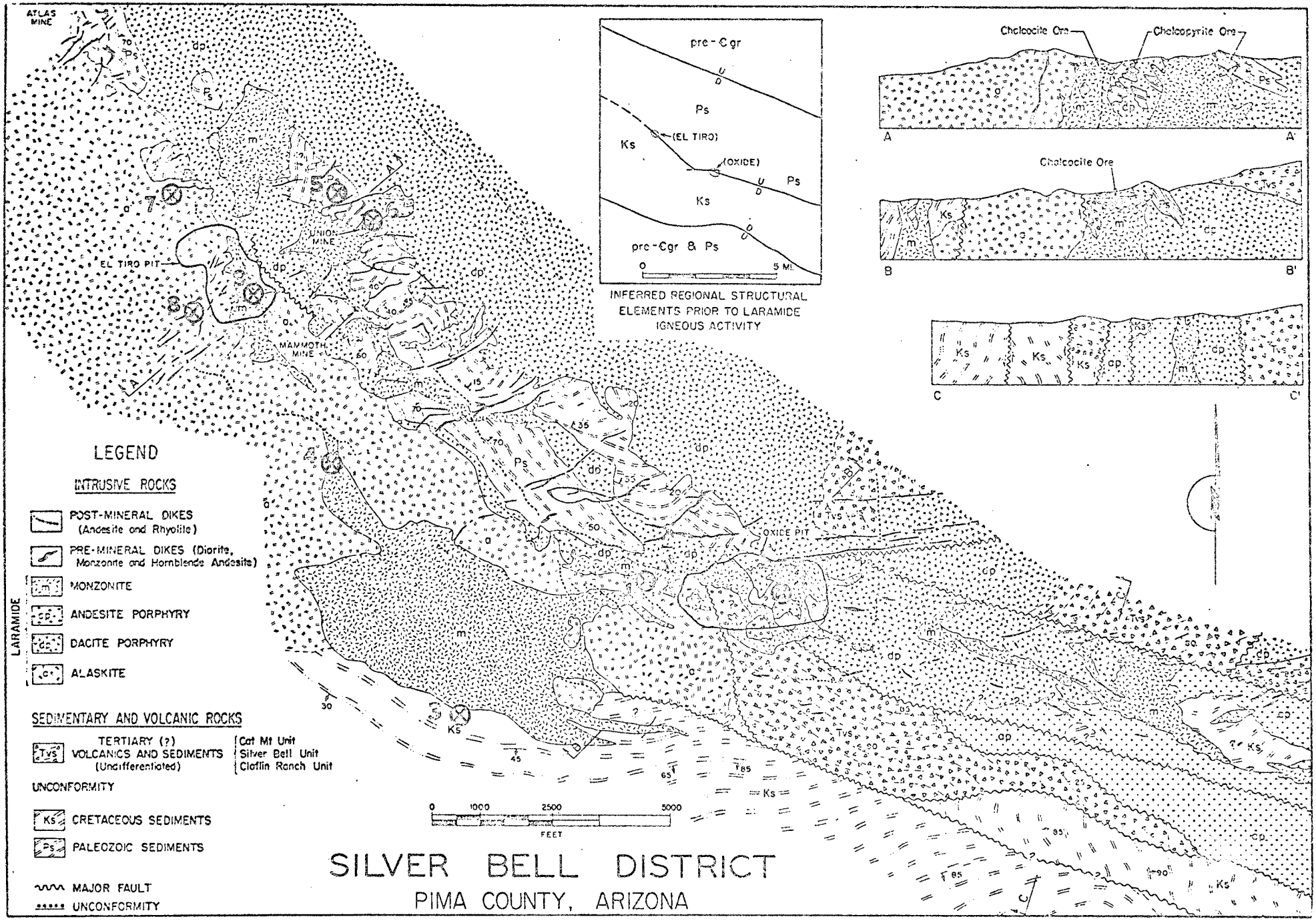

SILVER BELL DISTRICT

PIMA COUNTY, ARIZONA

✧ ✧ ✧ STRUCTURE AND MINERALIZATION AT SILVER BELL, ARIZONA

BY KENYON RICHARD AND JAMES H. COURTRIGHT

INTRODUCTION

This material was originally published (12) in November 1954. Exploration and mining during subsequent years have provided additional information; accordingly, a number of revisions of text and figures are included herein. Basic concepts, however, remain essentially the same as originally presented.

Watson (oral communication, 1962) has prepared a doctoral dissertation based on detailed mapping in the Silver Bell Mountains. Mauger et al. (9) are making potassium-argon age determinations of most of the igneous rocks in the district. These two lines of research should, among other things, materially improve upon the knowledge of certain age relations that are noted only briefly herein.

Silver Bell is 35 airline miles northwest of Tucson, Arizona, in a small rugged range rising above the extensive alluvial plains of this desert region. Its geographical relation to other porphyry copper deposits of the Southwest is shown on the inset map in the lower left corner of figure 1. The climate is semiarid. Altitudes range from 2,000 to 4,000 feet.

Opening of the Boot mine, later known as the Mammoth, in 1865, was the first event of note in the district's history. Oxidized copper ores containing minor silver-lead values were mined from replacement deposits in garnetized limestone and treated in local smelters. Copper production had approached 45 million pounds by 1909 when the disseminated copper possibilities in igneous rocks were recognized. Extensive churn-drill exploration was carried out during the next 3 years and resulted in the partial delineation of two copper sulfide deposits—the Oxide and El Tiro. Although the then submarginal tenor discouraged exploitation of these disseminated deposits, selective mining of ore bodies in the sedimentary rocks continued intermittently until 1930, providing a production total of about 100 million pounds of copper.

The American Smelting and Refining Co. began exploratory and check drilling in 1948 and subsequently made plans for mining and milling the Oxide and El Tiro ore bodies at the rate of 7,500 tons per day. Production began in 1954 and has been maintained at a rate of about 18,000 tons of copper annually.

GENERAL GEOLOGY

Formations ranging in age from Precambrian to Recent are exposed near Silver Bell. The more erosion-resistant of these—Paleozoic limestone and Tertiary(?) volcanics—predominate in the scattered peaks and ridges comprising the Silver Bell Mountains. Porphyry copper mineralization occurs along the southwest flank of these mountains in hydrothermally altered igneous rocks. These are principally intrusives which cut Tertiary(?), Cretaceous, and older sediments and are considered to be components of the Laramide Revolution.

For three-fourths of its length, the zone of alteration strikes west-northwest (fig. 1). There now is no single structure that accounts for this alignment. However, indirect evidence suggests that a fault representing a line of profound structural weakness existed in this position prior to the advent of Laramide intrusive activity. This line will hereafter be referred to as the "major structure." It was largely obliterated by the Laramide intrusive bodies, but it effected a degree of control on their emplacement, as evidenced by their shapes and positions. The influence of fault structures on the shapes of intrusives in other porphyry copper districts has been noted by Butler and Wilson (2).

As shown on the inset map on figure 2, a fault of parallel trend and considerable displacement lies to the north. This fault is now marked by a line of small intrusive bodies. To the south is a third fault of large displacement. Evidence of its age in relation to the Laramide intrusions and mineralization is not recognized, but its conformance in strike with the other two major faults is significant. These three breaks establish a pronounced trend of regional faulting, and it has been suggested (11) that they be named, from south to north, the Waterman thrust, the Silver Bell fault zone, and the Ragged Mountains fault. The two northerly ones are high angle, and the southerly one may be

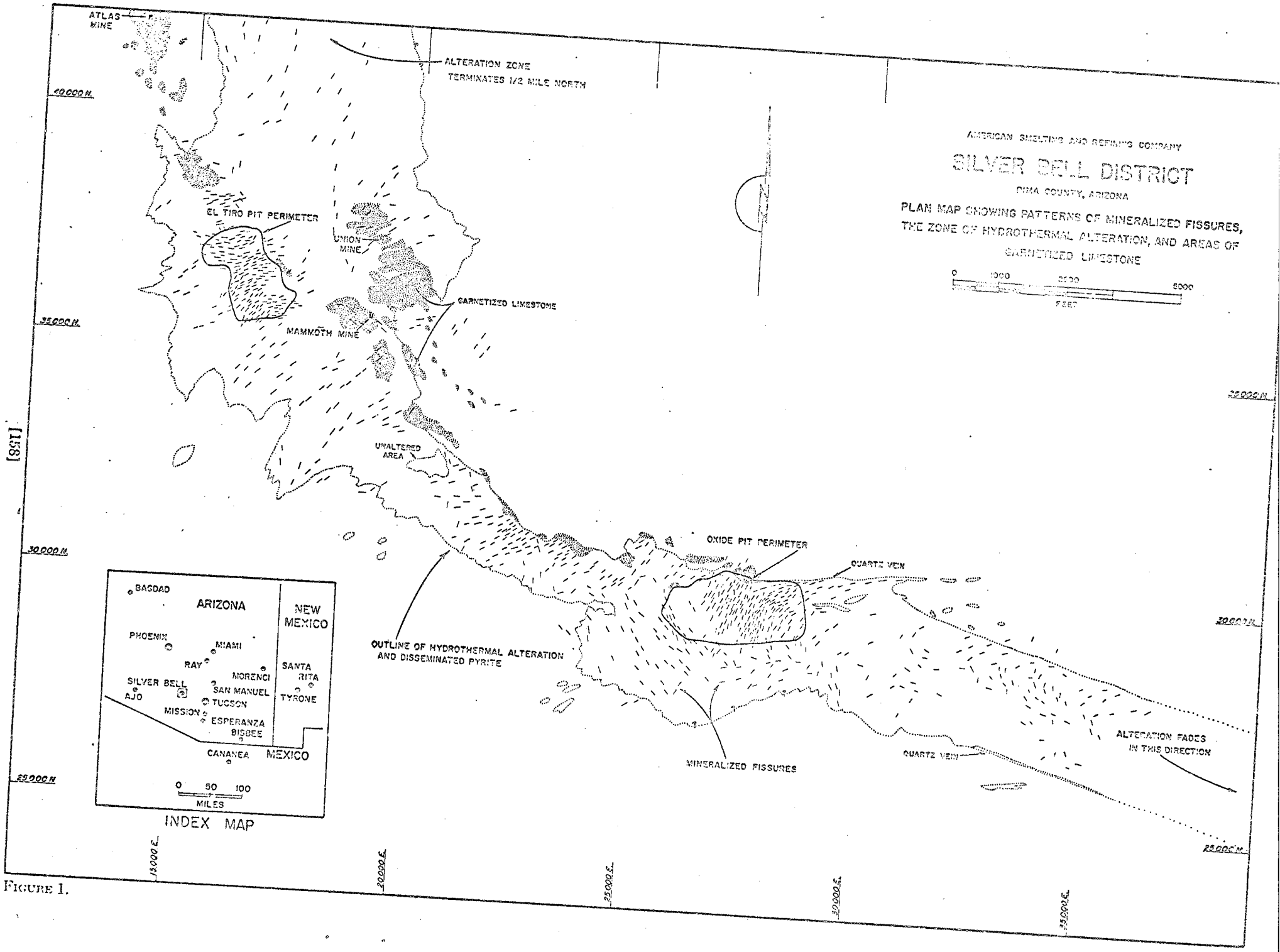
AMERICAN SMELTING AND REFINING COMPANY
SILVER BELL DISTRICT
PIMA COUNTY, ARIZONA
PLAN MAP SHOWING PATTERNS OF MINERALIZED FISSURES, THE ZONE OF HYDROTHERMAL ALTERATION, AND AREAS OF GARNETIZED LIMESTONE
0 1000 2000 5000
FEET
ATLAS MINE
ALTERATION ZONE TERMINATES 1/2 MILE NORTH
EL TIRO PIT PERIMETER
UNION MINE
GARNETIZED LIMESTONE
MAMMOTH MINE
UNALTERED AREA
OXIDE PIT PERIMETER
QUARTZ VEIN
OUTLINE OF HYDROTHERMAL ALTERATION AND DISSEMINATED PYRITE
MINERALIZED FISSURES
QUARTZ VEIN
ALTERATION FADES IN THIS DIRECTION
40000 N.
35000 N.
30000 N.
25000 N.
15000 E.
20000 E.
25000 E.
30000 E.
35000 E.
BAGDAD
ARIZONA
NEW MEXICO
PHOENIX
MIAMI
RAY
MORENCI
SANTA RITA
SILVER BELL
AJO
SAN MANUEL
TUCSON
TYRONE
MISSION
ESPERANZA
BISBEE
CANANEA
MEXICO
0 50 100
MILES
INDEX MAP

FIGURE 1.

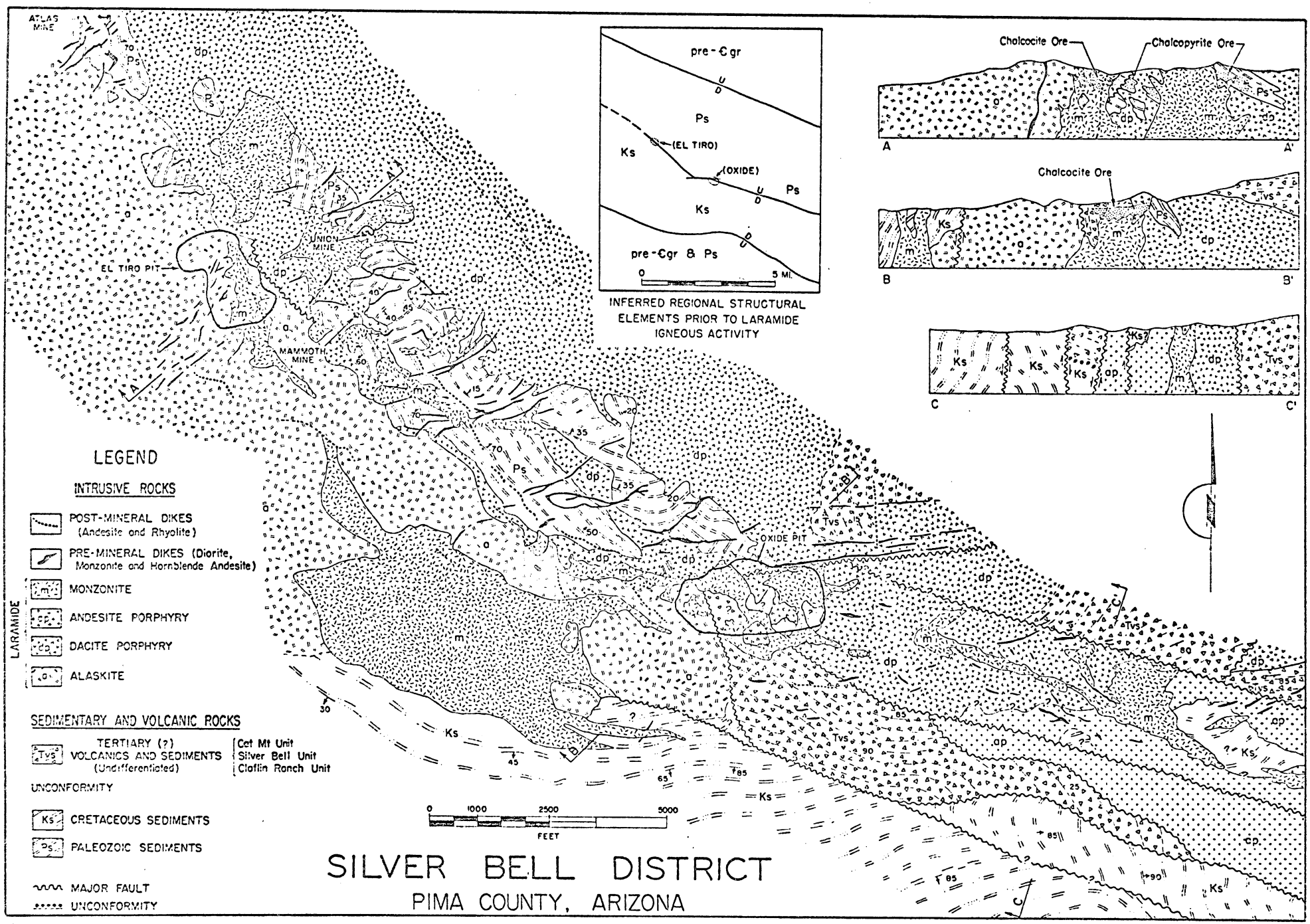
SILVER BELL DISTRICT
PIMA COUNTY, ARIZONA
LEGEND
INTRUSIVE ROCKS
POST-MINERAL DIKES (Andesite and Rhyolite)
PRE-MINERAL DIKES (Diorite, Monzonite and Hornblende Andesite)
LARAMIDE
MONZONITE
ANDESITE PORPHYRY
DACITE PORPHYRY
ALASKITE
SEDIMENTARY AND VOLCANIC ROCKS
TERTIARY (?) VOLCANICS AND SEDIMENTS (Undifferentiated)
Cat Mt Unit
Silver Bell Unit
Claflin Ranch Unit
UNCONFORMITY
CRETACEOUS SEDIMENTS
PALEOZOIC SEDIMENTS
MAJOR FAULT
UNCONFORMITY
FEET
ATLAS MINE
EL TIRO PIT
UNION MINE
MAMMOTH MINE
OXIDE PIT
INFERRED REGIONAL STRUCTURAL ELEMENTS PRIOR TO LARAMIDE IGNEOUS ACTIVITY
pre-Cgr
Ps
Ks
(EL TIRO)
(OXIDE)
pre-Cgr & Ps
Chalcocite Ore
Chalcopyrite Ore

FIGURE 2.

reverse. Stratigraphic separations on these faults are on the order of several thousand feet.

The local Paleozoic section is 4,400 feet thick (10). It is composed predominantly of limestone with a basal quartzite member. The Cretaceous section appears to be more than 5,000 feet thick, but this figure is not a result of careful measurement. Conglomerate, red shale, and arkosic sandstone characterize the lithology. Volcanic and sedimentary rocks of early Tertiary(?) age aggregate more than 2,000 feet in thickness. Three units are recognized by the writers (14): (a) the Claflin Ranch (earliest)—conglomerate and coarse sandstone made up largely of igneous fragments and containing a few pyroclastic interbeds; (b) the Silver Bell—andesite porphyry breccia, principally of mudflow origin; and (c) the Cat Mountain[1]—pyroclastics, composed mainly of ashflows (oral communication, Watson, 1962).

Intrusion of alaskite marked the beginning of Laramide igneous activity. It was emplaced as an elongate stock with its northeast side closely conforming to the major structural line for a distance of nearly 4 miles. The alaskite was at one time regarded as a thrust block of Precambrian rock (6); however, clear evidence of its intrusive relation with Paleozoic limestone and Cretaceous(?) arkose has since been found.

The intrusive activity was at this stage interrupted by an interval of erosion, resulting in partial exposure of the alaskite stock, followed by deposition of the Claflin Ranch, Silver Bell, and Cat Mountain units. (These three units are grouped as Tertiary(?) volcanic and sedimentary rocks on figure 2 herein, and were termed "dacite agglomerate" on figure 2 (12) by Richard and Courtright.) A similar sequence has been recognized by the writers elsewhere in the Southwest (14).

The next event was the intrusion of a large stock or sill of dacite porphyry about 3 miles in width and at least 6 miles in length in a northwesterly direction. Its main mass is outside and along the northeast edge of the mineralized zone. Although its southwesterly side consists of irregular stocks, sills, and dikes extending into the mineralized zone, these apophyses of the dacite porphyry are limited in this direction by the major structural line. A number of large pendants of folded and faulted Paleozoic sedimentary rocks occur in the southwest edge of the dacite porphyry. Thus, it is inferred that the original major fault between the Paleozoic and Cretaceous(?) sedimentary rocks became a contact between alaskite and Paleozoic sedimentary rocks and then a contact between dacite porphyry and alaskite.

Andesite porphyry may have been intruded later than the dacite porphyry, but relations are not clear; it may be simply a facies of the latter.

[1] K-Ar ages of 56 to 70 m.y. have been obtained for various Cat Mountain Rhyolite occurrences by Damon et al. (3). According to Holmes (5), Tertiary time beginning is 70±2 m.y.

Subsequent parallel faulting along the major structural line sliced the volcanic and Cretaceous (?) rocks into horst and graben structures. These faults are remarkably persistent southeasterly, extending several miles beyond the map. They probably extended through the northwest part of the district, but there is little direct evidence. The formation of these faults indicates at that time a still existent deep-seated zone of weakness along the major structural line.

Monzonite stocks and contemporaneous dikes were then emplaced along and near this line, obliterating parts of the faults described in the foregoing paragraph. The stocks are elongate parallel to the major structural line; but the dikes trend across it, for the most part, with an average east-northeast strike. The dikes are elements of an extensive swarm having a general northeasterly trend and occurring throughout the Silver Bell Mountains.

Systems of close-spaced *parallel* fractures then developed. These systems are distributed along the major structural line and generally strike across it.

Alteration and sulfide mineralization took place next. The deposition of sulfides, particularly chalcopyrite, was controlled in detail by the cross-trending fractures. Although these are distributed along the major structural line as a narrow band, it is notable that throughout much of its length there are now no fault structures to account for the trend of this zone.

Post-sulfide dikes of andesite and rhyolite represent the last intrusive activity in the immediate district. Curiously, most of these andesite dikes are parallel to the major structure, although it would seem that the cross-breaking fractures represented available lines of weakness. This serves to emphasize the major structural line as being a profound deep-seated zone of weakness persisting through a long period of time.

Uplift and erosion of the region exposed the lean primary mineralization to processes of leaching and enrichment, resulting in the accumulation in the district of a thin blanket of chalcocite. Two open-pit ore bodies occur in this blanket.

Remnants of flows of andesite and basalt occur in the flats surrounding the Silver Bell range. In at least one locality to the east these flows are nearly flat and overlie conglomerate, which dips about 25° and contains boulders and fragments eroded from *completely* leached capping of the mineralized zone. Damon et al. (3) have determined an age of 27.9 m.y. for these flows. This is particularly interesting because it indicates that, prior to that date, there existed an environment permitting formation of leached capping and, presumably, a chalcocite zone.

STRUCTURAL CONTROL OF HYPOGENE MINERALIZATION

As in the majority of porphyry copper deposits, the principal primary sulfide minerals at Silver Bell are

pyrite and chalcopyrite. Although occurring as discrete grains, they are more abundant—accompanied by quartz—in systems of veinlets or seams that are usually near vertical in attitude and persistently parallel. Varying in thickness from paper thin to several inches and in spacing from inches to several feet, these thin sulfide sheets occur as groups of various sizes in the narrow northwest-trending zone of hydrothermal alteration. (Due to the small scale, any single line in the pattern of "Mineralized Fissures" on figure 1 diagrammatically represents a large number of parallel veinlets, rather than an individual.) In detail the average individual fissure appears as a thin quartz-sulfide seam encased by a rather uniform band of sericite. The fissures are predominantly oriented in the northeast quadrant; a small proportion strike northwest and a few are random. From a broad viewpoint there are, among these systems or groups, no intersections of consequence. Within a group, changes in strike occur gradually and result in curving trends. As noted earlier, these groups of mineralized fissures are distributed along the major structural line, and it is assumed that they were formed in response to deep-seated uniform stress related to that line.

At least a few hundredths of 1 percent copper is present nearly everywhere in the zone of disseminated sulfides; better values occur where there are veinlets; and the best values occur where the veinlets are close spaced. The two comparatively large groups of these close-spaced structures coincide with the positions of the two ore bodies (fig. 1). However, the actual structural, mineralogical, and lithological distinctions among these and other smaller groups are minor, and the factors that controlled the position and size of these two groups are not clearly evident. A strong east-west fault that terminates in the Oxide area may have influenced the concentration of fracturing there, and at El Tiro the sharp bend in the alteration zone and the group of northeast-striking dikes likewise may indicate a cross-trending line of weakness that localized stresses. Nonetheless, the importance of these structural conditions is not clearly demonstrated, and no good evidence is found to explain the structural cause of the more intense fracturing which localized the two ore bodies in their present positions in preference to other locations along the major structural line.

Outside the zone of alteration the dacite porphyry is finely fractured and jointed in most of its large exposed area. In sharp contrast to the systems of parallel fissures in the alteration zone, these fractures in the dacite porphyry are almost completely of random orientation; parallelisms are rare and traceable for only a few inches or feet. They are pre-mineral in age where they are found in the alteration zone in the westerly and southwesterly parts of the dacite porphyry. It would seem that in physical aspect this formation was exceptionally well prepared to be mineralized—perhaps better than the rocks of the ore-zone proper. The fact that it was mineralized only locally may be accounted for, in part, by the absence of *systematic* fractures. That is, only the systems of parallel fractures were connected with the deep-seated source of mineralization, and the pervasive breaking of the dacite porphyry did not alone qualify it for mineralization.

Excepting the post-mineral andesite dikes, all igneous rocks in the narrow northwest-trending zone shown on figure 1 are hydrothermally altered. Variations in the intensity or in the completeness of the process have been subdivided by Kerr (6) into five stages. His analysis demonstrated, among other things, that the known ore bodies are in the more strongly altered areas. The area outlined by the writers on figure 1 includes all degrees of alteration, but no differentiation is made. It merely represents the areal extent of bleached-appearing igneous rocks showing evidence in the leached outcrops of pre-existing disseminated sulfides—principally pyrite. The transition to relatively fresh rock is quite sharp in many places, particularly along the contact with sedimentary rocks and on the faults in the southeast part. However, along most of the southwest margin the transition is gradational, and the limit is an arbitrary line.

Tactite—composed essentially of garnet, diopside, other lime-silicate minerals, and quartz—is confined to a narrow belt along the southwest margin of the limestone pendants, except near the Mammoth and Union mines where it has replaced the full width of the sedimentary block. There, parts of the tactite contain sufficient disseminated chalcopyrite to be classed as low-grade ore. As in the Mission deposit (13), this mineralized tactite is regarded by the writers as having been formed by the same processes that altered and mineralized the intrusive rocks. Thus, it is a product of hydrothermal metasomatism rather than contact metamorphism caused by the dacite porphyry and the monzonite as proposed by Stewart (15).

SUPERGENE ENRICHMENT

The two ore deposits consist of rudely tabular accumulations of chalcocite from 100 to 200 feet thick. Lying beneath about 100 feet of leached capping, they were formed by twofold to threefold enrichment of the copper contained in the primary mineralization. Typical ore is composed of altered rock and sulfides in a ratio of about 10:1 by weight.

Most of the capping over the ore bodies contains less than one-tenth of 1 percent copper as cuprite or other oxidation products mingled with the limonite. Occasionally, somewhat higher values occur where copper has been precipitated as silicates and carbonates by reactive gangue material present in less altered rock. In the ore bodies where alteration is strong and the gangue is nonreactive, the upper limit of the sulfide zone (or the base of oxidation) appears on open-pit

bench faces as a sharply defined highly irregular interface. Only rarely is there a transition zone of mixed sulfide and oxide copper minerals. Some of the irregularities of the base of oxidation are caused by displacement on post-chalcocite faults, but most seem to be due to variations in rock permeability. This is evidenced by the dense siliceous character of a few sulfide remnants occurring well up in the leached zone and by leached indentations of the sulfide zone along many of the fissures.

The present water table at Silver Bell is well below the chalcocite zone, a condition that exists in many of the porphyry copper districts (4). This indicates that the Silver Bell chalcocite zone now is in an environment of oxidation, and it should be undergoing leaching rather than enrichment. This current climatic cycle may have been relatively short and dry and may have caused only minor modifications of the chalcocite blanket.

The base of oxidation conforms in general shape to modern topography, although local relief is more than 200 feet. This rude conformance would seem to require a relatively wet climate with the water table being no more than a few tens of feet below the ground surface as the modern physiography developed.

In the early days at Morenci, Lindgren (7) observed that oxidation and leaching had, in some instances, penetrated along fissures down through the chalcocite into underlying primary sulfides; he also observed that erosion of Chase Creek Canyon had left the principal chalcocite zones stranded high above the canyon bottom, indicating that the chalcocite formed originally about an ancient water table several hundred feet above the present water table. Although erosion at Silver Bell has not penetrated as deeply as at Morenci, its chalcocite zone currently is in a similar unbalanced environment of oxidation with no appreciable enrichment now taking place. Reshaping of the upper surface of chalcocite zones in both districts to conform to the existing ground surface appears, then, to have occurred during formation of the modern topography but at some time prior to the current dry climatic cycle.

LEACHED OUTCROPS

In the formation of many disseminated chalcocite deposits the enrichment process is presumed to have taken place progressively—copper having been repeatedly dissolved, carried downward, and precipitated. It has been well established by Blanchard (1), Locke (8), and others that under these conditions "limonites" of certain colors and textures are left behind in the leached capping as evidence of the preexisting chalcocite. The Silver Bell district provides exceptionally good examples of this phenomenon, but limonites of chalcocite derivation are not confined to the outcrops over the ore bodies. They are widely dispersed through the zone of alteration. Proper interpretation of their significance in respect to ore possibilities has rested mainly on quantitative rather than qualitative appraisal. Mapping of the Silver Bell outcrops on this basis has provided a valuable guide in exploration drilling for the last 15 years. Results have demonstrated that the pattern of relatively strong chalcocite at depth is reflected in the outcrops by the distribution and abundance of diagnostic limonites.

It may be of interest at this point to mention the ancient excavations that are numerous in the outcrops of the mineralized zone at Silver Bell. There is evidence indicating that they are several centuries old. Since there are no precious metals or visible copper in these cuts, it is plausible to assume that the limonite and clay minerals were considered valuable, perhaps for pottery or warpaint. Thus, in the history of leached-outcrop investigations, it seems that some early Arizona Indian tribe deserves at least honorable mention.

Previous work and acknowledgments.—The first scientific study of the district was published in 1912 by Stewart (15). Considerable field and laboratory work has been done in more recent years by several groups and individuals, including the writers, all reporting privately to the American Smelting and Refining Co. Roland Blanchard conducted leached-outcrop studies in part of the area. Harrison Schmitt, H. M. Kingsbury, and L. P. Entwistle mapped structure and mineralization in the central part of the district. P. F. Kerr studied the alteration features and later published a comprehensive paper (6) on the district. Thomas Mitcham mapped structural features in the surrounding area. The writers have drawn considerably on these and other unpublished data, particularly in compilation of the geologic map. The high quality and usefulness of this material is gratefully acknowledged, but unfortunately it is not feasible to give special individual credits. Thanks are due the American Smelting and Refining Co. for permission to publish this paper.

LITERATURE CITED

1. Blanchard, Roland, 1939, Interpretation of leached outcrops: Jour. Chem., Met. and Min. Soc. of S. Africa, May.
2. Butler, B. S., and Wilson, E. D., 1938, Clifton-Morenci district: Arizona Bur. Mines Bull. 145, p. 74.
3. Damon, et al., 1963, Correlation and chronology of ore deposits and volcanic rocks: Univ. Arizona, Ann. Progress Report no. 5.
4. Emmons, W. H., 1917, The enrichment of ore deposits: U.S. Geol. Survey Bull. 625.
5. Holmes, Arthur, 1960, A revised geologic time-scale: Edinburgh Geol. Soc. Trans., v. 17, p. 183–216.

6. Kerr, P. F., 1961, Alteration features at Silver Bell, Arizona: Geol. Soc. America Bull., v. 62, p. 457–480.

Lindgren, Waldemar, 1905, The copper deposits of the Clifton-Morenci district: U.S. Geol. Survey Prof. Paper 43, p. 206.

8. Locke, Augustus, 1926, Leached outcrops as guides to copper ore: Baltimore, Williams and Wilkins.

9. Mauger, R. L., Damon, P. E., Gilletti, B. J., 1963, Age of ore deposition within the southwestern copper metallogenetic province in Arizona: Am. Inst. Mining Metall. Petroleum Engineers, Dallas, Texas, February.

10. McClymonds, N. E., 1959, Paleozoic stratigraphy of the Waterman Mountains, Pima County, Arizona: Arizona Geol. Soc., Southern Arizona Guidebook II.

11. Mitcham, T. W., 1955, Discussion of paper, Structure and mineralization at Silver Bell, Arizona: Am. Inst. Mining Metall. Petroleum Engineers, v. 202, p. 300.

12. Richard, Kenyon, and Courtright, J. H., 1954, Structure and mineralization at Silver Bell, Arizona: Mining Eng., November, and Am. Inst. Mining Metall. Petroleum Engineers Trans., v. 199, p. 1095–1099.

13. ——— 1959, Some geologic features of the Mission deposit: Arizona Geol. Soc., Southern Arizona Guidebook II.

14. ——— 1960, Some Cretaceous-Tertiary relationships in southern Arizona and New Mexico: Arizona Geol. Soc. Digest, v. III.

15. Stewart, C. A., 1912, The geology and ore deposits of the Silver Bell mining district, Arizona: Am. Inst. Mining Metall. Petroleum Engineers Bull., v. 65, p. 455–506.

UPDATING THE GEOLOGY AND STRUCTURAL ORE CONTROLS AT SILVER BELL, ARIZONA

by Barry N. Watson
ASARCO Geologist

A talk to be presented to the Mining Geology Division of the Arizona Section of A.I.M.E. on May 20, 1968.

One of the more complete stratigraphic sections in southern Arizona can be pieced together in the Silver Bell area. Much of the geology has been worked out by ASARCO geologists, while a few important areas have been mapped by students as thesis problems. Other portions of the Silver Bell area have yet to be mapped in any kind of detail, and some of this yet-uncharted geology could well be critical to a better understanding of the complex Mesozoic and Cenozoic stratigraphy.

It is my strong belief that a knowledge of certain of the stratigraphic units in the Silver Bell area--their lithologic characters and structural settings--would be of considerable help to field geologists dealing with similar phenomena elsewhere in southern Arizona. Parts of the Silver Bell stratigraphic section are accessible only by washes or somewhat obscure truck trails, and other portions of the section are on, or readily reachable only by passage through, private property owned by ASARCO.

In the following, I will attempt to briefly describe the geologic history of the Silver Bell area, with particular emphasis on the Mesozoic Era. My knowledge of the area has been greatly enhanced through field excursions and conversations with Harold Courtright, Kenyon Richard, Jim Briscoe, Craig Clarke, Chuck Haynes, Nick Nuttycombe, Joy Merz, Fred Graybeal and Dr. Willard Lacy. I must take, however, the responsibility for the interpretations drawn herein.

Figure 1 is a location map showing the principal topographic features mentioned below. Figure 2 is my diagrammatic representation of the Silver Bell stratigraphic column.

PRECAMBRIAN

Pinal Schist

The only outcrop of the basement Pinal Schist known to the author in the Silver Bell vicinity straddles the El Paso Natural Gas pipeline road about two miles east of Ragged Top. Relationships with other rock units are obscured by cover, except on the south where the schist is bounded by a mid-Tertiary dike filling the major WNW-trending Ragged Mountain fault.

FIGURE 1. Location map.

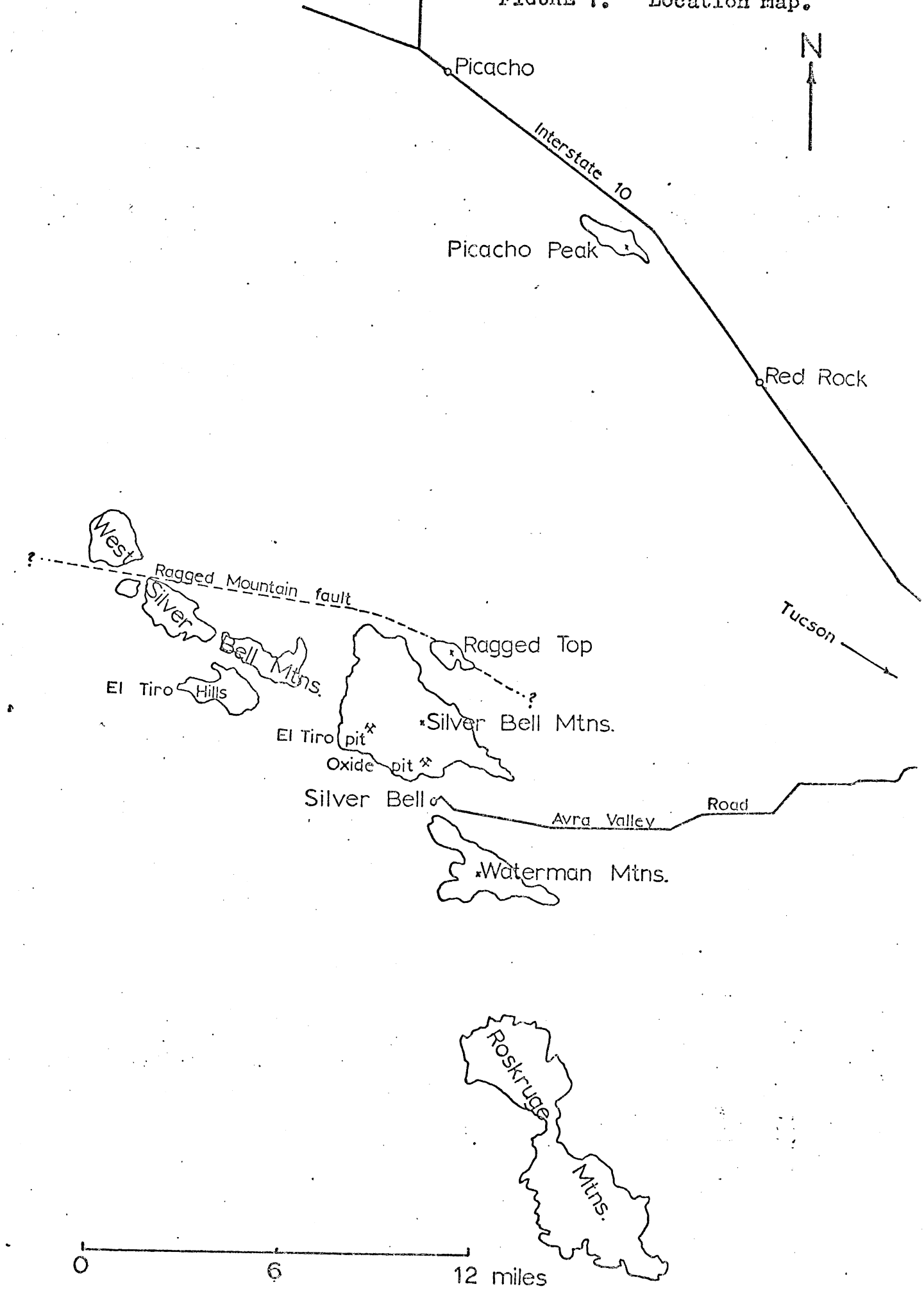

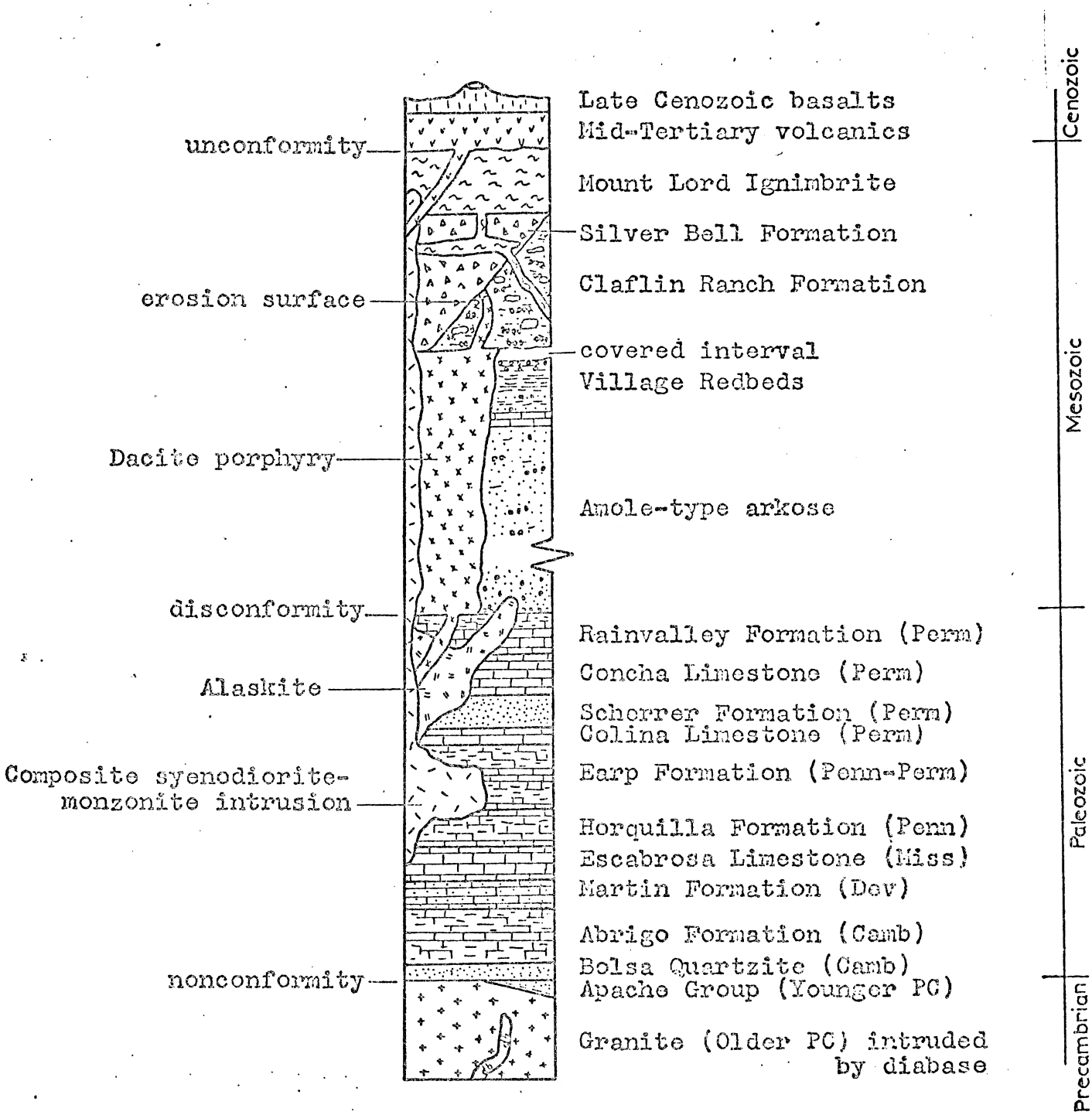

FIGURE 2. Diagrammatic geologic column of the Silver Bell area. Maximum known thicknesses for Paleozoic and Mesozoic rocks are shown. Scale of column: 1"=2000'.

Many fragments (ranging up to boulder size) of Pinal-like schist are seen in Cretaceous sediments just south of Ragged Top, indicating the presence of a considerable area of that schist at the surface in the near vicinity during the Laramide igneous activity.

Granite

A coarse-grained granite is found extensively to the north of the Ragged Mountain fault. Large and numerous quartz grains--frequently .25 inch in diameter--are set among pinkish crystals of feldspar and clumps and books of biotite. In many places orthoclase porphyroblasts up to an inch in length are common. This granite megascopically resembles the Precambrian Oracle granite seen near the town of Oracle.

Paleozoic sediments in the Waterman Mountains southeast of Silver Bell are also underlain by porphyroblastic granite.

Apache Group

Younger Precambrian Apache Group metasediments lie on granite just northeast of Ragged Top. Locally more than 200 feet thick, these south-dipping beds are sharply cut off to the south by the Ragged Top intrusive which wells up along the Ragged Mountain fault. The Apache Group stratigraphy here is not well worked out, but it appears as if a few tens of feet of probable Pioneer Formation (mixed sandy and shaly beds) are overlain by 2-3 feet of Barnes Conglomerate, which is in turn overlain by thin-to moderately thick-bedded quartzites of the Dripping Springs Quartzite.

Apache Group metasediments are missing in the Waterman Mountains where McClymonds (1957) notes Cambrian Bolsa Quartzite to conformably overlie basement granite.

Diabase

Well-altered diabase of possible Precambrian age irregularly intrudes the granite on the northern slopes of Ragged Top. As it is found only within granite, it's relative age cannot be stated with certainty. The principal period of Precambrian diabase intrusion in southern and central Arizona is post-Apache Group.

PALEOZOIC ERA

The Paleozoic stratigraphy of the Waterman Mountains has been deciphered by McClymonds (1957) and Ruff (1951) who mapped a well-faulted pile of limestones, quartzites, siltstones, and shales amounting to a thickness of 4,400+ feet. In the Silver Bell Mountains, Paleozoic stratigraphy was unravelled by Kingsbury, Entwistle and Schmitt in 1941 in a private report to the American Smelting and Refining Co. Merz (1967) undertook the difficult study of the altered and mineralized Paleozoic sediments on Union Ridge east of ASARCO's El Tiro pit. The alteration and mineralization of these Union Ridge sediments will be described in the next paper this morning.

The Paleozoic section in the Silver Bell Mountains is well faulted, locally intensely altered, and generally inundated by various Laramide intrusive units. Although each of the Paleozoic periods represented in the Waterman Mountains also show in the Silver Bell range, the section in the latter is obviously incomplete. A brief tabulation of units with thickness estimates is presented below:

Permian quartzites, limestones, shales..	550 ft. approx.
Pennsylvanian Horquilla Limestone.....	220 ft. max.
Mississippian Escabrosa Limestone.....	275 ft. max.
Devonian Martin Formation.....	300 ft. max.
Cambrian Abrigo Formation.....	430 ft. max.
Cambrian Bolsa Quartzite.....	230 ft. min.
Total.....	2,005± ft.

In the El Tiro Hills section of the West Silver Bell Mountains, Clarke (1965) mapped 1,200+ feet of uppermost Permian sediments. Approximately 300 feet of quartzites and dolomitic limestones belonging to the Scherrer Formation are overlain by ±420 feet of Concha Formation Limestone and ±550 feet of Rainvalley Formation limestone and argillite. These Permian rocks protrude from alluvial cover and are overlain by Mesozoic sediments.

MESOZOIC ERA

Amole-type arkose

A clearly exposed contact between Mesozoic and Paleozoic sediments is found in the El Tiro Hills where Clarke (1965) has mapped an estimated 5,000+ feet of probable Cretaceous Amole-type sediments overlying Permian Rainvalley rocks. The basal Amole-type units, lying on a disconformity, is a massive arkosic conglomerate containing rounded quartzite cobbles up to several inches in diameter. This unit of the Cretaceous (?) is several feet thick; the remainder is generally more thinly bedded.

Hayes and Drewes (1968) consider the Amole Arkose of the Tucson Mountains to be more or less a time-equivalent of the lower Middle Cretaceous Bisbee Group sediments. If the Amole-type materials in the El Tiro Hills can be considered correlative with the Amole Arkose, then Clarke's basal quartzite pebble conglomerate qualifies as a far-western equivalent of the basal Bisbee Glance Conglomerate. The presence of Cretaceous (?) beds lying disconformably on the uppermost Permian Rainvalley certainly suggests that the Silver Bell area did not experience, at least locally, the degree of structural unrest manifested farther to the east.

Another interpretation suggested by the near-conformable nature of the Paleozoic-Mesozoic contact related to recent U.S. Geological Survey recognition of Triassic sediments in southern Arizona. Possibly the hiatus between Permian and Mesozoic deposition is not as great as might be thought, and the lowermost Amole-type sediments are of Triassic age?

A few tuffaceous beds are scattered through the Amole-type arkoses, indicating periodic volcanic activity in the general region. Red-colored shales and conglomerates are found here and there through the sequence and are most prevalent in the upper portions. A 20-30-foot thick sandy limestone occurs near the top of the exposed older Cretaceous beds.

The Amole-type sediments are overlain in angular unconformity by interbedded tuffs and coarse clastic sediments of the Claflin Ranch-type. A similar mid-to late Cretaceous unconformity has been noted elsewhere across southeastern Arizona. It is felt that this unconformity reflects initial upheaval related to Laramide deformation.

Amole-type arkoses, conglomerates and sandstones also crop out in the valley between the Waterman and Silver Bell Mountains. Immediately overlying the arkoses near the southeast corner of the older Silver Bell tailings dam is a limestone unit probably exceeding 200 feet in thickness. Donald Bryant of the University of Arizona was able to identify recrystalized pelecypods here as of definite Cretaceous age. Outside of the Bisbee Group Mural Limestone, this localized unit is probably the thickest Cretaceous limestone known in southcentral Arizona.

Village Redbeds and red conglomerates

A sequence of red-colored clastics is found overlying the limestone unit and Amole-type arkoses south of the Silver Bell tailings dams. These clastics, which also underlie Silver Bell village, are locally several hundreds of feet thick, but faulting and alluvial cover prevent thickness determinations. The author originally considered this unit to be an equivalent of the Recreation Redbeds of the Tucson Mountains. However, detailed mapping plus radiometric age-dating have recently proven the Recreation Redbeds to be of pre-Amole age, and evidence is now overwhelming that red coloration represents restricted environmental conditions that could, and do, appear at various times throughout the Mesozoic. Consequently, I am here designating the Cretaceous redbeds and red conglomerates near the Silver Bell townsite the "Village Redbeds".

In places redbeds and light-colored Amole-type arkoses are found interbedded, suggesting a somewhat gradual transition from the Amole to the Village environment. Several hundred feet of red silts, sands and arkoses occur in the lower portions of the Village Redbeds and are seen to grade upward to red conglomerates. At first these conglomerates contain only sedimentary detritus. Higher in the sequence igneous materials begin to appear, however, and in the uppermost known portions the red conglomerate consists almost entirely of purple andesitic fragments set in a detrital matrix. Deformation of an ancient Silver Bell landscape and a gradual increase in volcanic activity is readily evidenced in the continuing deposition of the redbeds and red conglomerates. Thus the transition from normal Cretaceous subaerial sedimentation to coarse and rapid Laramide accumulation is not always marked by an obvious stratigraphic break.

The Village red conglomerates are cut off by a major WNW-trending fault in the tailing pond area, and their relation to overlying units is not presently known.

Claflin Ranch Formation

The Claflin Ranch Formation is something of a catch-all term, and the rocks it represents are not limited to any one specific time of deposition. The formation represents a type of sedimentation associated with a terrane undergoing volcanic upheaval and rapid erosional deformation. Thus, in the Silver Bell Mountains where Richard and Courtright first used the name (1960), the conglomerates, mudflows, landslide blocks, aeolian tuffs, water-lain tuffs and pyroclastic layers included within the Claflin Ranch Formation have ambiguous relationships with associated volcanic units. They are pre-dacite and post-dacite, pre-Silver Bell andesite and post-Silver Bell andesite. In the West Silver Bell Mountains Claflin-like conglomerates are interbedded with pyroclastics and overlie earlier Cretaceous sediments by angular unconformity.

The thickest continuous Claflin Ranch sequence in the Silver Bell Mountains--approximately 1800 feet--occurs southwest of Ragged Top. This accumulation is, at least in good part, pre-dacite porphyry (the earliest of the Laramide volcanic and sub-volcanic rocks in the Silver Bell range). Coarse, greenish clastic materials megascopically identical with parts of the Claflin Ranch Formation are found as a matrix of the Tucson Mountain Chaos in the Tucson Mountains. Claflin Ranch-type rocks also are seen in roadcuts north of Sonoita along Arizona State Highway 83.

It seems reasonable to expect that the Claflin Ranch-type of surface accumulation of detrital and volcanic debris might be found throughout southern Arizona wherever Laramide volcanic piles exist. Such depositional sequences--seemingly thickest in earlier Laramide time--would run the gamut from fairly thin-bedded sands to chaotic masses of landslide-block accumulations.

Alaskite

Richard and Courtright (1966), in accounting for the WNW-striking zone of alteration at Silver Bell, conclude that "indirect evidence suggests a fault representing a line of profound structural weakness existed in this position prior to the advent of Laramide intrusive activity." This line is referred to as the "major structure." They go on to note that this major structure "was largely obliterated by the Laramide intrusive bodies, but it effected a degree of control on their emplacement, as evidenced by their shapes and positions."

The first indication of activity along the Silver Bell fault zone came in early Laramide time with the intrusion of a coarsely granitoid alaskite along the southwest side of the

major structure. This alaskite, which contains a very low ferromagnesian mineral content, intrudes Paleozoic sediments and Cretaceous Amole-type arkoses in the El Tiro area. Aplite dikes are found through the alaskite, and, locally, fine-grained border phases of alaskite are found in contact with other rock units.

The alaskite is one of the principal hosts for the later porphyry copper mineralization. This coarse-grained felsic rock locally shows high chalcopyrite-to-pyrite ratios.

Dacite porphyry

The dacite porphyry is a sub-volcanic rock characterized by numerous rounded or triangular quartz "eyes" set in a very fine-grained matrix. Orthoclase and sanidine phenocrysts, vague but consistent flow structure, and up to 20% of xenoliths are also commonly seen. Chemically, the dacite porphyry is more accurately a quartz latite porphyry.

The dacite occurs extensively northeast of the major structure in the form of sills and dikes within Paleozoic and Mesozoic sediments. The largest body of the porphyry--a sill ± 3,400 feet thick--occupies the stratigraphic interval in the Silver Bell range proper where Amole-type arkose should occur. This sill is floored by Paleozoic sediments and roofed by an 1800-foot sequence of Claflin Ranch materials. The dacite-Claflin Ranch contact is gradational over several feet, but dikes of dacite porphyry are found locally in the overlying Claflin Ranch beds.

An explosive history for the dacite porphyry is strongly suggested by the numerous xenoliths, the large fragments of quartz, and the shards of former glass in the matrix. The nature of the rock is believed to reflect an emplacement by fluidization in the following manner:

The gas-and fragment-charged dacite porphyry magma (actually quartz latite in composition, suggesting greater viscosity and more explosive potential) rose along the Silver Bell fault zone into Paleozoic strata. The higher the porphyry magma ascended, the more the confining pressure decreased, causing exsolution of gases and thus lending an explosive and dilative nature to the intrusive material.

Its extension to the southwest blocked by the large body of alaskite, the dacite porphyry welled up, sending small dikes and sills northeastward into the Paleozoic beds. Damp Amole-type Cretaceous (?) sediments were reached and more gas evolved. The magmatic material, expanding constantly, spread laterally to the northeast in the weak Cretaceous (?) sediments. Dilation occurred, as did the incorporation of fragments broken by churning gas action.

The dacite porphyry probably surfaced in one or more places, venting gases as it did. Gas also escaped laterally through the just-formed sill and vertically into overlying Claflin Ranch sediments. The heat and vapor action altered the immediately overlying quartzo-felspathic clastic sediments, giving rise to the gradational contact seen today.

The dacite porphyry was a poor host rock for porphyry copper mineralization because of its flinty, "tight" nature.

Silver Bell Formation

The Silver Bell Formation (Richard and Courtright, 1960) consists of laharic, autobrecciated, and intrusive andesitic to dacitic breccias, andesitic to dacitic flows, and andesitic intrusions. These materials overlie Claflin Ranch sediments and dacite porphyry in the Silver Bell Mountains. The rugged nature of the basal Silver Bell contact and the fact that it locally lies on unroofed dacite porphyry points to a period of rapid uplift and erosion following intrusion of the dacite porphyry sills.

Purplish Silver Bell-type breccias are seen to be interlayered in places with overlying Mount Lord Ignimbrite. Such a transition from andesitic activity to more felsic and explosive volcanism is seen throughout the world and is commonplace in the Laramide rocks of southern Arizona and southwestern New Mexico.

It is believed that the Silver Bell Formation is roughly correlative with the Demetrie Formation of the Sierrita Mountains, the Picacho Peak volcanics (Briscoe, 1967), the Owl Head volcanics, and that portion of the Cloudburst Formation north and east of the San Manuel mine.

Mount Lord Ignimbrite

A welded ignimbrite lithologically similar to, and stratigraphically a time-equivalent of, the Cat Mountain Rhyolite of the Tucson Mountains overlies the Silver Bell Formation in the Silver Bell Mountains. This quartz latitic ignimbrite is up to 800 feet thick, including an 80-foot thick cap of lithic vitric tuff. As Silver Bell Peak was formerly known to residents of the area as "Mount Lord" and since the peak is composed of the pyroclastic unit, the name "Mount Lord Ignimbrite" has been given to this Cat Mountain-type unit.

Intrusive ignimbrites--genetically related to the Mount Lord Ignimbrite, and megascopically and petrographically identical with it--occur as dikes and sills in the underlying Silver Bell Formation and dacite porphyry. These feeder materials once en route to the surface spread along bedding and formational contacts, apparently when vents became choked.

The Cat Mountain Rhyolite of the Tucson Mountains evinces an average age of 68 million years (Damon, 1968), and it is felt that the Mount Lord Ignimbrite is of similar age.

Syenodiorite porphyry

The syenodiorite porphyry is an early and somewhat extensive pyroxene-bearing phase of the composite intrusive thought to be related to the copper mineralization at Silver Bell. Later phases of this composite intrusive are monzonitic and quartz monzonitic. The syenodiorite porphyry is found principally in the southeastern portion of the Silver Bell Mountains. It occurs as massive bodies in Oxide pit (where it was previously called both "andesite" and "dacite") and east of Oxide pit along the major structure, and is found as east-trending dikes north of Oxide pit in the mountain range.

The syenodiorite porphyry is the best host rock in Oxide pit. It shows the highest primary copper sulfide content of any of the igenous rocks at Silver Bell and has allowed precipitation of a substantial chalcocite blanket.

Only occasional dikes of syenodiorite porphyry are seen in El Tiro pit.

Monzonite porphyry

The later monzonitic and quartz monzonitic phases of the composite intrusion are found as massive bodies scattered along the major structure. They occur also as generally east-trending dikes in the mountain range to the northeast of the major structure.

The principal porphyry copper mineralization followed emplacement of the monzonite porphyry, and a zone of alteration was superimposed on the major structure. K-Ar age-dating (Mauger, Damon and Giletti, 1965) has shown that the solidification of the monzonite porphyry and the subsequent hydrothermal alteration occurred at approximately 65 million years and within a short enough time span so that, considering the limits of error of the age-dates, the two events are radiometrically indistinguishable. I do not mean to imply here that the Silver Bell deposits are to any great extent syngenetic as has been suggested recently (Mauger, 1966). It may be that a small amount of chalcopyrite became trapped as discrete grains in the monzonite magma at the time of solidification. The great preponderance of copper mineralization, however, was emplaced in the various host rocks through veins, veinlets, and hairline fractures with values diffusing into wallrocks, possibly with the aid of a certain amount of igneous rock recrystallization.

It is interesting to note that both the Oxide and El Tiro orebodies occur at structural intersections (see Figure 3). Oxide pit is located at the junction of the WNW-trending major structure with an ENE-trending swarm of syenodiorite and monzonite porphyry dikes. Similarly, El Tiro pit exists at the junction of the major structure with a northeast-trending swarm of monzonite porphyry dikes.

FIGURE 3. Dike swarms related to mineralization at Silver Bell

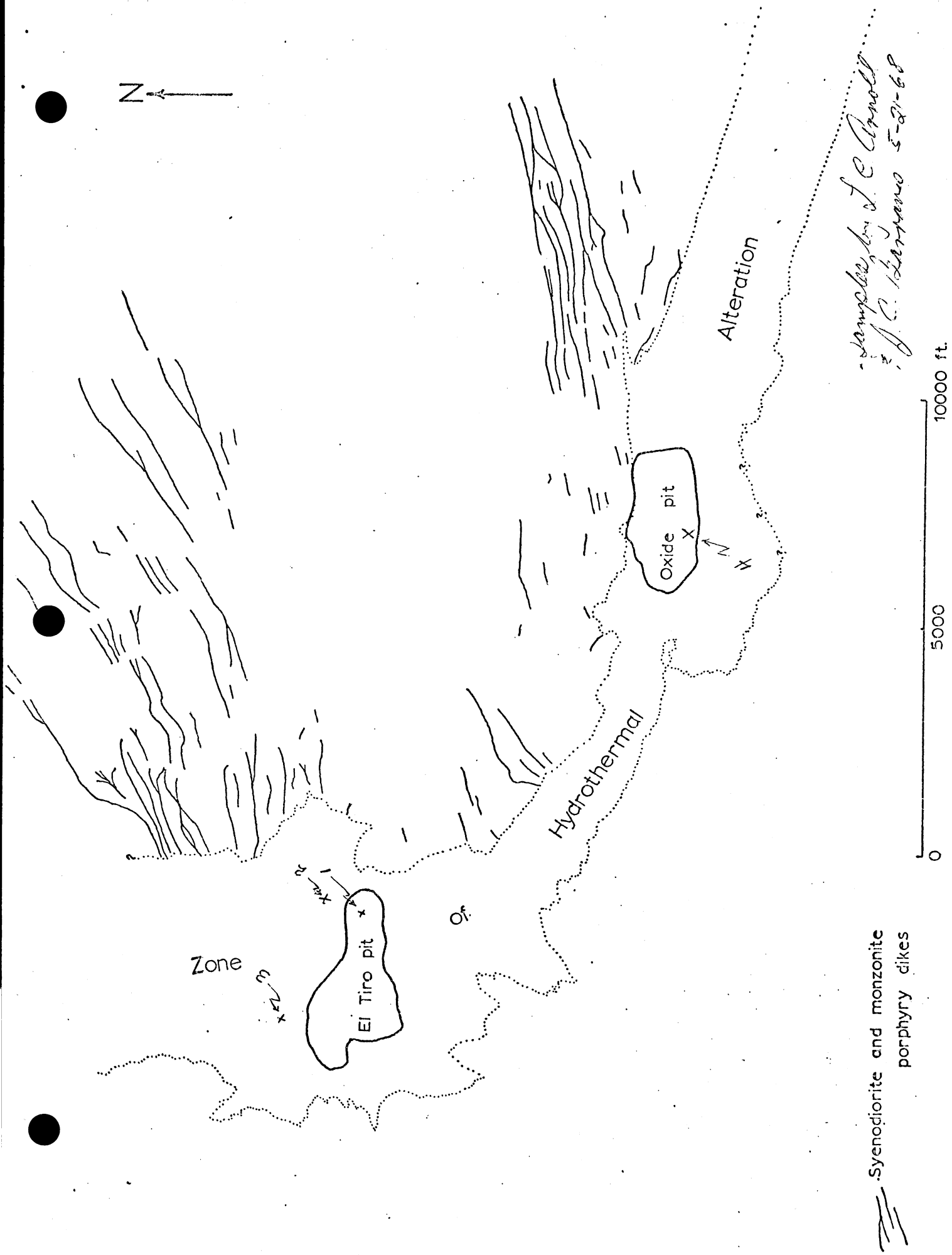

CENOZOIC ERA

It is preferred here to set the Mesozoic-Cenozoic time boundary at 63 million years as defined by Folinsbee, Baadsgaard, and Lipson (1961). This allows the Silver Bell mineralization to fall at the end of the Cretaceous Period.

Regional northeasterly tilting of 20°-30° occurred sometime between the emplacement of the composite Laramide intrusion and the mid-Tertiary volcanism. It probably was a result of late Laramide upheaval. This tilting, shown by the present orientation of Laramide depositional units, appears to have taken place by rotation of WNW-elongate, fault-bounded blocks in the Silver Bell area.

The mineralized rocks at Silver Bell were exposed to weathering and probably supergene enrichment in early Tertiary time. This is strongly suggested 3 miles east of Oxide pit where pieces of leached capping were found in a conglomerate immediately underlying an andesite flow dated at 28 million years (Damon and Mauger, 1966). A mid-Tertiary period of rhyolitic to andesitic volcanism evinced widely over southern Arizona probably covered and thus preserved the Silver Bell mineralization. This mineralization has been exhumed in more recent times and is presently undergoing destruction through weathering processes.

North-northwest-trending quartz latite porphyry and andesite porphyry dikes of the mid-Tertiary volcanic epoch cut all earlier rock units in the Silver Bell Mountains. The quartz latite dikes have a strangely discontinuous line of outcrop which is caused not by faulting, as has been previously suggested by Schmitt (1941), but by intrusion into a very broken and faulted terrane. A few of the andesite porphyry dikes are conspicuous in El Tiro pit where they are locally collectors of green copper oxide.

The Ragged Top Latite Porphyry dated at 25±1.0 million years (Mauger, Damon and Giletti, 1965) intruded the prominent Ragged Mountain fault which had dropped Laramide rocks on the south some 5,000-7,000 feet against Precambrian granite. Andesitic and rhyolitic flows of probably similar age are seen several miles west of Ragged Top in the northeastern part of the West Silver Bell Mountains.

A late and minor lead-silver-copper mineralization is found in the Silver Bell range. North-trending epithermal veins carrying galena, native silver and cerargyrite with a barite-quartz-calcite-fluorite gangue were mined in the early days. Copper stain is seen on the old dumps. This later period of mineralization has been superimposed very locally on the porphyry copper deposits to the south. On the other hand, a mid-Tertiary quartz latite porphyry dike cuts one of the epithermal veins, thus establishing a general minimum date to this mineralization.

Quaternary-Tertiary basalt cones and flows are found north of the Ragged Mountain fault.

SOURCES USED

Briscoe, J.A., 1967, General geology of the Picacho Peak area, Pinal County, Arizona: Unpublished Master's thesis, Univ. Ariz.

Clarke, C.W., 1965, The geology of the El Tiro Hills, West Silver Bell Mountains, Pima County, Arizona: Unpublished Master's thesis, Univ. Arizona.

Damon, P.E., and Mauger, R.L., 1966, Epeirogeny-orogeny viewed from the Basin and Range Province: Soc. Mining Engineers Trans., v. 235, p. 99-112.

Damon, P.E., 1968, Application of the potassium-argon method to the dating of igneous and metamorphic rock within the Basin Ranges of the Southwest: Ariz. Geol. Soc. Southern Arizona Guidebook III, p. 7-21.

Folinsbee, R.E., Baadsgaard, H., and Lipson, J., 1961, Potassium-argon dates of Upper Cretaceous ash falls, Alberta, Canada: Annals of the New York Acad. Sci., v. 91, art. 2, p. 352-359.

Hayes, P.T., and Drewes, H., 1968, Mesozoic sedimentary and volcanic rocks of southeastern Arizona: Ariz. Geol. Soc. Southern Arizona Guidebook III, p. 49-58.

Kingsbury, H.M., Entwistle, L.P., and Schmitt, H., 1941, Geology and ore deposits of Silverbell, Arizona: private report.

Mauger, R.L., 1966, A petrographic and geochemical study of Silver Bell and Pima mining districts, Pima County, Arizona: Unpublished Ph.D. dissertation, Univ. Arizona.

Mauger, R.L., Damon, P.E., and Giletti, B.J., 1965, Isotopic dating of Arizona ore deposits: Soc. Mining Engineers Trans., v. 232, p. 81-87.

McClymonds, N.E., 1957, The stratigraphy and structure of the Waterman Mountains, Pima County, Arizona: Unpublished Master's thesis, Univ. Arizona.

Merz, J.J., 1967, The geology of the Union Hill area, Silver Bell district, Pima County, Arizona: Unpublished Master's thesis, Univ. Arizona.

Richard K., and Courtright, J.H., 1960, Some Cretaceous-Tertiary relationships in southern Arizona and New Mexico: Ariz. Geol. Soc. Digest, v. III.

_____ 1966, Structure and mineralization at Silver Bell, Arizona: Geology of the Porph. Copper Deposits, SW No. America, Univ. Ariz. Press, p. 157-164.

Ruff, A.W., 1951, The geology and ore deposits of the Indiana mine area, Pima County, Arizona: Unpublished Master's thesis, Univ Arizona.

Watson, B.N., 1964, Structure and petrology of the eastern portion of the Silver Bell Mountains, Pima County, Arizona: Unpublished Ph.D. dissertation, Univ. Arizona.

_____ 1965, Geology of the area east of Oxide pit, Silver Bell, Arizona: private report.

_____ 1968, Intrusive volcanic phenomena in southern and central Arizona: Ariz. Geol. Soc. Southern Arizona Guidebook III, p. 147-154.